University of California
Santa Barbara

Looking under the light pulse: an integrative case study on the mating behaviors of Caribbean sea fireflies (Crustacea, Ostracoda, Cypridinidae)

A dissertation submitted in partial satisfaction
of the requirements for the degree

Doctor of Philosophy
in
Ecology Evolution & Marine Biology

by

Nicholai Marcus Hensley

Committee in charge:

Professor Todd H. Oakley, Chair
Professor Thomas L. Turner
Professor Trevor J. Rivers

September 2020

The Dissertation of Nicholai Marcus Hensley is approved.

Professor Thomas L. Turner

Professor Trevor J. Rivers

Professor Todd H. Oakley, Committee Chair

August 2020

Looking under the light pulse: an integrative case study on the mating behaviors of Caribbean sea fireflies (Crustacea, Ostracoda, Cypridinidae)

by

Nicholai Marcus Hensley

For Mom, who taught me to dream.
To Dad, who taught me love.
And a brother-in-arms.
`10.09.1990 - 08.24.2005`

Acknowledgements

Many thanks are deserved by my advisor, Todd H. Oakley, whose clear thinking and dogmatic use of the Socratic method has helped shape how science is seen by me. As important was his commitment to creating a convivial lab environment, and whose members over the years I consider true colleagues, including (but not limited to): Daniel I. Speiser, Johanna T. Cannon, Jessica A. Goodheart, M. Desmond Ramirez, Andrew J. M. Swafford, Natasha Picciani, and Emily S. Lau. I am particularly honored to have spent much of my graduate education with Emily A. Ellis, the best lab mate and dive-buddy someone could ask for. You all have made this journey better in every facet.

I thank my collaborators Gretchen A. Gerrish and Trevor J. Rivers, and also James G. Morin and Elizabeth Torres, for introducing me to these elegant underwater gnats (sea fireflies, fire fleas, seed/disco/techno shrimp, umihotaru, ostrocads, etc.). Also to Yasuo Mitani and the other members of AIST Sapporo for their hospitable treatment of a graceless scientist abroad, and John Lew for his guidance on the nature of light and statistics. My sincerest gratitude to the UCSB EEMB department, especially Cathi Arnold, Shelly Vizzolini, and Andi Jorgensen, without whom we all would have fallen by the wayside long ago. To Thomas L. Turner and Scott A. Hodges, your leadership in Evolution Seminar was a motivating force for good, critical science. Zac Cabin, Evangeline Ballerini, and Natalie Love all made the 4th floor corridor a better place to work every day, each in their own way. I am also grateful for a number of academic mentors/models that I've had the privilege of knowing over the years, and who inspired me to pursue research: Daniel T. Blumstein, David A. Gold, Matthew B. Petelle, Greer A. Dolby, and Jonathan P. Drury. And as a mentor, it was my great honor to host a number of undergraduate and high school students during these trials and tribulations, each who helped buoy my passion for science with their own.

Emotional support was provided by family, friends, and a consistent practice of mindfulness at my local yoga and coffee haunts. To my Father, Mother, Christopher, Lola, and Pops: I would have never gotten this far without you. I owe you more than I know, and I love you. To my friends who've graciously hosted my couch-surfing serfdom: I'm not a"real" doctor like half of you, and as such can never repay you, but I'll always be thankful (S. Pattison, A. Payson, A. Andersson, T. Webb, S. Nguyen, M. Mansour, E. Black, L. Hunt, and K. McCarty). Until the next reunion. To Andrea N. Chan, who has tolerated my frumpy, grumpy ways ever since that fateful day at Bodega Marine Lab, and in stark contrast to the rainbow tapestry of her life. Gotta Get Back. Always. And to my cohort (Eric W. Slessarev & Claire Kouba, Michael P. Shahandeh, Kristen Peach, and Laura Drake-Schultheis), for providing years of commiseration and joy: I owe you my laugh lines. We'll always have Santa Barbara.

Curriculum Vitæ

Nicholai Marcus Hensley

Education

2020	**Ph.D.** in Ecology, Evolution, & Marine Biology
	University of California, Santa Barbara
2018	**M.A.** in Ecology, Evolution, & Marine Biology
	University of California, Santa Barbara
2012	**B.S.** in Ecology, Behavior, & Evolution
	Minor in Conservation Biology
	University of California, Los Angeles
	Magna Cum Laude, College Honors, Departmental Highest Honors

Publications

Research Articles

1. Picciani de Souza, N., Kerlin, J. R., Jindrich, K., **Hensley, N. M.**, Gold, D. A. & Oakley, T. H. Light modulated cnidocyte discharge predates the origins of eyes in Cnidaria. Authorea doi: https://doi.org/10.22541/au.159626523.36299944 (Aug 2020 - in review).
2. **Hensley, N. M.**, Ellis, E. A., Leung, N. Y., Coupart, J., Mikhailovsky A., Taketa, D. A., Tessler, M., Gruber, D. F., De Tomaso, A. W., Rivers, T. J., Gerrish, G. A., Torres, E. & Oakley, T. H. Selection, drift, and constraint in cypridinid luciferases and the diversification of bioluminescent signals in sea fireflies. bioRxiv doi: https://doi.org/10.1101/2020.01.23.917187 (Aug. 2020 - in revision).
3. **Hensley, N. M.**, Ellis, E. A., Gerrish, G. A., Torres, E., Frawley, J. P., Oakley, T. H. & Rivers, T. J. Phenotypic evolution shaped by current enzyme function in the bioluminescent courtship signals of sea fireflies. Proceedings of the Royal Society B 286, 20182621 (2019).
4. Gold, D. A., Nakanishi, N., **Hensley, N. M.**, Hartenstein, V. & Jacobs, D. K. Cell tracking supports secondary gastrulation in the moon jellyfish Aurelia. Development Genes and Evolution 226, 383–387. ISSN: 1432-041X (Nov. 2016).
5. Gold, D. A., Nakanishi, N., **Hensley, N. M.**, Cozzolino, K., Tabatabaee, M., Martin, M., Hartenstein, V. & Jacobs, D. K. Structural and Developmental Disparity in the Tentacles of the Moon Jellyfish Aurelia sp.1. PLOS ONE 10, 1–12 (Aug. 2015).
6. **Hensley, N. M.**, Drury, J. P., Garland Jr., T. & Blumstein, D. T. Vivid birds do not initiate flight sooner despite their potential conspicuousness. Current Zoology 61, 773–780 (2015).

7. **Hensley, N. M.**, Elmasri, O. L., Slaughter, E. I., Kappus, S. & Fong, P. Two species of Halimeda, a calcifying genus of tropical macroalgae, are robust to epiphytism by cyanobacteria. Aquatic Ecology 47, 433–440. ISSN: 1573-5125 (Dec. 2013).
8. **Hensley, N. M.**, Cook, T. C., Lang, M., Petelle, M. B. & Blumstein, D. T. Personality and habitat segregation in giant sea anemones (Condylactis gigantea). Journal of Experimental Marine Biology and Ecology 426-427, 1–4. ISSN: 0022-0981 (2012).

Writings for Science Communication

1. **Hensley, N. M.** Larger than life experiments expose the machinery inside elephant trunks. Society of Integrative and Comparative Biology (2020).
2. **Hensley, N. M.** The Devil Wears Prada: Birds Have Designer Cheats to Make The Bland Look Beautiful. Society of Integrative and Comparative Biology (2020).

Funding

1. American Microscopical Society Student Research Fellowship, June 2020, $1000
2. NSF Postdoctoral Research Fellowship in Biology, October 2020 - 2023, $15000 per yr.
3. NSF Graduate Research Opportunities Worldwide, July 2019, $5000
4. Smithsonian Tropical Research Institute, May 2018, $1500
5. American Museum of Natural History Lerner Gray Memorial Fund, May 2018, $2081
6. UC Santa Barbara Department of Ecology, Evolution, & Marine Biology Block Grant, April 2018, $1600
7. Sigma Xi Grant-In-Aid-of-Research, January 2015, $700
8. Society for the Study of Evolution Rosemary Grant Award for Graduate Student Research, May 2014, $2337

Fellowships & Awards

1. NSF Postdoctoral Research Fellowship in Biology, October 2020 - 2023, $54000 per yr.
2. NSF Graduate Research Opportunities Worldwide, January - April 2020, $6459.72
3. UC Santa Barbara Academic Senate Doctoral Student Travel Grant, June 2019, $1350
4. Worster Award for the development of graduate and undergraduate research, May 2019, $2500
5. Smithsonian Tropical Research Institute Short Term Fellowship, May 2018, $3000

6. NSF East Asia & Pacific Summer Institute Fellowship, June - August 2017, $5400
7. UC Santa Barbara Graduate Student Association Travel Award, 2015/2017/2018/2019, $200 ea.
8. NSF Graduate Student Research Fellowship, 2015 - 2018, $34000 per yr.
9. NSF Graduate Student Research Fellowship Honorable Mention, 2014
10. UC Santa Barbara Regents Special Fellowship, 2013 - 2015, $24000 per yr. + $5000
11. UC Los Angeles 15th Annual Biology Research Symposium Undergraduate Poster Award, June 2012
12. UC Los Angeles Ecology & Evolutionary Biology Special Faculty Award, June 2012
13. NSF Research Experience for Undergraduates, July 2011, $4000

Teaching & Professional Experience

Teaching Assistantships

1. UC Santa Barbara EEMB 102: Macroevolution, Spring 2019/2020
2. UC Santa Barbara EEMB 116: Invertebrate Zoology II, Spring 2015
3. UC Santa Barbara EEMB 138: Ethology/Behavioral Ecology, Winter 2015/2019
4. UC Santa Barbara EEMB 112: Invertebrate Zoology I, Fall 2014/2019
5. UC Los Angeles EEB 100L: Introduction to Ecology and Behavior Laboratory, Spring 2013
6. UC Los Angeles EEB 153: Ecological Responses to Environmental Variables, Fall 2012

Workshops & Job Experience

1. Workshop on Molecular Evolution, Marine Biological Laboratory in Woods Hole, 2018
2. Evolutionary Quantitative Genetics Workshop, Friday Harbor Laboratory, 2018
3. Cypridinid Ostracod Workshop, 2015
4. International Frozen Zoo Cell Culture Seminar, San Diego Zoo Institute for Conservation Research, 2014
5. Laboratory Technician, UC Los Angeles Department of Ecology & Evolutionary Biology, March - August 2013

Service & Outreach

- Founder/Organizer, UC Santa Barbara EEMB Professional Development Workshop
- Student Representative, UC Santa Barbara EEMB Faculty Search Committee
- Co-founder/Organizer, OUTReach Seminar Series
- Organizer, UC Santa Barbara EEMB Graduate Student Symposium

Abstract

Looking under the light pulse: an integrative case study on the mating behaviors of Caribbean sea fireflies (Crustacea, Ostracoda, Cypridinidae)

by

Nicholai Marcus Hensley

Some of the most extreme and diverse phenotypes in nature are mating behaviors. Poised to be an engine for biodiversity during the speciation process, and some of the most rapidly evolving traits, these extreme phenotypes are widely studied at the whole organism-level, yet intractable at other levels of biological organization due to their inherent complexity as an emergent property. Although we have a strong theoretical understanding of the ecological processes that contribute to the diversification of these behaviors, we have few studies able to resolve how evolution acts on the genome to generate such diversity. Our understanding of the genetic basis of behavior is much more limited than other phenotypes, and even more so when we wish to understand how behaviors diverge between species. In this thesis, I present a series of integrative studies dissecting the contribution of important proteins on the phenotypic evolution of mating behaviors, focusing on the fantastical displays of Caribbean ostracods (affectionately, "sea fireflies"). Males of 100 species use secretions of bioluminescent, mucus-like proteins to attract females, creating diverse patterns that vary between species and guide females towards individuals during the mating spree. I present evidence that functional and molecular divergence of these proteins contributes to changes in their light-producing function. In theory, this links to mating display structure, as it may influence the visible duration of individual bioluminescent secretions. By analyzing in vivo and in vitro differences in protein function, I find that the evolutionary lability of this display duration may be

constrained by its underlying mechanisms. Differences in these mechanisms contribute to the overall form of single pulses within a mating display, and molecular patterns of evolution point towards both purifying and diversifying selection acting on protein function. Lastly, using artificial playback experiments, I present further evidence that male displays influence female behavior, supporting the idea that these signals may be under sexual selection but not necessarily important in sea firefly speciation. Together, these data lend credence to the hypothesis that key genes can be hotspots of evolutionary divergence during species radiation but that their effects might be contingent upon other constraints, showcasing how diverse evolutionary forces are important in the evolution of behavior.

Contents

List of Tables

List of Figures

Chapter 1

Introduction

Complex phenotypes are replete in nature, concomitant with the biodiversity of life. An enduring question in evolutionary biology is how diversity of form evolves, and if by looking amongst these tangled banks, can we derive rules that predict such riotous evolution. Of particular interest are the evolution of animal behaviors. As emergent phenotypes at the intersection of genetics, development, and the environment, animal behaviors are widely associated with differences in fitness. Behaviors can also alter evolutionary rates and influence macroevolutionary patterns of diversity. Most prominently, shifts in some behaviors seem key to many bursts of speciation, and even claimed as causal. Thus understanding the mechanisms of divergence in behavioral phenotypes can inform us of behavior's broader evolutionary consequences, from phenotypic disparity to their role in structuring ecological interactions and driving species diversity. What genetic factors influence behavioral form and diversity over time? Are these factors shared across species, and when (if ever) are they important during speciation? What ecological factors select on these loci in the genome for behavioral divergence? In my thesis, I investigate how a single orthologous gene family may play a key role in the diversification of animal behavior using a unique system - the bioluminescent mating displays of cypridinid ostracods (Arthropoda, Crustacea, Ostracoda, Cypridinidae).

A major goal in dissecting the genetic basis of differences in such complex phenotypes is to understand if phenotypic evolution is repeatable at the genetic level: are specific loci always the target of evolutionary change during diversification? Theoretically, genes in key positions are disproportionately susceptible to produce change as evolutionary hotspots [122, 201]. This may be due their unique position in development, increased mutational target size, or other genomic properties that increase local mutation rates (e.g. *Pel* fragility in sticklebacks near *Pitx1* [238]). Classically, while coding changes are expected to produce large effects due to changes in gene function, alterations of regulation can avoid pleiotropic catastrophe with refined expression [202, 79]. Regulatory changes

are known to increase morphological disparity (e.g. Drosophila trichomes [129, 207], avian skull shape [185, 247]). Such cis-regulatory mutations are more prevalent for certain phenotypes over others [202]. More recent work suggests that an "omnigenic model" of phenotypic architecture, invoking genome-wide pleiotropy, is expected for complex phenotypes. Pleiotropy may constrain the available evolutionary solutions that produce phenotypic changes. Notably, comparisons for many phenotypes (like behavior) are only just becoming possible due to the inherent difficulty in generating data to answer these questions. Like most quantitative phenotypes, animal behaviors generally have a complex genetic architecture [110, 2]. More empirical examples are necessary to clarify how evolution creates behavioral diversity over time.

Some of the greatest behavioral diversity occurs in mating systems associated with adaptive radiations, and the interaction between sexes allows for complex patterns of phenotypic co-evolution [194, 145]. Thus species radiations are excellent systems to address mechanisms of behavioral diversification, as done with cichlid [246] and mormyrid fishes [6], *Drosophila* flies [63], *Heliconius* [133] and other butterflies [125], and *Laupala* crickets [187]. Sexual selection is invoked in many species radiations, with specific predictions on its genetic signature (reviewed by [131, 105]). Famously, Fisher [51] and Lande [109] developed simple population genetic models that predict how the exaggeration of secondary sexual traits should evolve over time. The genetic architecture of these traits is just as complex as traits under natural selection [2], and they seem to be just as heritable [165]. In particular systems, loci for sexually selected traits and corresponding preferences segregate together [234, 188], but other systems demonstrate complex trait-preference architecture [157, 113]. Contrary to some predictions, these areas are not associated with decreased rates of chromosomal recombination or inversions [16]. In ruffs [107] and white-throated sparrows [224], large inversions are linked with different reproductive morphs behaviors within these species, but only simple changes in enzyme

regulation are needed to generate differences in the color of canaries [57].

One of the most successful examples of mechanisms shaping behavioral divergence are odorant receptors; lying at terminal nodes of genetic pathways in order to integrate chemical information into a neurosensory context, these gene families have been targets of selection in many systems, especially for successful species recognition and mate choice [4, 50, 21, 183]. These receptors demonstrate both coding and expression changes that modify sensitivity to environmental cues, ultimately changing behavior (briefly reviewed in [24]). For example, in moths, differences in male sensitivity to female pheromone blends has been attributed both to switches in ligand affinity for expressed olfactory receptors (OR), and to which subsets of ORs are expressed in specific sensory neurons [69]. This also seems to be true for fly species with host-plant switches between species [115, 126], or changes in cuticular hydrocarbon profiles involved in insect mating [62, 111, 100]. And OR changes in sensitivity and ligand-binding are implicated in host switches for human-feeding mosquitoes subspecies [127].

Other genes of varying network position have also played key roles in species' behavioral divergence. Both opsins and other GPCRs seem repeatedly to be hotspots of evolutionary change between species [12]. Opsins are more terminal genes in a sensory network, but GPCRs can occupy many levels given their cellular function. Conversely, Cande et al. [25] did not find an association between the genes fruitless and doublesex and mating signal production in Drosophila species, despite being characterized as master regulators of sexual behavior [39]. Likewise, some sexually dimorphic traits have unique signatures of gene expression, network position, and genomic position [120, 72]. Together, these examples illustrate that certain genes and evolutionary changes may be poised to create divergent sexual behaviors within and between species, but consensus from empirical examples continues to defy theoretical expectations and generalization (but see [244]). Developing examples to test the genomic signatures of sexual selection

and behavioral divergence will be key in marrying these two theories.

Cypridinid ostracods are a promising group to investigate these questions because a key enzyme (c-luciferase) integral to their mating behaviors has been previously characterized. These small crustaceans inhabit the world's waters and are 500 m.y. diverged from the last common ancestor of other (more delicious) crustaceans. Within the family Cypridinidae, they have independently evolved bioluminescence to use light for self-defense [139]. When attacked by a predator, a luminous ostracod exudes a cloud of mucus outside its body that contains the enzyme c-luciferase and substrate vargulin, which react with oxygen to form light. This biochemical reaction is ATP independent [104] and is well described with first-order kinetics (assuming oxygen is freely available in sea water [192, 193]). In about 100 Caribbean species, defensive bioluminescence has been co-opted for use in complex mating displays [141]. Male cypridinid ostracods secrete discrete, species-specific patterns of bioluminescent pulses to attract females, who follow these trains of signals to intercept the male's trajectory [170, 171]. Females will even respond positively to artificial displays made of LEDs [171]. Natural courtship trains vary little within species, but widely between them in a number of ways, like in the duration of individual pulses in a single train, or the distance and timing between pulses [29, 141].

The genetic basis of light production has been previously characterized by isolating both the enzyme and the substrate [204, 220, 74, 213, 146]. We know that c-luciferases (enzyme) from different species vary in their ability to oxidize vargulin (substrate), changing the relative light output [146]. We also know that light emission varies across species in other ways: the rate of light emission can decay differently [220, 173, 152, 204], and the color can even appear different to the human eye [74]. However, no study has quantified this variation broadly or in a comparable manner, leaving our ability to infer the relative contribution of variation in enzymatic ability to variation in courtship displays without. Because of its simplicity and high diversity, this system has potential to inform us about

how behaviors, specifically courtship displays, diversify across many species.

In Chapter 2, I set a foundation for understanding the causes and consequences of variation in bioluminescence amongst cyprindid ostracods. These results support a hypothesis one aspect in ostracod mating displays - the duration of visible light from single pulses - may be evolutionarily constrained by the underlying biochemical mechanisms that produce light. I gathered light emission data from *in vivo* bioluminescent expression of living animals across 16 species, and within a phylogenetic comparative framework, found that a metric of enzyme function negatively, nonlinearly correlates with differences in pulse duration. These unexpected results show that variation in bioluminescence relates to mating display variation across species, and that enzyme function does not predict equal change across species in this phenotype. Even during diversification across a candidate gene that may be uniquely posed to create diversity, we may not be able to confidently predict which evolutionary changes may become prevalent to generate phenotypic outcomes.

In Chapter 3, I use a combination of molecular analyses and techniques, paired with simple modeling, to characterize the function and evolution of new c-luciferase orthologs across species. I discover and validate a handful of these bioluminescent proteins in three separate expression systems, and demonstrate that protein function has diversified across species in both kinetics and relative efficiency. By analysing patterns of nucleotide substitution, I propose candidate sites that demonstrate molecular signatures of purifying and diversifying selection in relation to enzyme function. Together, I use simple models to show how these differences impact the development of the phenotype during courtship. This has important implications for how behavioral signals in this system may co-evolve with receiver visual physiology, a key prediction in studies of animal communication and sexual selection.

In Chapter 4, I explore how female behavior responds to variation in male signaling

across four species of ostracods. As these signals are important during mate choice and speciation, females preferences for these signals are likely to be a key driver of prezygotic isolation and evolutionary diversification. Female preferences for mating displays can also evolve in response to complex environmental shifts, such as secondary contact with heterospecifics that share their habitat. Sampled with varying ecology in mind, and tested across different courtship display variations using artificial playback experiments, these results confirm that female ostracods actively respond to the presence of lights that simulate the signals of conspecific males. However, this change in behavior (increase in swimming speeds and directedness of motion) differs among species and is correlated with the complexity of their natal signaling conditions.

In Appendices A - C, I provide supplemental data and analyses to contextualize the main findings of each data chapter (2 - 4, respectively).

In Appendix D, I provide initial data that support the hypothesis that behavioral divergence may precede postzygotic reproductive isolation among closely related ostracod species. Between two congeners of the *Photeros* clade, I quantify gross morphology, behavioral and genetic divergence, developmental differences, and perform interspecific crosses to show they are interfertile. Although the current description of these two species is informal, these data indicate that prezygotic reproductive barriers, like the mating displays of bioluminescent cypridinid ostracods, may be contribute to speciation in this group.

1.1 Permissions and Attributions

- Chapter 2 was previously published as, "Hensley NM, Ellis EA, Gerrish GA, Torres E, Frawley JP, Oakley TH, Rivers TJ. 2019 Phenotypic evolution shaped by current enzyme function in the bioluminescent courtship signals of sea fireflies. Proc. R.

Soc. B 286: 20182621". It is reproduced here with the permission of The Royal Society Publishing; permission conveyed through the Copyright Clearance Center, Inc. http://dx.doi.org/10.1098/rspb.2018.2621

- Much of Chapter 3 has been submitted to the pre-print service bioRvix as, "Selection, drift, and constraint in cypridinid luciferases and the diversification of bioluminescent signals in sea fireflies. 2019. Hensley NM, Ellis EA, Leung NY, Coupart J, Mikhailovsky A, Taketa DA, Tessler M, Gruber DF, De Tomaso AW, Rivers TJ, Gerrish GA, Torres E, Oakley TH. bioRxiv 2020.01.23.917187". It is reproduced here in-part, and under Creative Commons Attribution License, CC-BY 4.0. https://doi.org/10.1101/2020.01.23.917187. Other majors aspects of Chapter 3 were undertaken in continued collaboration with Komatsu Mami, Jessica A. Goodheart, Emily S. Lau, John Lew & Yasuo Mitani.

- Chapter 4 is the result of a collaboration with Gretchen A. Gerrish, Raj Saha, Trevor J. Rivers & Todd H. Oakley.

- Appendix A is the Supplementary Information for Chapter 2

- Appendix B is the Supplementary Information for Chapter 3

- Appendix C is the Supplementary Information for Chapter 4

- Appendix D is the result of a collaboration with Katherine Peterson, Noelle M. Lucey, Gretchen A. Gerrish, Trevor J. Rivers, & Todd H. Oakley. Much of these data were collected by K Peterson under the auspices of the Worster Award.

Chapter 2

Evolutionary trajectory of bioluminescent mating displays constrained by current enzyme function

2.1 Introduction

Disparate courtship behaviours are often a hallmark of species radiations [117, 169, 45], such that learning how differences evolve is critical to understanding the origins of biodiversity. Like other phenotypes, courtship displays are sensitive to natural selection, stochasticity, and historical and developmental constraints, with the interaction of these factors determining overall phenotype [197, 19, 47]. When predicting how such phenotypes evolve, it can be useful to build a theoretical space relating structure to function to better understand both realized and potential diversity; such "phenospaces" give us insight into the evolutionary process. This has been particularly well-used in functional morphology to describe how the evolution of biomechanical performance (a metric analogous to behavioural output) may be enabled [230] or constrained [162] due to differences in morphological traits. For example, in the courtship behaviours of woodpeckers, this approach has shown that morphological constraints in one aspect of the phenotype can be ameliorated by sexual selection acting to elaborate overall signal design in other ways [134]. However, behaviours are a non-additive output from many biological levels, not just morphology, and we might expect that variation in any one level can contribute to phenotypic evolution. Thus, given sufficient understanding of the relationship between structure and function, we can extend this approach to any level of biological organization and begin to understand if and how variation in biological organization leads to variation in courtship phenotypes.

Unlike morphology, studies on biochemistry are either more difficult to link directly or less commonly connected with phenotypic evolution. Even though biochemistry may be studied by measuring biochemical functions, the best assessments for how it affects phenotypic evolution generally come from studies of particular proteins, like how haemoglobin changes relate to shifts in altitudinal home range [206]. But in mating phenotypes

specifically, linking biochemical variation to behaviour is less well demonstrated. Most famously, in many insects, changes in the metabolic pathways creating cuticular hydrocarbon (CHC) profiles led to differences in recognition-semiochemicals, both in kind and composition (briefly reviewed in [81]). Even outside insects, most work on biochemical variation connecting to animal communication has focused on pheromones (for some examples, see Animal Behaviour Volume 97 Special Section: Biochemistry & Animal Communication). Other studies, like in bioluminescent taxa such as fireflies, have shown that changes in colouration between species are due to changes in the biochemical binding of the substrate [158]. And in weakly electric fishes, differences between species in their communication signals have been linked to differences in the voltage-gated potassium channels that contribute to the neuronal action potentials and subsequent discharge rate in their electric organs [209]. These studies provide important initial insights on how biochemical variation can influence the production of mating signal phenotypes, albeit with a skewed focus on pheromone research. Here, using a phenospace and comparative data set, we show how variation in biochemical kinetics can lead us to evolutionary inferences about behavioural diversity broadly.

Generally, phenotypes may change via two mechanisms: first, evolution may alter the identity of components contributing to the phenotype ("what it is" - like gene or enzyme sequence and function); and second, evolution may alter the implementation of those components ("how they are used" - like expression levels, concentration, ratios, or interactions). Bioluminescent cypridinid ostracods (commonly umihotaru, or "sea fireflies") comprise a species-radiation of marine crustaceans that share an enzymatically well-studied light reaction, allowing us to ask how enzyme identity and implementation interact during the diversification of luminous courtship signals. Both sexes produce anti-predator light pulses that cause predators like fish to spit out their potential ostracod prey, and which can be experimentally induced [173], but only male cypridinids secrete

species-specific patterns of bioluminescent pulses to attract females [170, 171]. These courtship trains vary little within species but widely between them, like in the number of pulses and direction of propagation, duration of each pulse, and timing between pulses [29, 141]. Upon detecting a single display comprised of many individual pulses, females will alter their swimming trajectories to intercept a male's predicted position in the water column [171]. Other receivers like competing males have highly plastic responses and depending on how close they are to a display, will: (1) sneak onto the display of another male, (2) begin to produce their own display in loose synchrony with a competitor (called entrainment), (3) or will choose to make their own independent display [172].

In these single display trains, each pulse is comprised of mucus secreted outside the body, containing the luciferase enzyme (hereafter "c-luciferases") plus a conserved substrate (vargulin or cypridinid luciferin [138]), which react with oxygen to form light (Fig. 2.1A). The reaction is ATP-independent [104] and well-described with first-order kinetics, meaning that reaction rates depend only on substrate concentration, as oxygen is freely available in seawater [193, 192]. After secretion, light production over time has phases: upon addition of the substrate, light production should rise rapidly ("Rise Phase", Fig. 2.1A, red zone) to a maximum that correlates with the amount of active c-luciferase excreted; as the reaction stabilizes, c-luciferase oxidizes excess vargulin creating a plateau in the amount of observed light over time ("Plateau Phase", Fig. 2.1A, yellow zone); finally, the substrate becomes limiting and the reaction decays exponentially ("Decay Phase", Fig. 2.1A, blue zone). As this rate of decay in light is determined by c-luciferase becoming substrate limited, and not the total c-luciferase amount or relative c-luciferase:vargulin ratio (implementation), decay should reflect the inherent enzyme function (identity). The sequence of c-luciferase is known [146, 213] and is the only identified enzyme that oxidizes vargulin to produce light in ostracods [128, 219, 218]. Orthologous c-luciferase enzymes from two other species differ in their bioluminescent reaction, specifically in their

affinity for vargulin [146]. These features in particular provide an excellent system for understanding how biochemical variation contributes to courtship display diversification.

Within ostracods, the relative contributions of identity and implementation to phenotypic evolution are unknown. On one hand, changes in the functional kinetics of c-luciferase enzymes (identity) across species could influence light production and alter courtship pulses; theoretically, enzymes with faster reactions will consume finite levels of secreted substrate more quickly, leading to shorter pulse durations. At the same time, changing the ratio of the reactants (implementation) could explain differences in duration of courtship pulses, as suggested in [173]: here, less excess substrate relative to the enzyme amount could also produce shorter pulses (by reducing the length of time in the plateau phase). Because cypridinid bioluminescence is secreted outside the body without further input, by mapping the relationship between enzyme performance and phenotype, we can simultaneously infer aspects about enzyme implementation. In a theoretical phenospace describing the duration of natural courtship pulses (Fig. 2.1B), c-luciferase identity (measured by the decay activity of the enzyme; from Fig. 2.1A, blue zone) and implementation (estimated as a proportion of time in the plateau phase of a pulse; from Fig. 2.1A, yellow zone) can combine differentially to produce similar total pulse durations. From this model we may predict that the power to describe changes in the pulse duration phenotype varies across enzyme identity as it interacts with enzyme implementation.

We hypothesize that as species diverged, bioluminescence reactions also diverged, contributing to variation in courtship signals. We predict different species' luminous reactions have different light-production abilities, which relate to variation in the pulse duration of courtship signals. By measuring the decay of light production (an inherent aspect of bioluminescent reactions) in many species, and comparing those kinetics to the durations of courtship pulses in situ, we find that changes in enzyme function are non-

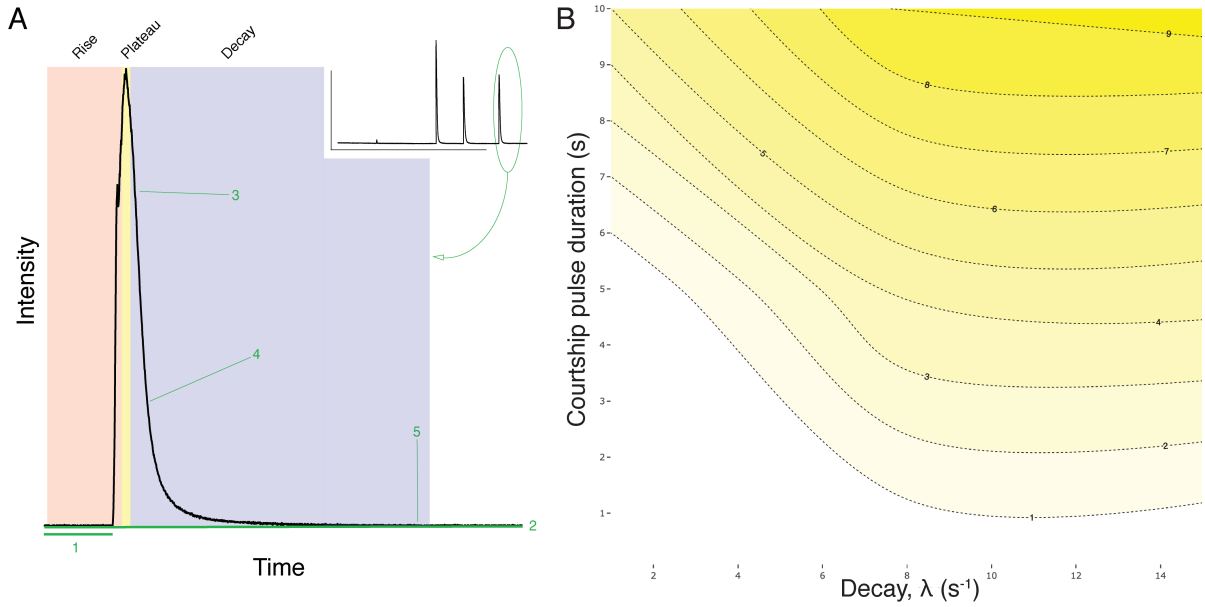

Figure 2.1: Phenotyping of bioluminescent waveforms. (A) Exemplar file depicting the parsing and model fitting of individual bioluminescent peaks. Single peaks are identified from a time series of stimulated bioluminescent events (inset, circled). Shaded zones are: (red) the rise of a pulse as enzyme and substrate are secreted, (yellow) the plateau as the enzyme is saturated with substrate, and (blue) the pulse decay as the enzyme is substrate limited. Numbers indicate (1) the background voltage removed; (2) the minimum voltage to be kept in the analysis; (3) the beginning of the exponential decay; (4) time point at which the reaction reached half its maximum length; (5) overall decay length. During parsing, waveform axes were rescaled. (B) Different combinations of the decay equation constant λ (x-axis; as blue zone from 1A) and the plateau phase duration (dashed isoclines where darker = longer phase duration; as yellow zone from 2.1A) can generate similar total pulse durations (y-axis). Generated from hypothetical data.

linearly and negatively correlated with changes in pulse duration across species. From this, we infer that both enzyme identity and implementation must contribute to disparity in courtship signals between species. As the power of enzyme identity to describe

pulse duration diminishes, enzyme implementation must take precedence. Our ability to evaluate identity and implementation simultaneously leads to the inference that the path of evolutionary diversification may depend on current phenotype: fast pulses may more often diversify by changing components (implementation), while slow pulses may evolve by changing enzyme kinetics (identity). These results provide a clear example of how both identity and implementation influenced diversification of behavioural phenotypes across species, and the power that illustrating this pattern in a phenospace has on revealing the role historical constraint may play in phenotypic evolution.

2.2 Results

2.2.1 Decays vary across species

We fit mathematical models to measures of light production over time in stimulated anti-predator pulses (Fig. 2.1A); different species have different decay constants in spite of significant variation in maximum intensity (λ constant Fig. 2.2B; Linear mixed effect model, Species $p < 0.001$, Max Intensity $p < 0.0093$; for full model details and other decay parameters see Appendix A).

2.2.2 Differences in decay explain differences in courtship pulse duration across 16 species

λ explains variation in courtship pulse durations (Fig. 2.3, Generalized nonlinear least squares $p < 0.0001$, Bonferroni corrected $p < 0.0001$, Table A.2), and its effect is not equal for all species. We discovered the relationship between courtship pulse duration and λ best fits a negative, nonlinear pattern (Fig. 2.3, Table A.1). On average, species with shorter pulse durations have higher, and therefore faster, decays. However, the strength

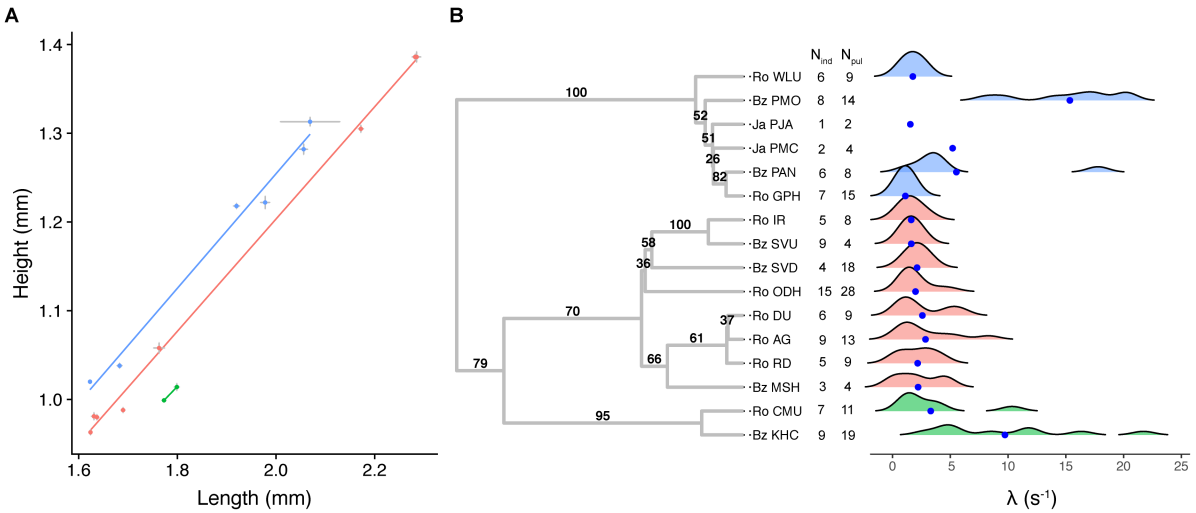

Figure 2.2: Different decay constants (λ) between species indicate differences in enzyme activity. (A) Body height (H) and length (L) measures (mean +/- SE) for 16 inferred species. Data and best fit trend lines are colored by genera, with different genera having different L:H slopes: *Maristella* = red, *Photeros* = blue, *Kornickeria* = green, or Other = grey. Data from Table A.3. (B) Density plots with means (blue dots) are the interpolated distribution of each species' decay constant. Nind and Npul indicate the number of individuals and pulses, respectively, sampled. For species with less than 3 estimates, no density plot could be generated. Decays are mapped onto a mitochondrial phylogeny and colored by genus as in (A). Bootstrap values from 1000 bootstraps are mapped to the branches preceding their respective nodes. The first two letters of each ID are country of origin (Bz = Belize, Ja = Jamaica, Pa = Panama, Jp = Japan, Pr = Puerto Rico, Ro = Roatan), followed by a species-specific identifier. Most are undescribed, but described species are as follows: PMC = *Photeros mcelroyi*, PJA = *Photeros jamescasei*, PMO = *Photeros morini*, PAN = *Photeros annecohenae*, MSH = *Maristella chicoi*, and KHC = *Kornickeria hastingsi carribowae*. Note that decays below zero are an artifact of the smoothing function in generating the density plot.

of this pattern changes as pulse durations shorten and decays increase, generating a nonlinear effect. The preferred model (smallest residual squared error) was an inverse relationship between pulse duration and λ; generally, inclusion of a phylogeny (based on AICc values) was not preferred, but in some cases was sensitive to whether certain species were included Table A.2. Excluding highly influential species in a reduced dataset (N = 14) had the same qualitative results as the full model. Analyses with or without weighting on standard error usually changed the model AICc values and sometimes model results Table A.2.

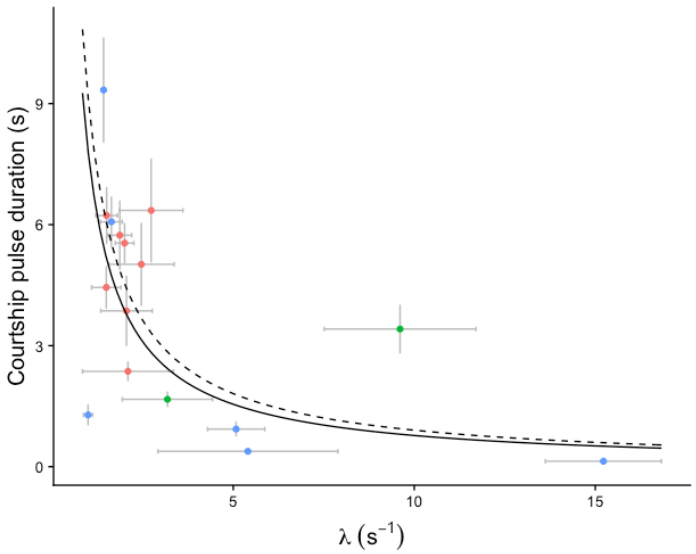

Figure 2.3: Enzyme identity (λ) describes some, but not all, differences between species in courtship duration. Scatterplot of courtship pulse duration and λ for 16 species (mean +/- SE in grey). Given the nonlinear relationship between pulse duration and enzyme function, identity has less explanatory power at high λ values. Colored by genera (*Photeros* = blue, *Kornickeria* = green, *Maristella* = red), with best fit regression estimates from an inverse model, including all data, excluding phylogeny, and without weights as a solid line and with weights as dashed line (from Table A.2).

2.3 Discussion

We provide evidence that differences in biochemical reaction rates are associated with evolutionary divergence in behavioural phenotypes. By analysing variation in bioluminescent pulses of ostracods, we infer that both changes in c-luciferase enzyme function (identity) and implementation contributed to the diversification of courtship pulse duration in their mating displays. Between species, we found consistent differences in the decay constants of stimulated luminescence (Fig. 2.2) explain some variation in the duration of natural courtship pulses (Fig. 2.3). One potential mechanism for increasing bioluminescent courtship diversity is changing enzyme function. In enzymatics, the parameters V_{max} and K_m describe an enzyme's ability to proceed through a reaction (see Supplement A for further discussion). By increasing V_{max} or decreasing K_m (Appendix A, Eqns A.1 and A.2), secreted c-luciferase will deplete the secreted substrate more quickly, such that decay rates could increase and courtship pulse duration will decrease. However, changes in the implementation of secretion components must also contribute to phenotypic differences in courtship pulse duration because residual variation in courtship pulse duration not due to enzyme function must be due to implementation (Fig. 2.3). There are multiple ways this could occur, including changes in enzyme:substrate ratios or unknown accessory components. Different species likely change the amount of substrate secreted, which alters the plateau phase of single pulses (yellow zone of Fig. reffig:label2AA), thereby increasing or decreasing the overall duration of courtship pulses. Our data remain agnostic as to which particular implementation changes take place.

Changing both identity and implementation within these enzyme reactions could potentiate a high diversity of phenotypes in courtship pulse duration. Dual mechanisms underlying the phenotype may allow for evolutionary exploration of phenotype-space along more than one avenue simultaneously. By relying on more than one mechanism,

courtship pulse duration could vary either enzyme ability or usage and produce multiple solutions towards a phenotypic state [230], as predicted by our phenospace. For any given pulse duration, there are multiple combinations of enzyme function and reactant implementation that produce the same result (Fig. 2.1B). This many-to-one mapping would result in a high level of convergence despite unique evolutionary pathways in functional underpinnings (e.g. as with haemoglobin [149]). Therefore, both a high level of convergence and high level of disparity are reasonable expectations when increasing the number of different mechanisms generating a phenotype.

Importantly, the tendency for evolutionary change in courtship pulse duration to be mediated by changes to enzyme function or implementation depends on the current phenotype, suggesting that historical contingency shapes phenotypic patterns. As overall courtship pulse duration decreases, the changes in the enzymatic reaction rate describe less of the phenotype, as indicated by the nonlinear trends that best fit our data (Fig. 2.3, Table A.1, Fig. A.6). Therefore, the residual variation due to implementation increases inversely with phenotypic state. At longer courtship pulse durations, enzyme function strongly influences the duration, so evolutionary changes in enzyme implementation (such as enzyme:substrate ratios) may not be used to evolve phenotype very much. Conversely, at short courtship pulse durations, where changes in function more weakly influence courtship pulse duration, evolution may change implementation of the reactants to drive phenotypic differences between species. Thus, the ability for evolution to alter the phenotype may depend on the phenotype's current reliance on either mechanism. Such dependence implies that courtship pulse duration is sensitive to historical contingency, as discussed in the literature [245] and implied with unique behavioural phenotypes [15, 164] but rarely demonstrated (but see [235]). Our data provide a possible example as to how contingency arises at a mechanistic level, with reliance on either identity or implementation predicting the evolutionary trajectory of the phenotype.

Even though examples of both are known, the relative contributions of identity and implementation to evolution are still debated, not only for behaviour, but also for other phenotypes [203, 79]. One reason for continued debate is that few studies have taken a pluralistic approach (but see [41]), leading to a limited ability to conclude how identity and implementation might jointly affect evolutionary change [223, 25]. To understand best how different types of change impact evolutionary divergence, both must be evaluated to gauge their presence and efficacy for producing diversity. By conceptualizing our phenotype in a way that captures the relationship between these two mechanisms (Fig. 2.1B), we have been able to make new inferences on the evolution and disparity of ostracod courtship signals.

The relationship inferred between identity and implementation has multiple, potential explanations. First, limitations in c-luciferase function to describe changes in courtship pulse duration may be due to intrinsic enzyme properties, like maximum performance rate [1]. Alternatively, identity may be constrained by the inability to optimize all enzyme properties simultaneously (e.g. trade-offs in function and stability [215] at the protein level). Changing implementation could compensate for either of these, reminiscent of hypotheses on minimizing pleiotropic effects from coding changes [203]. Teasing apart a causal relationship between c-luciferase sequence and courtship pulse duration, as well as testing the connection between identity and implementation, will be possible in future molecular work because c-luciferase functions can be quantified *in vitro* [146, 104].

Conclusions In discovering unappreciated variation in the duration of light pulses of ostracod bioluminescence, we have generated testable hypotheses about: (1) the relationship between genotype and phenotype, and (2) mechanisms of its diversification. Our data support the hypothesis that variation in courtship pulse duration between species is associated with changes in both c-luciferase function and the behavioural regulation of the bioluminescent reactants, providing a new example of how variation in biochemistry

can influence the evolution of behavioural phenotypes. Each of these mechanisms have a limited, potentially interacting, role in shaping this behavioural phenotype in evolutionary time. The influence of either mechanism in shaping phenotypic diversity may depend on the phenotype's current reliance on function or implementation, which may explain why processes like historical contingency arise in phenotypic evolution.

2.4 Materials & Methods

2.4.1 Animal Collection and Identification

We identified and collected different species from Jamaica, Honduras (Roatán), Belize, Puerto Rico, and Panamá based on unique display traits in their bioluminescent signals (direction of display initiation, courtship pulse timing, and microhabitat [141, 59]). We swept through a single species' display with hand-nets of 125μm mesh [139]. Animals were sorted by their relative length:height ratio (characteristic of species and genera [59, 140]; Table S3) measured on a Nikon SMZ-745 or SMZ-460 microscope (Mellville, NY, USA) with an eyepiece micrometre. During phenotyping, animals were housed in plastic Ziploc containers (Racine, WI, USA) with new seawater kept at ambient temperatures. Most species are unknown or only anecdotally recorded (JG Morin & GA Gerrish, unpublished field notes). We report species by their field identifier, with ongoing work to describe them. As a note, bioluminescence is found in cypridind ostracods worldwide, but previous [29] and on-going [44] analyses suggest that mate signalling is found only within Caribbean species. So although bioluminescence is best known from species in Japan, these lack any mating signal for comparison.

2.4.2 Induced Bioluminescence Phenotyping and Data Processing

We adapted PMT recording methods from [173]. We induced bioluminescence via mild electric shock with an Arduino Uno (Fig. A.1.B #4) and captured light output over time (intensity measured in volts, denoted I) with an RCA 931-A Photomultiplier tube (PMT; Harrison, NJ, USA; Fig. A.1.B #2) in a custom brass housing. Animals were placed in a scintillation vial within the housing (Fig. A.1.B #3) with enough fresh seawater (approx. 2 mL) to submerge the tips of two silver wires, creating a cathode and anode. The PMT was connected to an analog data acquisition device (Dataq Instruments, Akron, OH, USA; model DI-158U for Jamaica; model DI-155 for other countries; Fig. A.1.B #5). To visualize and record both stimulus and light output, we split the Arduino output into an electronic breadboard (Fig. A.1.B #6), with one half on the scintillation vial nodes and the other half into the data collector. We covered the entire PMT housing with an opaque box (24-gallon Rubbermaid Action Packer; Atlanta, GA, USA) to block ambient light. We automatically analysed data using a custom script in RStudio (vers. 1.0.136) with R (vers. 3.3.1). We cut files (Fig. 2.1 inset) to focus on the decay at the end of each defensive pulse (Fig. 2.1C blue zone). For details and code, see Appendix A.

Using the program "nlsLM" in the 'minpack.lm' package, we fit different exponential models to the decay of each defensive pulse in order to describe differences in bioluminescent production ability as enzyme identity. First, we used a model previously used to identify cypridinid decay constants [173]:

$$I = I_0 e^{-\lambda * t} \tag{2.1}$$

In Eqn 2.1, I is the voltage observed at time t, I_0 is the initial voltage at $t = 0$ (to be

estimated), and the decay constant to be estimated is λ. Other models of biochemical reactions were fit to these data as well. Please see Appendix A for further details. For all decay parameters estimated from any model, we averaged multiple values for each individual if possible; species are averages of as many individuals as possible (details in Tables A.4 - A.6 in Appendix A). We also applied these models to previously published decays from two other Japanese species for comparison (see Appendix A).

2.4.3 Natural Courtship Phenotyping

We used WebPlotDigitizer [175] to extract average courtship pulse duration data from the first 3 pulses of measured displays from [141] and [59] for which we had corresponding species (N = 8). We used the first three courtship pulses because these may represent the 'initiation' phase of the signal [170], and are expected to be the most variable in duration within and between species. The original data plotted are species' averages per pulse with no intrapulse variation reported, and therefore, none to extract. For specifics, see Appendix A.

For an additional 10 species, we used video recordings of individual displays from the field to quantify pulse duration. Using a Sony A7S with attached Atomos Shogun in a custom underwater housing, individuals were recorded by following their single courtship displays while on SCUBA. A reference of known length was used to standardize focus, focal length, and provide a scale while filming. We extracted pulse duration data from as many individuals as possible manually. These data were extracted along with other metrics of each courtship display as part of a forthcoming publication (GA Gerrish et al. in preparation). For data, metadata, and further methods see Appendix A.

2.4.4 Transcriptome Processing and Mitochondrial Phylogeny

Species traits may appear similar simply due shared ancestry, therefore it is necessary to use a phylogenetic approach when comparing traits across species to make inferences about their evolution [137]. We generated a mitochondrial phylogeny from transcriptomes of each species stored in RNALater prepared using Illumina v2 or v3 kits in accordance with standard procedures (Fig. 2.2). We sequenced on platforms including NextSeq (UC Santa Barbara), HiSeq (UC Davis), and MiSeq (Novogene). We trimmed adapter sequences and low-quality forward and reverse reads (scores < 20) using TrimGalore v0.4.1 [8]. Using a blast database of the *Vargula hilgendorfii* mitochondrial genome (GenBank #AB114300), we queried trimmed reads against this reference using BLAST 2.5.0+ [23] and removed any read not with 'Family Cypridinidae' in the top 5 hits. We then used Trinity v2.2.0 [66] to assemble decontaminated reads into contigs and calculated the species tree in IQ-TREE v1.6.1 [153]. ModelFinder [94], implemented in IQ-TREE to determine the best-fit model (GTR+F+I+G4) with 20 maximum likelihood best tree searches and 1000 bootstraps. For further details, see Appendix A.

2.4.5 Statistical Analyses

We hypothesize that differences in courtship pulse duration are due to differences in c-luciferase activity, a function of enzyme identity. First, in order to look at c-luciferase activity differences, we compared estimates of the decay parameters (λ) across species using a linear mixed effect model ("lme" in the 'nlme' package of R) with species and max intensity per induced pulse as fixed effects, and country of origin and individual as random effects. We included max intensity (Fig. 2.1A; height in yellow zone), an imperfect proxy for the amount of reactants secreted, as a covariate because it may also influence decay estimates (see Appendix A for a discussion on this). Decay parameters

were log-transformed to meet assumptions of linearity and residual normality.

Secondly, we hypothesized that enzyme identity (as decay from stimulated defensive pulses) described variation in natural courtship pulse duration. Before phylogenetic correction, we explored the relationship between decay parameters and natural courtship duration using different linear and non-linear models (Table A.1), and subsequently with and without the presence of certain species (see Appendix A). After plotting the data and seeing that the best fit model was nonlinear, we used our phylogeny in phylogenetic generalized nonlinear least squares (PGNLS) regressions. Using the "gnls" functions in the 'nlme' package, we regressed the decay constant against courtship pulse duration. We fit the correlation option with a Brownian motion (BM) transformation of the phylogeny ("corBrownian" in 'ape'). To account for variation in both our decay estimates and natural courtship pulse duration, we used the weights option with the standard error of each measure ([137, 179], for code see Appendix A). To compare nonlinear model fits, we used the maximum likelihood estimate of the residual standard deviation of the error; support for phylogenetic or non-phylogenetic models was compared using AICc. We report all comparisons in Table A.2.

2.5 Relevant Supporting Information

2.5.1 Ethics statement

All organisms were collected in accordance with the regulations of the Jamaican National Environment and Planning Agency (Permit Ref. #18/27), the Belize Fisheries Department (Permit #000003-16), the Honduran Department of Fish and Wildlife (Permit #DE-MO-082-2016), the Puerto Rican Department of Natural and Environmental Resources (DRNA; Permit #2016-IC-113), and Panamanian Ministry of the Environment

(MiAMBIENTE; Permit #SE/A-33-17).

2.5.2 Author Contributions

TJR, NMH, and THO conceived of the study. NMH, JPF, and TJR collected induced bioluminescence data. GAG and TJR recorded natural courtship pulse videos, and GAG measured pulse duration data. EAE generated the phylogenies with some sequences provided by ET. NMH extracted data from the literature, performed data analysis, and statistics. NMH and THO wrote the manuscript with comments from all other authors. All authors collected specimens.

2.5.3 Acknowledgements

We thank James G. Morin, Mitchel McCloskey, Yexin Jessica Li, Sarah M. Schulz, Nicholas J. Reda, and Vanessa L. Gonzalez for assistance with animal collection; Morris Aguilar for transcriptome preparation; and Eric W. Slessarev, Andrew J. Swafford, and Vanessa L. Gonzalez for computational analyses. We also thank field station staff members for their assistance with logistics: Cheryl and Danny Thacker (Smithsonian Institute Carrie Bow Caye Field Station), Captain Snow (University of West Indies Discovery Bay Marine Lab), and Plinio Gondola and Arcadio Castilla (Smithsonian Tropical Research Institute at Bocas del Toro). We are grateful for the UCSB Statistical Consulting Laboratory and two reviewers for improving the clarity of the manuscript.

2.5.4 Funding

This work was supported by the National Science Foundation (to authors THO (DEB-1457754), GAG (DEB-1457439), ET (DEB-1457462), and senior advisor James G. Morin). Supplementary research funds were provided by the Sigma Xi Grants in Aid

of Research (G20141015722209) and the Society for the Study of Evolution Rosemary Grant Research Award to NMH. NMH was supported by the UC Regents Special Fellowship and the National Science Foundation Graduate Research Fellowships Program. EAE was supported by the UC President's Dissertation Fellowship.

Chapter 3

Molecular evolution of cypridinid-luciferase and diversification of bioluminescent signals in sea fireflies

3.1 Introduction

Evolutionary biology is challenged with describing how diverse processes can generate vast differences in phenotypes. Darwin himself best described this as, "...from so simple a beginning endless forms most beautiful and most wonderful have been, and are being, evolved" [38]. The advent of the Modern Synthesis solved issues of heritability unbeknownst to Darwin, but a major obstacle to this endeavor still remains in the form of development. Namely, that mapping heritable, genotypic changes to phenotypic diversity is nontrivial for any given phenotype. Phenotypic diversity is closely associated with adaptation and speciation, placing questions of development squarely within the realms of larger evolutionary themes [180, 79]. Despite recent advances in targeting the loci of an adaptive phenotype or a genomic region associated with speciation, tracking the causal mechanisms through development can rarely be done across the breadth of such diversity but offers much in knowledge [54]. The best characterized system is that of butterfly color patterns, where the genomic regions and adaptive value of differences in wing coloration patterns are well researched [91, 11, 93]. From these studies, we have gained novel insight into how pleiotropy [10, 231], genomic modularity [177], and hotspots of evolutionary divergence [91, 9] all may contribute to phenotypic variation. However, for complex phenotypes like animal behavior, difficulty in mapping genotype to phenotype only compounds, as such diversity is generated at different levels of biological organization and timing ([42]; but see [195, 80] for conceptual advancements). Expanding our tools and systems will allow us to look broadly for generalities in how evolution tinkers to create the panoply of biological variety.

For coding regions of the genome, genotypic differences that cause amino acid replacements may have large effect functional consequences on phenotypic outcomes [70, 48]. Although the ubiquity of coding versus regulatory changes on phenotypic evolu-

tion are believed to be heavily biased towards cis-regulatory changes because they may avoid catastrophic pleitropic consequences [203, 237], coding changes are still powerful engines of phenotypic change [79]. Traditionally, candidate regions for study have been identified because changes in coding regions can have large effects, making them prone to discovery. However, bottom-up approaches like quantitative trait mapping have also verified that protein-coding regions can be important to evolutionary change (for examples see Gephebase, [35]). Studies of protein function best demonstrate this, and research programs espousing such a "functional synthesis" [40] have made headway into understanding how mutation [161], epistasis [148], and historical constraint [199] can influence the phenotypic outcomes, especially those controlled by enzymes proteins. Many of these key phenotypes are morphological (e.g. pelage color across many vertebrates via MC1R, [176]) or physiological (e.g. hemoglobin binding to oxygen [147]; ion-channel responsiveness [209]), and are one or several steps removed from variation in behavioral phenotypes (but see opsin color sensitivity in cichlids, [184]; and odorant sensitivity in orchid bees, [21]. Our work presented here, and further work to connect across levels of biological organization in diverse systems, can help alleviate this biological and taxonomic limitation.

Mathematical models have been useful for understanding how genetic and molecular variation map to phenotypic possibilities [22]. Modeling is a powerful approach: models built from strong theory and compared to empirical data may reveal biologically unique cases where conceptual frameworks explain (or fail to explain) specific observations. Such phenospaces, parameterized off real data, have revealed the role stochastic forces can play in the development of phenotypes [95], and how nonlinear dynamics may be quite prevalent [101]. Most famously, Alan Turing developed the reaction-diffusion model to understand how vertebrate coloration patterns might arise from simple molecular diffusion gradients and local interactions [222]. Since his work, others have developed

many descendent models with appropriate modifications to explain striping patterns [119], and even shifts in digits during the evolutionary shift in limb usage [159, 191, 33]. Noticeably, most of these models attempt to explain morphological characteristics by mapping gene expression data onto morphogenic fields. However, given sufficient understanding of the molecular processes underlying other phenotypes like behaviors, such modeling should be equally fruitful to understand the genotype-phenotype map.

Bioluminescent ostracods in the Family Cypridinidae are a unique and charismatic candidate clade to ask questions about the evolution of behavioral phenotypes. On moonless nights in the Caribbean Sea, male ostracods swim into the water by the hundreds and produce species-specific bioluminescent patterns to attract mates [29]. There are approximately 100 species of these small crustaceans (mostly undescribed; [140]), and they share a common enzymatic basis for the production of this behavior [192]. By secreting a catalytic monooxygenase ("c-luciferase") with a high-energy substrate ("vargulin") into discrete packets of mucus, male ostracods create trails of light that act like airplane runways [170], allowing females to locate and track their position during mating swarms [171]. Although these complex mating displays are multivariate, differing in a variety of attributes like the timing and number of discrete pulses per train [59], once secreted outside the body, changes in c-luciferase function and reactant concentration should drive how much light is produced in a single pulse (hereafter pulse duration; [192]). Thus, by characterizing variation in these two components (enzyme function and reactant concentrations), we can begin to derive a mechanistic and functional explanation for diversification in the complex mating displays of sea fireflies.

C-luciferases may be expressed *in vitro* to test biochemical functions [214]. Despite the potential value of bioluminescence for genotype-phenotype relationships, including some work in other organismal groups [49, 229], previous studies characterizing luciferase genes of cypridinid bioluminescence exist for only two species [146, 213], which show cypridinid

luciferases evolved independently of other luciferases, have a signal peptide leading to secretion outside cells, and possess two Von Willebrand Factor-D (VWD) domains [155]. In c-luciferases, a plethora of disulfide bonds between conserved cysteines [146, 84, 88] as well as post-translational N-linked glycosylation are both thought to be important for proper folding and function [240, 136]. Previous mutagenesis experiments in ortholog have identified amino acid sites that affect enzyme function and shift the color of emitted light [98].

Here, we characterize new c-luciferase genes for phylogenetic analyses in combination with molecular signatures of diversification and functional assays of bioluminescence. By incorporating estimates from purified enzymes and mathematical modeling, we better map the genotype-phenotype landscape for a single aspect of these complex behavioral displays - pulse duration. In single secretions, the biochemical reaction between c-luciferase and vargulin follows Michaelis-Menten enzyme kinetics, where the reaction rate can be determined by c-luciferase and vargulin concentrations. Classic Michaelis-Menten models can be used to understand product formation given the following parameters: substrate concentration ([S]), enzyme concentration ([E]), catalytic rate of product formation (k_{cat}), and the Michaelis-Menten constant, a measure of substrate affinity (K_m). In the bioluminescent displays of ostracods, product formation is equivalent to the amount of light produced over time. Using these data as parameters for a phenotypic model incorporating c-luciferase function and enzyme:substrate ratios, we find that species occupy different areas of the pulse duration landscape. Changes in any one of these parameters may reliably predict evolutionary divergence in phenotype across species.

3.2 Results

3.2.1 Discovery of new, putatively functional c-luciferase genes & expression

From previously generated transcriptomes, we discovered 20 new putative luciferases from whole-body transcriptomes of cypridinid ostracods (Fig. 3.1). These putative luciferases bear multiple hallmarks of c-luciferase, including two Von Willebrand Factor-D (VWD) domains, a signal peptide, and conserved cysteine sites [155, 213, 146].

3.2.2 Validation of exemplar c-luciferase proteins in three expression systems

Using *in vitro* expression in mammalian, yeast (Fig. 3.2A and 3.2B, respectively), and silkworms (Fig. 3.3), we tested the ability of putative c-luciferases to catalyze light reactions. We selected five exemplar species representing different genera of bioluminescent Cypridinidae. For each luciferase construct, light levels increased significantly after the addition of the substrate luciferin or compared to negative controls (Fig. 3.2; Table B.1). Adding luciferin to biological media often produces light [228] that varies across biological replicates. We note this variation, yet also report statistically significant differences in light production after adding substrate (for yeast), or between c-luciferase secreting-cells and cells or media alone (for HEK293 cells and yeast; Fig. 3.2). This is consistent with the putative c-luciferases across multiple genera of Cypridinidae being functional c-luciferases.

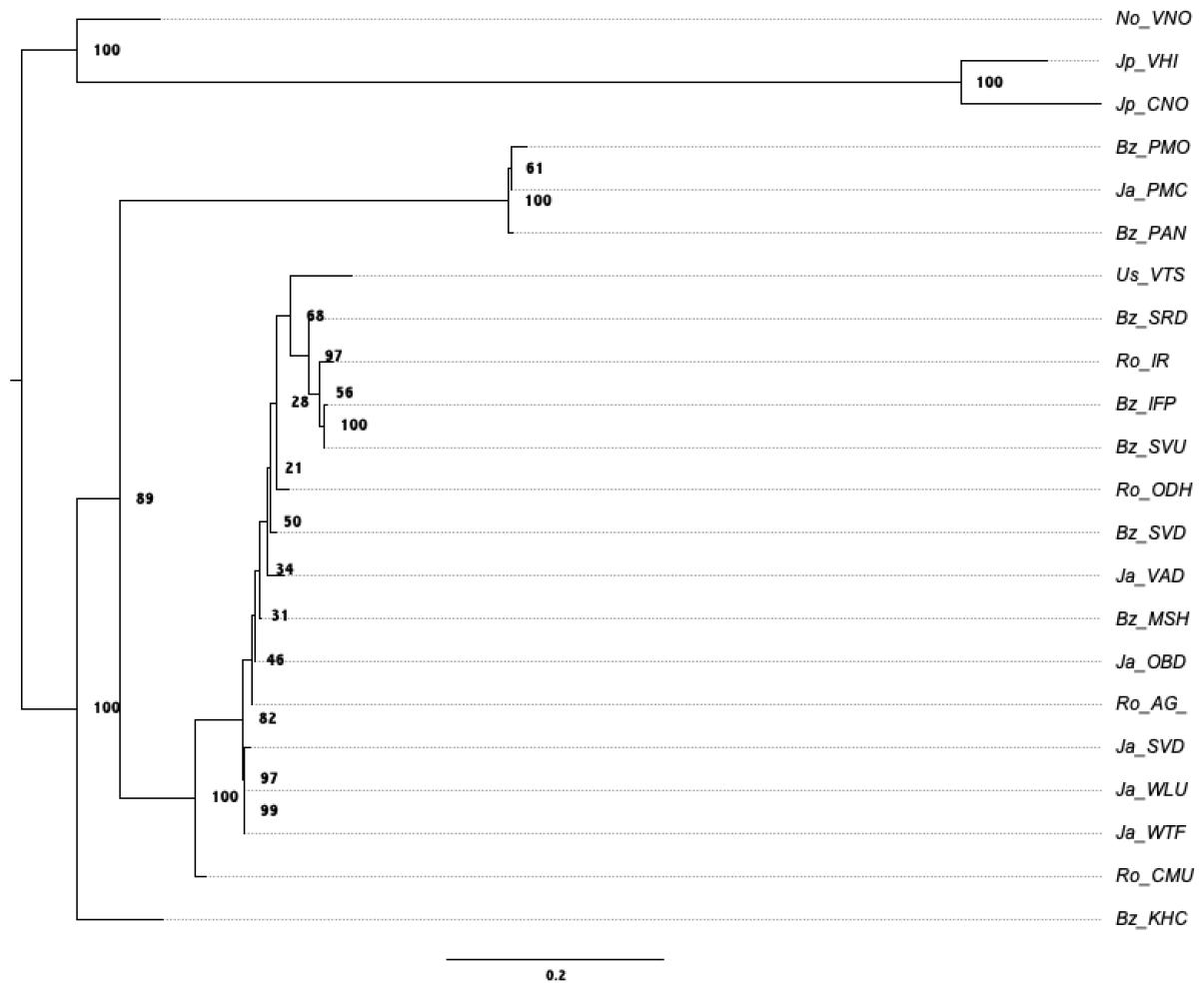

Figure 3.1: Protein phylogeny of 20 new putative c-luciferases from cypridinid ostracods. Branch lengths indicate amino-acid changes. Previously published sequences "Jp_VHI" and "Jp_CNO" from *Vargula hilgendorfii* and *Cypridina noctiluca*, respectively. Tree is rooted at the origin of mate signaling.

3.2.3 C-luciferase homologs differ in their relative light emission efficiency and Michaelis-Menten enzyme kinetics

Homologs differ from one another in both k_{cat} and K_m (Table 3.1). Using separate assays, we also report that the relative emission efficiency (the number of photons produced per unit substrate per unit enzyme, herein as RLU/uM) differs between orthologs (Table 3.2).

Species	Dataset Date	Corr.	Variable	Value	SE	T	P	RSE	DF
TL1 - Bz SVU	02Mar2020	No	k_{cat}	1.494E+07	1.645E+05	90.85	0.0000	6.64	2498
TL1 - Bz SVU	02Mar2020	No	K_m	13.61	0.30	46.05	0.0000	-	-
TL1 - Bz SVU	02Mar2020	Yes	k_{cat}	1.494E+07	1.645E+05	90.85	0.0000	6.64	2498
TL1 - Bz SVU	02Mar2020	Yes	K_m	13.61	0.30	46.05	0.0000	-	-
TL2 - Bz PMO	11Mar2020	No	k_{cat}t	5.111E+05	8.348E+03	61.22	0.0000	1.67	3505
TL2 - Bz PMO	11Mar2020	No	K_m	19.20	0.59	32.59	0.0000	-	-
TL2 - Bz PMO	11Mar2020	Yes	k_{cat}	1.179E+06	1.075E+05	10.97	0.0000	2.56	189
TL2 - Bz PMO	11Mar2020	Yes	K_m	65.16	9.33	6.98	0.0000	-	-
TL3 - Bz PAN	11Mar2020	No	k_{cat}	5.481E+05	9.870E+03	55.53	0.0000	1.90	3505
TL3 - Bz PAN	11Mar2020	No	K_m	17.77	0.61	29.03	0.0000	-	-
TL3 - Bz PAN	11Mar2020	Yes	k_{cat}	1.597E+06	1.531E+05	10.43	0.0000	2.59	538
TL3 - Bz PAN	11Mar2020	Yes	K_m	95.52	12.85	7.43	0.0000	-	-
TL4 - Bz MSH	11Mar2020	No	k_{cat}	3.231E+07	3.977E+05	81.24	0.0000	1.74	3498
TL4 - Bz MSH	11Mar2020	No	K_m	44.70	0.83	53.96	0.0000	-	-
TL4 - Bz MSH	11Mar2020	Yes	k_{cat}	2.918E+07	3.878E+05	75.25	0.0000	2.16	2716
TL4 - Bz MSH	11Mar2020	Yes	K_m	37.11	0.76	48.74	0.0000	-	-
TL5 - Bz KHC	28Feb2020	No	k_{cat}	1.860E+07	1.456E+05	127.76	0.0000	1.05	2498
TL5 - Bz KHC	28Feb2020	No	K_m	17.97	0.23	78.44	0.0000	-	-
TL5 - Bz KHC	28Feb2020	Yes	k_{cat}	1.845E+07	1.430E+05	129.06	0.0000	1.06	2474
TL5 - Bz KHC	28Feb2020	Yes	K_m	17.68	0.22	79.24	0.0000	-	-

Table 3.1: Michaelis-menten kinetics for different orthologs derived from initial velocity data. Units for kinetic parameters are in: kcat (1/s), Km (μM). Corr. indicates whether the dataset in the regression excludes counts that overlap with the distribution of counts from the control (substrate only plus buffer) reactions; whether the datasets differ can be seen in the degrees of freedom (DF). All p-values < 0.05. RSE is the residual squared error of the weighted model, all of which are weighted by the variance in each substrate concentration measure.

Sample	Species	Dataset Date	Time (s)	Substrate conc. (μM)	Total Emission (RLU)	Rel. Em. Eff. (RLU/μM substrate)	Specific Activity (RLU/μM protein)	RLU/μM sub./μM pro.
TL1	Bz SVU	11Mar2020	900	50	6.86E+05	1.37E+04	4.73E+09	9.46E+07
TL2	Bz PMO	11Mar2020	900	50	2.50E+05	4.99E+03	1.62E+09	3.24E+07
TL3	Bz PAN	11Mar2020	900	50	1.77E+05	3.54E+03	1.15E+09	2.30E+07
TL4	Bz MSH	11Mar2020	900	50	5.19E+06	1.04E+05	3.58E+10	7.16E+08
TL5	Bz KHC	11Mar2020	900	50	6.18E+06	1.24E+05	3.72E+10	7.45E+08

Table 3.2: Relative Emission Efficiency and specific activity differ between c-luciferase homologs.

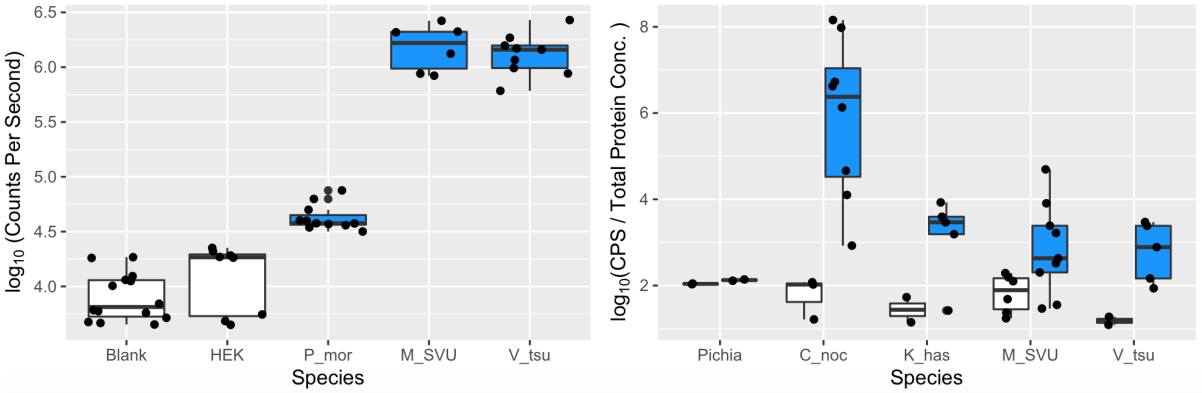

Figure 3.2: Exemplar luciferases are functional. (A) Light produced after addition of luciferin to putative c-luciferase constructs from different species, measured in log Counts Per Second. Controls include blank cell culture media and HEK cells with no construct. Constructs are: (1) *Photeros morini* (P_mor), *Maristella* sp. SVU (M_SVU), and *Vargula tsujii* (V_tsu) (B) Log counts per second normalized by total protein concentration for four c-luciferase constructs expressed in yeast *Pichia*. Measures are before the addition of the substrate luciferin (grey) and after (blue). Control is *Pichia* cells alone. Constructs are: (1) the host strain of *Pichia* without a luciferase as a negative control, (2) a sequence known from *Cypridina noctiluca* (C_noc) as a positive control, (3) a novel sequence from *Kornickeria hastingsi carriebowae* (K_has), (4) a novel sequence from an undescribed species from Belize, "SVU" (nominal genus *Maristella*), and (5) a novel sequence from the California sea firefly *Vargula tsujii*. Each datum is an average of three technical replicates.

3.2.4 Expression of c-luciferase orthologs at the site of bioluminescence

From four species, we detected 543 transcripts that are related to previously characterized orthologs at an E-value of 0.0001 or less. Of these, 230 were detected in our RNA Taq-seq data from at least one biological replicate. Transcripts with an E-value of 0.0 (exact matches to the query) had higher expression levels than imperfect yet highly matching (low-scoring) transcripts (Fig. 3.4; Wilcoxon Rank Sum Test, $p < 0.05$). On average, those most highly expressed in the upper lip of different species have the lowest E-scores. This pattern suggests that the genes we identified as potential homologs and closely related to c-luciferase are more highly expressed at the site of bioluminescence

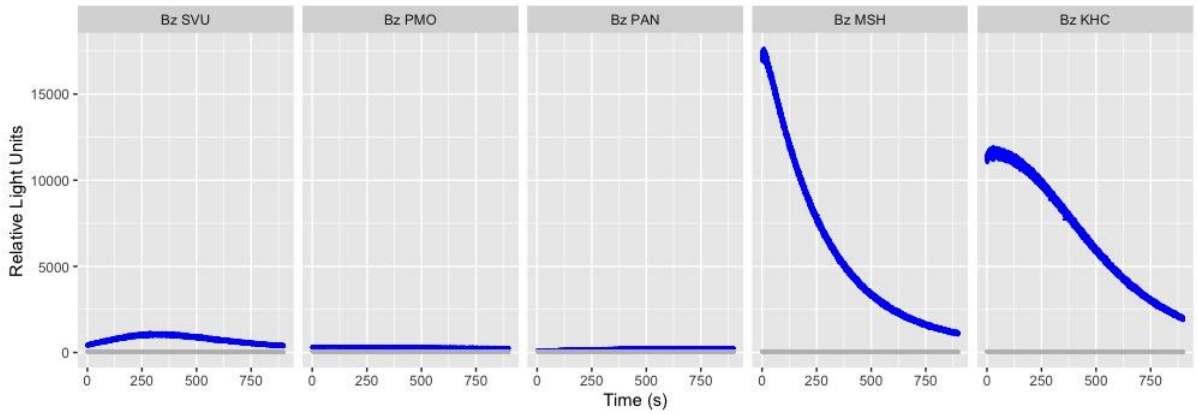

Figure 3.3: Exemplar progress curves for orthologs expressed and purified from transgenic silkworm homogenate (insect cells). Each facet is a different species (left to right: nominal *Maristella* sp. "SVU", *Photeros morini*, *Photeros annecohenae*, *Maristella chicoi*, *Kornickeria hastingsi carriebowae*). Grey line in each facet is the same control sample showing background luminescence. Assays performed with 1.5 x 10^{-4} μM luciferase and 50μM substrate.

than other, more distantly related genes. For total gene expression counts see Table B.2.

3.2.5 Molecular evolution of c-luciferase function: evidence for candidate sites

Using mixed effects maximum likelihood in HyPhy [144] on a subset of our discovered c-luciferase genes (N = 13), we found ratios of synonymous to non-synonymous substitution rates in c-luciferases to indicate six sites consistent with significant episodic diversifying selection (Table 3.3), distributed throughout the gene. "Episodic" diversifying selection refers to sites with elevated dN:dS along a proportion of branches of the gene tree. According to Fixed Effects Likelihood (FEL) analysis [106], 178 c-luciferase sites have significantly low rates of dN:dS (p-value < 0.051), consistent with purifying (negative) selection, and two sites with significantly high dN:dS, consistent with pervasive positive selection, or sites with elevated dN:dS for the entire gene tree. Of note,

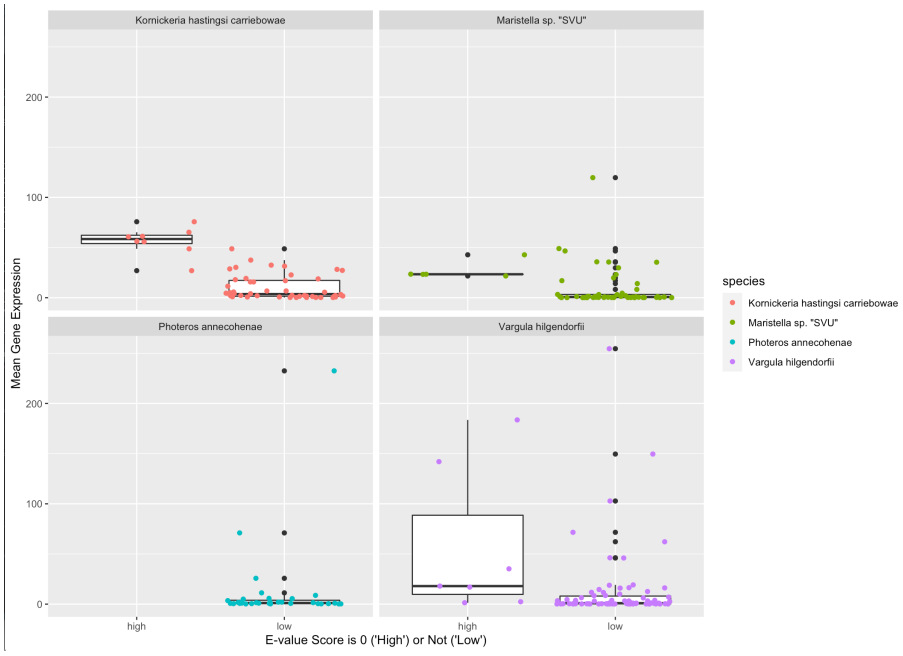

Figure 3.4: Relative gene expression from RNA Tag-seq data show that c-luciferase homologs are more highly expressed in the upper lip than other transcripts. Genes that perfectly matched the *Cypridina noctiluca* BLAST query were re-labeled as "high" scoring, and all other scores were discretized to "low". See Tables B.2 for gene expression summary.

our alignment with newly discovered c-luciferases shows that only 32 of the 34 cysteine residues are conserved, and 23 demonstrate significant patterns of purifying selection.

Our analysis using BUSTED[S] yields very strong statistical support ($p < 0.0001$) for episodic positive selection, without specifying which sites or branches are under selection. However, BUSTED[S]-MH fails to find significant support for episodic diversifying selection ($p = 0.1835$), which uses a model aimed to account for non-independent, adjacent nucleotide substitutions. We hypothesize dN:dS tests may be overly conservative when using models that incorporate multi-hit substitutions because comparative data may often fail to distinguish simultaneous substitutions versus multiple, single substitutions. Our aBSREL analysis indicated two branches of the c-luciferase phylogeny are under positive selection, both which are terminal branches (*M. chicoi* and *P. mcelroyi*).

aBSREL failed to support our *a priori* hypothesis of increased selection on the branch leading to *Photeros*, the only genus with very rapid courtship pulses. Multihit indicates that models incorporating either two, three, or three hit islands substitutions are preferred to single mutation models or other, less complex models (Likelihood Ratio Tests, $p < 0.001$). However, the impact of this varies by site (Fig. B.1 and Table 3.3). Across all sites, 25/610 (4.09%) strongly prefer a multinucleotide substitution event (Evidence ratio greater than 5).

From FEL and MEME, we found two sites and seven sites with dN:dS ratios consistent with pervasive or episodic diversifying selection (dN > dS; p-value < 0.051), respectively (see Github repository for full data). Our ANOVA results indicate that one of these sites in particular, site 160, is correlated significantly with light decay of c-luciferases (Table 3.3), and may be under diversifying (positive) selection (MEME, $p < 0.051$). Two other sites (19, 232) were initially identified by our modeling approach as significantly related to light decay but these relationships dissolved with iterative removal of other sites.

Site (*Cypridina*)	**Site (Aligned)**	**ANOVA P-value**	**HyPhy MEME P-value**	**HyPhy FEL P-value**	**Multihit - 2 hits**	**Multihit - 3 hits**
19	41	0.1384	0.03	0.79	35.1240	6.2700
160	189	0.0032*	0.05	0.35	0.1690	1.0440
232	261	0.1123*	0.00	0.27	65.5060	0.5830

Table 3.3: Candidate sites associated from ANOVA analyses with phenotypes and their inferred processes of molecular evolution (diversifying selection) based on estimated rates of synonymous to non-synonymous substitution ratios from HyPhy MEME and FEL tests. Columns from Multihit list the evidence ratio preferring a model of di- or trinucleotide substitution, respectively, over a model of a single substitution at that site. *Results from a PGLS model where PGLS and OLS fits were equivalent. All other ANOVA p-values are reported from models preferring an OLS fit based on comparison of AIC scores.

3.2.6 Modeling pulse duration phenotypes

Using Eqn. 3.3 and 3.4, we generate an expected phenospace for pulse duration given the range of parameter values we measure (Tables 3.1 and 3.2) and from the literature [146] for k_{cat}, K_m, and the relative emission efficiency. As seen in Fig. 3.5A, there are multiple combinations of catalytic rates and enzyme affinities that will produce similar pulse durations. Notably, the mediating power of enzyme affinity to affect predicted pulse duration is ablated at high catalytic rates.

We find similar results with the amount of light output at the 10th timestep in a series (Fig. 3.5B). However, as expected from Michaelis-Menten dynamics, we see that enzyme affinity best mediates the light output at high catalytic rates; this pattern is inversely related to the kinetics determining the predicted total duration of single pulses.

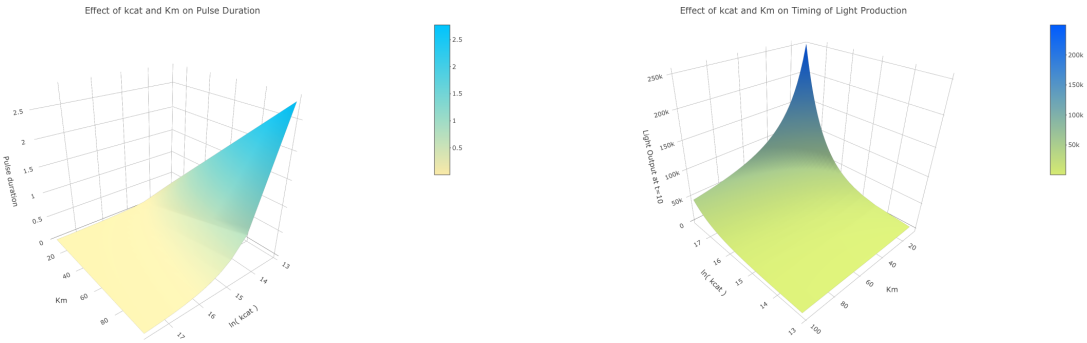

Figure 3.5: (A; left) Phenotypic predictions for pulse duration from Eqn. 3.4 across the same orders of magnitude measured in this experiment. From cream to blue is an increase in pulse duration (longer overall time of visible light) in arbitrary units (z-axis), as predicted by values of k_{cat} (natural log transformed, y-axis) and K_m (x-axis). (B; right). Phenotypic predictions for the amount of light produced at t = 10 from Eqn. 3.3. Given different parameter rates, varying amounts of light would be visible at time t = 10 (arbitrary units). From green to blue corresponds to an increase in the amount of visible light (z-axis). X and Y axis as in (A). Note: We did not plot the results of variation in Relative emission efficiency, as it is a scaling factor in our models and would affect the range of the z-axis.

3.2.7 Models based on measured enzyme functions do not predict pulse duration

In comparing our newly measured enzyme kinetic parameters with observed pulse durations (data from [76]), we find that our corrected K_m values are negatively trending with pulse duration (Table 3.1; Fig. B.2) although our pattern is not statistically significant (Pearson's correlation = -0.861, t = -2.9313, df = 3, p = 0.061). This result is counterintuitive with predictions from models based on Michaelis-Menten kinetics: as enzyme affinity increases (which is measured inversely, and therefore whose value goes down), the reaction rate increases and substrate is consumed more quickly. Rapid consumption of finite substrate should equate to shorter pulse durations. From this theory, and which we recapitulate mathematically (Fig. 3.5A), K_m values should be positively correlated with pulse duration (high K_m equates to a low affinity, resulting in a slower reaction rate, and therefore a long pulse duration). However, we find the opposite pattern. Indeed, when using all measured kinetic parameters (k_{cat}, K_m, and relative emission efficiency) to predict the time to decrease to 1 x 10^{-6} of the original substrate concentration (arbitrarily chosen) given the same starting substrate and enzyme conditions across all five species, we find that Eqn. 3.4 does not recapitulate the biological pattern (Fig. 3.6; Pearson's correlation = -0.785, t = -2.1938, df = 3, p = 0.1158).

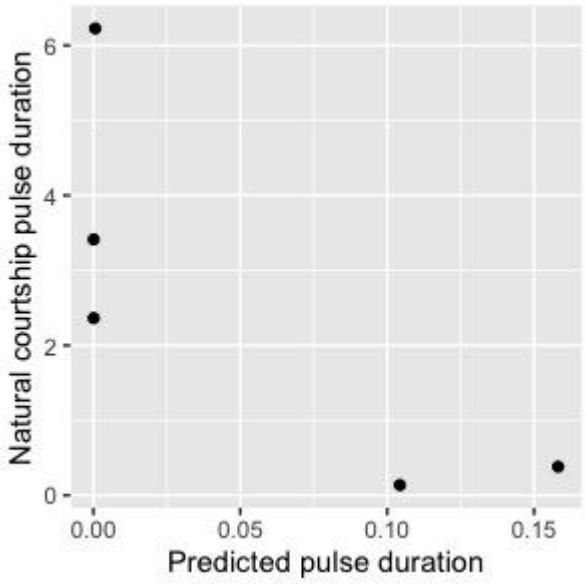

Figure 3.6: No correlation between predicted pulse duration (x-axis; arbitrary units) and the observed natural courtship pulse durations (y-axis, in seconds; as from [76]

3.3 Discussion

Our data demonstrate the c-luciferase orthologs have different enzyme functions, which should predict differences in the form of mating displays between species. Species with displays typified by longer pulse durations like *K. hastingsi carriebowae* and *M. chicoi* have high performing enzymes, and vice versa. We also found that rapidly acting enzymes also release more light per unit substrate, which implies a positive correlation between enzyme functions (relative emission efficiency & rate of light production, Fig. B.2). By incorporating these parameters into classic Michaelis-Menten models describing single pulse durations and brightness, we have developed a theoretical expectation of how protein function and expression should influence the evolution of mating display diversity in cypridinid ostracods. Unexpectedly, our measured kinetic parameters seem to trend opposite of these phenotypic predictions and which we discuss below. Different types of genomic changes are primed to drive phenotypic evolution at this locus, itself a potential

hotspot for increasing biodiversity.

C-luciferase may act as an hotspot for evolutionary divergence in the communication behaviors for Caribbean cypridinid ostracods. This may be because of its unique position during the development of the phenotype. As best said by Martin and Orgozozo [122], "specialized genes may drive the evolution of specialized traits." Confirming that our homologous proteins are the most highly expressed of related genes in the upper lip (the site of bioluminescent secretion in ostracods), differences in c-luciferase relative emission efficiency (Fig. 3.5B) and catalytic rate (Fig. 3.5A) between species alter the total output and timing of light production, respectively, during each pulse in a mating display. Evolutionary divergence in these enzyme functions may be driven by coding changes in the primary structure of each protein. In other non-homologous luciferases from terrestrial fireflies and marine copepods, both emission efficiency and catalytic rate differ across homologs [154, 20, 212, 211]. Within species, like in the ctenophore *Mnemiopsis leideyi*, different protein isoforms have functional differences [182]. The independently evolved c-luciferase from ostracods is composed of two VWD-domains [155], which appear to be the fusion product from an ancient, lineage-specific expansion of these domains (Oakley et al., unpublished). As such, many related proteins with similar architectures and unknown functions may be found within cypridinids. Characterization of c-luciferase and other homologs will help illuminate the functional consequences of coding changes, as well as the functional evolution of these bioluminescent proteins.

Differences in molecular function could be shaped by natural and/or sexual selection. Patterns of variation in synonymous and nonsynonymous substitutions in c-luciferase sequences are consistent with selection and correlated to phenotypic variation of biochemical properties of light production. We found multiple sites (19, 160, and 232) in c-luciferases potentially evolving under episodic diversifying selection and which may be correlated with the rate of decay of light (Table 3.1). Of particular interest is site 160

because it is one of only a handful of sites that differs between *Photeros annecohenae* and *P. morini*, which vary greatly in their natural courtship pulse duration. Regardless of strong similarity in c-luciferases between these two species, their enzymes have dramatic differences in measures of decay rate that are related to duration of courtship pulses [76]. Although these substitution patterns suggest selection acting at the molecular level, the selective forces that influence rates of light decay at the organismal level are uncertain because there are very few experiments on the fitness effects of different ostracod signals [171]. We hypothesize pulse duration, in part dictated by enzyme kinetics [76], may be important for fitness via inter-specific anti-predator displays and/or through mate recognition or choice. Consistent with this hypothesis, there is extensive variation among species, with pulse durations in courtship signals ranging from approximately 0.15 - 9 seconds [76, 30]. Because the relationship between enzyme kinetics and pulse duration varies across species [76], selection on single sites associated with changes in c-luciferase function may be more episodic.

In addition to sexual selection, c-luciferase kinetics could also be under selection at the organismal level due to changes in environmental factors like temperature, pH, or salinity. Cypridinid luciferase is secreted externally and bioluminescent ostracods are globally distributed, so environmental factors affecting enzyme function could vary widely. Indeed, previous *in vitro* expression of *C. noctiluca* luciferase showed temperature-dependent differences in activity [240, 146]. Increased sampling of taxa living in different habitats, including deep-sea cypridinids, could allow testing of varying conditions and the role that adaptation may play in constraining or facilitating changes in enzyme function.

We believe our results document important functional sites in a single gene - some verified via previous mutagenesis experiments - that impact phenotypic diversity. Although some methods to detect diversifying selection are sensitive to false positives, we remain confident that our conservative estimates of function are exciting. Firstly, we

provide evidence of which sites may or may not be impacted by multinucleotide substitutions (MNS), one source of false inference (Table 3.3, Fig. B.1). Some have most likely been impacted by at least two mutations, but others remain confidently as single mutations that influence light production. Secondly, we agree with others [144, 242] that a model of pervasive selection at any single site is not expected *a priori* in many biological scenarios, as well as in our system. Numerous forces may act to drive functional evolution of c-luciferase across species (as we theorize above), and besides purifying selection acting to maintain critical light-production function, none of these regimes are expected to act towards the same phenotypic optima necessarily. As such, selection may be more transient on sites than strict models may be able to detect, as has been found in functionally-verified opsins [144]. And although MNS may increase false positives at sites assuming single hits, this does not mean that sites with true MNS may not be under positive selection as well. Lastly, on older genes or across wider scales of phylogenetic diversity, these models may not be adequate to estimate the substitution process because of the time for increased numbers of mutations to arise and fix. Without more complex molecular models, we cannot account for these biological possibilities. Further understanding of how site-specific changes alter enzyme function will clarify their roles in the evolution of signal diversity.

Biochemical constraints like pleiotropy could influence the evolution of bioluminescent phenotypes. In sea fireflies, we find a natural pattern of replacement from arginine (N) to aspartic acid (D) residues between non-signaling and signalling cypridinids at site 404. In the luciferase of the non-signaling species *C. noctiluca*, site 404 is part of a N-glycosylation site [136], and mutagenesis from N to D residues decreases relative light production [240]. The magnitude of this decrease is also epistatic with both sites 182 and 184 (both part of the same N-glycosylation site [240]). Although site 404 does not appear to be part of a putative glycosylation site in c-luciferases of courtship-signaling species,

these results indicate epistatic effects on protein functions in some species. It is possible that site-specific epistatic interactions changed during the evolution of c-luciferases, like in other proteins [160, 243].

Interestingly, we find that transgenically expressed c-luciferases originating from the genus *Photeros* do not produce luminescence on the same order of magnitude as other homologous genes from two other genera (*Maristella*, *Kornickeria*) despite being the most highly expressed (Fig. 3.4). Our data indicate that homologs from *Photeros* are only weakly able to produce luminescence, either as low levels of light (Fig. 3.2, and as found in *Pichia* yeast system; Hensley et al. in revision), or only at high concentrations of substrate (as in HEK cells; Hensley et al. in revision). This may describe the previously found nonlinear pattern between enzyme function and pulse duration [76], such that evolutionary changes are biased towards regulatory alterations in enzyme:substrate ratios as a compensatory mechanism to combat reduced light output among *Photeros* species. Conversely, evolution of epistatic interactions along the branch leading to *Photeros*, as proposed for other bioluminescence characteristics like color (Hensley et al. in revision), may make *Photeros* homologs sensitive to the expression system. Such system-level sensitivity has been noted with the non-homologous luciferases of copepods [121, 200], as well as failure to express ostracod luciferase in *E. coli* [88]. Testing different expression systems, with particular attention to the *Photeros* clade and leveraging new techniques, will help to resolve these contrasting hypotheses and clarify the genotype-phenotype map in ostracod mating displays.

Many-to-one mapping within the phenospace increases the available evolutionary solutions to predict changes in pulse duration phenotypes (Fig. 3.5). Besides differing in their catalytic rate, surprisingly, these enzymes also differ dramatically in their ability to yield photons during the bioluminescent reaction (REE; Table 3.2). Paired together, differences in relative emission efficiency and enzyme kinetics generate a predictable phe-

notypic space where similar optima (pulse durations) can be achieved by varying the components of the bioluminescent reaction (enzyme, substrate) as well as the intrinsic enzyme functions (relative emission efficiency, rate of light production, and substrate affinity). As species map to different phenotypic points in this space, alternative evolutionary solutions to generating phenotypic change become apparent. Species with poor substrate affinities can quickly cross isoclines of pulse durations given relatively small changes in affinity (Fig. 3.7A). Conversely, these same species may be constrained to a flat surface in the timing of light output (Fig. 3.7B), and can most rapidly move across the phenospace via changes in enzyme:substrate ratios (Eqn 3.3). These conclusions predict the types of genomic changes that may be most available to evolution to generate phenotypic diversity: coding changes may alter enzyme functions to an extent, whereas regulatory mutations are expected to alter the mixture of bioluminescent components within each pulse, as suggested in [173]. Trade-offs between these functions may constrain phenotypic solutions. Further expansion of molecular tools in this group, including biochemical and comparative population genomics data, can help resolve the influence of mutations at this locus versus others in patterning phenotypic diversity. Of particular interest is the relative contributions of regulatory versus coding changes in affecting mating signal diversity, as understanding the mutational landscape due to coding changes is now comparably tractable with *in vitro* expression (Hensley et al. in revision).

Changes in enzyme function may be driven by selection as it influences predicted pulse duration, constrained by molecular processes like gene-wide epistasis, or most likely both. The positive relationship between predicted light output and catalytic rate (Fig. 3.7B) suggests that mechanisms acting on the evolution of enzyme function could co-evolve with visual ability in intended receivers (seeking females and/or competing males). Many visual systems co-evolve with requisite signals to maximize information transfer [114, 205, 189]. Spatiotemporal variation in information - such as that proffered in

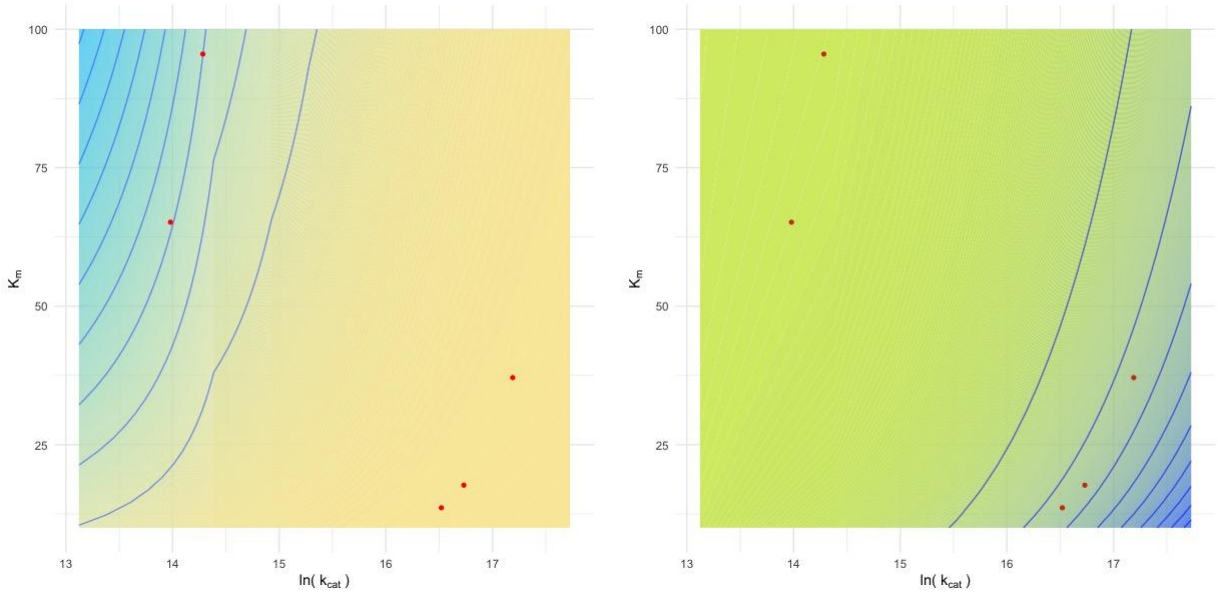

Figure 3.7: Placement of measured enzyme kinetic parameters (Table 3.1) onto phenotypic predictions from Eqn 3.4 for (A; left panel) pulse duration, and 3.3 (B; right panel) timing of light output. Colors as in Fig. 3.5, with shaded regions indicating either (A) longer pulse durations or (B) more light output at time-step 10. Each red datum is a species from Table 1 using the parameters from the corrected models.

the bioluminescent mating displays of Caribbean ostracods - may best be perceived by tuned visual systems. The variation in spatiotemporal display characteristics due to enzyme kinetics is well paired for future explorations using paradigmatic visual physiology techniques. Visual abilities like flicker-fusion rate and luminance sensitivity are prime candidates, as these metrics directly relate to the differences in pulse duration, timing, and brightness seen across the displays between species. Classical sexual selection models like the phenotypic tango (Fisher Lande Kirkpatrick process, [7]) predict that receiver ability and sender traits should track one another through phenotypic space over time. Preliminary data (J. Cohen, unpublished) indicate that species do have different visual capabilities. Future work looking at differences in visual sensitivity, mating display traits, and enzyme kinetics can test these co-evolutionary predictions at many levels of biological organization.

Conclusions Here, we explicitly model a behavioral phenotype in the bioluminescent mating displays of Caribbean cypridinid ostracods - also called sea fireflies. By purifying bioluminescent proteins and quantifying their relative emission efficiency and enzyme kinetics, we have parameterized a model describing how intrinsic enzyme function and extrinsic reactant ratios may influence the phenotype. The relative sensitivity to these different parameters suggests that different genomic changes may have alternative consequences for shaping evolutionary change, and also support the hypothesis that the c-luciferase enzyme could act as a genomic hotspot for phenotypic divergence in this behavior. With tests on molecular evolution, we provide potential candidate sites for discussion. Despite strong *a priori* expectations, we find that our parameterized model fails to predict *in vivo* behavioral characteristics. In proceeding to study visual physiology and by further characterizing the molecular basis for light production in sea fireflies, this system offers a new opportunity to explore the causes of diversification.

3.4 Materials & Methods

3.4.1 Animal collection

We identified most species by the patterns of male courtship signals, targeting each particular display type with a single net and later measuring length and height of individual animals using a dissecting microscope and ocular micrometer. Several of the species, especially from Panama, are undescribed and we refer to those here by field codes, consisting of two or three capital letters. We classify species into genera based on length:height ratio, which is a reliable genus-level characteristic [76, 168]. For transcriptomes, we preserved specimens in RNALater (Invitrogen) and stored at -20°C for later processing.

3.4.2 Luciferase discovery and amplification

We designed luciferase-specific primers (Table B.4) to amplify from cDNA and obtain sequences that do not include signal peptides (18 or 19 amino acids from the n-terminus, as inferred with SignalP) because we later used yeast-specific signal peptides during protein expression. we used an initial denaturation of 95°C for 2 min. For 30x cycles, we performed a 95°C denaturation step for 1 min., followed by an annealing phase at varying temperatures per species (*K. hastingsi*: 45.5°C, *P. morini*: 48°C, *M. sp.* SVU: 41.1°C , *M. sp.* SVD: 43.7°C, *M chicoi*: 41.4°C, *V. tsujii*: 45.5°C) for 1:45 min., and then by an extension step at 73°C for 1 min. For *V. tsujii* primers designed from the published transcriptome, we used thermal profile: 40 cycles of 94°C for 35s, 55°C for 30s, 72°C for 1min) and amplified the native signal peptide.

3.4.3 Ortholog inference and gene tree construction

We generated a gene tree of translated luciferase candidates and closely related genes. We used a published c-luciferase from V. hilgendorfii as a query in a similarity search using BLAST (E-value cut off 0.0001). In some cases, we did not obtain full-length luciferase transcripts in the assembly created by Trinity [71], which we attribute to polymorphism from pooling individuals. In these cases, we did a second assembly of luciferase fragments using cap3 [82] and selected the longest orfs as putative c-luciferases. We aligned these sequences using MAFFT [97]. We used IQ-TREE 1.6.12 [153] to select the best-fit model of protein evolution and to estimate the maximum likelihood phylogeny. We rooted this phylogeny using midpoint rooting to identify putative c-luciferases from new transcriptomes as orthologues to previously published c-luciferases.

3.4.4 Quantifying synonymous and non-synonymous rates of substitution

Many models and methods exist to quantify substitution rates of a gene under the assumption that rates of synonymous substitution represent rates of neutral mutation [102]. As such, ratios of non-synonymous to synonymous (dN:dS) rates inform evolutionary mechanisms, including positive selection [83]. Different approaches address different questions, such as whether individual sites, individual branches, or entire genes show signs of selection. For methods focused on individual sites, some methods assume a single dN:dS ratio at a site for the entire history of that site ('pervasive') [106]. Other methods allow for different ratios at a site along different branches of the gene tree ('episodic') [144]. Accuracy of these statistical methods are impacted by deviations from their assumptions, such as constant rates of synonymous substitutions across the phylogeny or independent mutations. The sensitivity of these methods means they must be interpreted with caution. At the same time, interesting patterns of substitutions generate testable functional hypotheses, especially in systems where enzymatic function can be measured following mutagenesis and *in vitro* expression. We believe episodic selection, where dN:dS is allowed to differ in different lineages, fits the biology of signal diversification better than pervasive selection because optima of signal phenotypes are expected to change commonly during evolution, such as to track shifts in mating preferences by courtship signals (i.e. phenotypic tango of the Fisher-Lande process [7]), and/or as predator behaviors co-evolve to combat the efficacy of defensive displays in a Red Queen scenario [225].

We aligned luciferase DNA by codon, first aligning amino acids in MAFFT [97], then matching DNA codons using pal2nal [208]. We used HyPhy [163] to compare ratios of synonymous to non-synonymous substitutions using various models. We used BUSTED[S]

with a correction for multiple hits to test the hypothesis that positive selection occurred at some (unspecified) point in the history of the gene [236]. We used FEL to look for evidence of pervasive positive selection on individual sites. FEL also reports sites showing significantly low dN:dS, consistent with purifying selection [106]. Because some *Photeros* species have very rapid courtship pulses, we tested for positive selection along the branch leading to *Photeros* using aBSREL [196]. Finally, we tested for episodic diversifying selection using MEME [144]. Both raw evolutionary rates (e.g. site heterogeneity in dS) and multinucleotide substitutions can increase rates of false positives [236, 226]. FEL, aBSREL, and MEME incorporate site-level heterogeneity into their models, and we used Multihit [116] to assess the evidence supporting a double or triple substitution over a single substitution at every site. Given our number of sequences (N = 15), we expect our identification of false positive sites to be relatively low (i.e. between 0-1%, [144]). We report uncorrected p-values in Table 1, but annotate both the uncorrected p-value cut-off of 0.05 and corrected q-value cut-off of 0.025 in Fig. S3 for ease of interpretation (correction for two branch-site tests: FEL and MEME).

3.4.5 Genetic correlation with c-luciferase function

We looked for amino acid changes associated with changes in light decay constant using previously published data [76]. We analyzed candidate mutations with an ANOVA to test for significant associations between variant amino acid sites and functions of c-luciferases, similar to methods for opsins and spectral absorbances [241]. To determine which sites were most highly correlated with each function, we used a model selection approach in the R package MuMIn [143]. We used the dredge function to test combinations of amino acid sites regressed against enzyme function, which formed different models. Dredge sorts models by AIC score. We tallied amino acid sites present in the

highest number of best-fit models, and then performed phylogenetically-informed least squares regression (PGLS) using a linear model with those sites and incorporating branch lengths from the gene tree transformed with a Brownian-motion model of evolution as a correlation structure into the residuals. We compared corrected and uncorrected models (i.e. with and without the phylogeny) using AICc of the maximum likelihood model fits. In most comparisons, AICc scores favored uncorrected, OLS fit models (Supplementary Table S3). In one case, OLS and PGLS fits were equivalent and we default to reporting results from a phylogenetically-corrected model (annotated in Table S1).

3.4.6 Protein expression and functional assays in mammalian cells

We expressed three luciferases in mammalian HEK293 cells. To construct a V. tsujii luciferase (VtL) expression vector, we first amplified VtL using primers with engineered restriction sites to clone into a pCR4-TOPO vector. We next excised VtL-pCR4 with XhoI and EcoRI (Promega), and subcloned into a modified pCMV3B mammalian expression vector with a C-terminal mCherry reporter (mCherry-C). The luciferase genes of P. morini and M. sp. SVU were synthesized and cloned into the mCherry-C vector by Genscript (Piscataway, New Jersey, USA) with flanking restriction enzyme sites. We planned to use mCherry to quantify the concentration of expressed luciferase, but we found high autofluorescence of cell media and/or other secreted proteins to preclude this use. We first transformed cloned constructs into competent *E. coli* cells using the One Shot Chemical Transformation Kit (Invitrogen), and cultured for 24 hours in standard lysogeny broth (LB) with 0.1% kanamycin at 37°C. We verified construct transformation using the engineered restriction enzyme sites in digests and compared them to their expected product size. We extracted these plasmids using the FastPlasmid Mini kit (Qaigen) and assessed

concentrations with the Qubit high standard DNA kit (Qubit). For transfection, we cultured mammalian HEK293 cells in Dulbecco's modified Eagle's medium (DMEM), supplemented with 10% fetal bovine serum (FBS) and penicillin/streptomycin (P/S) at 37°C with 5% CO_2. We then plated 5 x 10^4 cells in each well of a 24-well plate one to three days before transfection. Cell medium was changed to DMEM without serum and antibiotics before transfection. We transfected cells with 0.5 µg of vector using Lipofectamine 2000 (Invitrogen), performed according to the manufacturer's instructions. After 4 hours of incubation, we replaced the transfection medium with DMEM+FBS+P/S and allowed the cells to recover for 24 hours. We collected cells via trypsin digestion and reseeded them into 10mL of DMEM+FBS+P/S+1% G418 to select against untransfected cells in 90cm cell plates. We cultured the transfected cells for 3 to 5 days before harvesting and using in light catalysis assays.

3.4.7 Protein expression and functional assays in yeast cells

For expression in *Pichia* yeast, we cloned sequences into the pPICZ-αC vector at the XhoI and NotI sites following standard procedures (Invitrogen Easy Select *Pichia* kit). First, we analyzed predicted c-luciferases for the presence of a signal peptide at the n-terminal end using SignalP v4.1 [13]. We then designed primers for cloning and protein expression to amplify the entire c-luciferase sequence without the native signal peptide, beginning usually 51-54 bp inside the 5' end from the predicted start codon. 3' end primers excluded the native stop codon so that a fusion construct could be generated. Fusion constructs were made via the EasySelection *Pichia* expression kit (Invitrogen) using the pPICZ-αC vector according to the manufacturer's instructions. Briefly, we used the 5' XhoI site in order to generate fusion c-luciferases with an alpha secretion signal from yeast. We reconstructed the Kecx2 cleavage site with one Glycine Alanine

repeat region via PCR. On the 3' end, we used NotI; this would result in the addition of extra amino acids in our expressed proteins on the c-terminal end before inclusion of the fusion c-myc epitope and histidine tags. We transformed newly-made, linearized constructs into *Pichia* using electroporation with a BioRad Micro-Pulser using the Sc2 program (1.5 V).

After electroporation, *Pichia* were allowed to recover in selective media for an hour before plating. We initially selected for recombinant *Pichia* colonies using two concentrations of zeocin (100 and 500 mg/mL). After three days of growth, individual colonies were replica-plated at high zeocin concentrations (1,000 and 2,000 mg/mL) to try and screen for high copy-number integrants for our gene of interest. After one day, we selected single colonies that grew best at high zeocin concentrations to induce protein expression according to the manufacturer's guidelines.

To stabilize the pH of the media for extended expression, colonies were grown in 25mL buffered media with glycerol in baffled flasks until the OD_{600} reached 2.0 - 8.0. For our colonies, this occurred after 72 hrs due to suboptimal shaking conditions. We then calculated the amount of original growth we would need for an OD_{600} of 1.0 in 30mL expression media, spun down the appropriate volume of the original colonies at 3,000 g for 5min., removed the glycerol media, and resuspended the pellet in 30mL of buffered media with methanol in a 125mL baffled flask. Flasks were shaken in a table-top incubator at 29.5°C at 300 rpm for 3 days, with media supplemented with 100% methanol every 24 hrs to maintain a 0.5% volume of methanol in culture.

3.4.8 Protein expression, purification, and kinetics using silkworm

Synthetic constructs of putative c-luciferase candidates from 5 different species were ordered from Genscript, USA. Codon usage was optimized for insect expression (Genscript, USA). Each recombinant protein was expressed using a silkworm expression system by an outsourcing company (Sysmex, Japan). The recombinant protein was designed to possess 6x His-tag at its C-terminus. The crude body fluid containing the recombinant protein was collected and centrifuged at 100,000 x g for 1 h by Sysmex, and the supernatant (2mL) was delivered for further characterization.

We performed Ni-NTA resin purification of Histidine-rich proteins from this supernatant according to manufacturer recommendations (Qiagen). After washing 100μl of Ni-NTA resin with 50μl H_2O (3x times), and 50μl equilibration solution (10mM imidazole, 20mM TRIS; 3x times), we combined silkworm supernatant (100 - 200μl) with equilibration solution to a total of 500μl and mixed this dilution with the Ni-NTA agarose at 4°C for 1hr via slow rotation. We used a table-top centrifuge to collect the Ni-NTA beads and wash them 2x with a wash solution (40mM imidazole, 20mM TRIS) to remove low-affinity proteins. We then eluted high-affinity proteins using 50μl elution solution (200mM imidazole, 20 mM TRIS).

The subsequent elution was combined with 20mM TRIS to a volume of 2mL and desalted using PD10 desalting columns (Sigma Aldritch) with a total wash volume of 10mL of 20mM TRIS. We assayed fractions by adding vargulin substrate, pooled the most active fractions, and used centrifugal concentration to concentrate proteins above 50,000 NMWL (Amicon Ultra). We confirmed protein purity visually with SDS-PAGE and Coomassie staining. Protein concentration was measured with a Nanodrop assuming molecular weight and extinction coefficients from the known c-luciferase ortholog

of *Cypridina noctiluca* (MW = 62.1 kDA, e = 6.11), but corrected for each sequence post-hoc.

3.4.9 Light catalysis assay

To assess the ability of expressed genes to catalyze a light reaction, we harvested cell culture media from mammalian or yeast cells from each transfection (approximately 10 - 25mL per transfection), and concentrated it using 30,000 MWCO centrifugal filters (Amicon), spun from 30 - 240min. at 4,000 x g. After centrifugation, the protein solution was immediately collected for the assay. Varying volumes of concentrated protein solution and luciferin assay mix (Targeting Systems; prepared to manufacturer's specifications but with unknown concentration for mammalian cells; and for yeast, we procured vargulin from NanoLight Technology (Pinetop, AZ) and suspended it in 10mM TRIS to a working concentration of 0.01 ng/μl) were added together in a plate reader (Wallac). We measured luminescence in counts per second (CPS) for 10 seconds.

For light catalysis assays using silkworm-expressed proteins, we combined differing volumes of purified protein (known concentration) and diluted luciferin (starting from 100uM stock suspended in methanol; ATTO) to 100μl in 20mM TRIS HCl (pH 8.0). Assays were measured anywhere from 10 - 1200 seconds, depending on the experiment. To quantify the enzyme kinetic parameters (see below), we performed initial velocity experiments. We combined purified enzymes (either at 1.5×10^{-3} μM or 1.5×10^{-4} μM) with substrate concentrations ranging from 0.78125 to 50μM in a final volume of 100μl TRIS to perform light catalysis assays as above. Data were collected at 50 Hz, and we only retained the first 10 seconds of data for analysis in each experiment.

3.4.10 Michaelis-Menten kinetics

We used nonlinear regression in RStudio (v.1.2.1335) with the command nlsLM from the package 'minpack.lm' [46] to fit the observed count data to the standard Michaelis-Menten equation (below):

$$v = \frac{k_{cat} * [E] * [S]}{K_m * [S]} \tag{3.1}$$

and solving for the parameters k_{cat} and K_m. In our experiments, the initial rates (v) are the measured relative light units (RLU) from the microplate photometer, [E] is the known concentration of protein, and the [S] is the known concentration of substrate at the start of the experiment. k_{cat} is the rate of catalysis of the forward reaction as the enzyme:substrate complex dissociates and reaction products are formed; in our case, this is the rate at which light is produced in the bioluminescent reaction (units: 1/s). K_m is the Michaelis constant or enzyme affinity, which is the concentration at which the reaction reaches half its maximum rate; lower K_m values indicate a higher substrate affinity (units: substrate concentration, μM).

Although traditionally technical replicates at each substrate concentration are performed to account for variation in product formation, limited protein concentration and timing did not allow us to perform such replication. Instead, to account for relative error in each measure, we retain the first 500 data points (10 s) of the initial velocity measures for each concentration assay. Our rapid sampling rate and the separation of timescales in kinetic experiments [27] allows us to assume that substrate depletion is not relevant to each datum within this time scale, making them quasi-independent. We then used weighted nonlinear regression with a correction for the variance in each substrate assay, as variation across substrate concentration experiments is not typically uniform. To account for auto-catalysis of the substrate and spontaneous emission of light, we also performed control experiments (substrate only added to TRIS HCl buffer) at each sub-

strate concentration. As the origin of measured light counts is impossible to distinguish between enzymatic and non-enzymatic processes, we present our regression analyses in two ways: (1) without accounting for this background level of emission, and by only retaining counts in each substrate concentration assay that exceed 1 standard deviation above counts from the control experiment at the same substrate concentration (Table 3.1).

3.4.11 Gene Expression

To quantify gene expression at the site of bioluminescence (in the organ called the "upper lip"), we performed RNA Tag-seq to help capture lowly expressed reads. Light organs from the upper lips of individual ostracods (N = 2 - 5 males per species) were dissected and placed immediately into Trizol for subsequent RNA extraction. After sequencing, raw data were cleaned, filtered, and annotated on the Taq-seq pipeline (elimeyer.github.io). Expression files were then generated by comparing Taq-seq read count files to reference transcriptomes for each species. Reference transcriptomes were assembled via Trinity by using preliminary *Vargula tsujii* genome long reads as a scaffold for previously generated RNA short-reads [44]. Of the c-luciferase homologs from different species of ostracod expressed *in vitro*, we only had overlapping Tag-seq data from four species: *Vargula hilgendorfii*, *Photeros annecohenae*, *Maristella chicoi*, and *Kornickeria hastingsii carriebowae*. Unlike the other three reference transcriptomes, the *P. annecohenae* reference transcriptome did not possess a fully assembled luciferase (as mentioned previously). As such, we performed an additional assembly using CAP3; for these mapped reads, we simply added the transcript abundances together for each partial match if they were phased by CAP3 into a single contig.

3.4.12 Quantifying phenotypic space

Cypridinid bioluminescence follows first-order kinetics and may be described by Michaelis-Menten models [92]. We use two forms of the integrated Michaelis-Menten formula to mathematically quantify verbal arguments that demonstrate how pulse duration may be influenced by variation in enzymatic reaction rates. For a more detailed review on enzyme kinetic theory and the derivation of the Michaelis-Menten formula, please see Appendix A. First, to quantify the influence of kinetic parameters on the timing of light production during the secreted reaction (pulse duration), we used the integral of Eqn 3.1, as follows:

$$K_m = log_{10}(\frac{\frac{-S}{K_m} - 1}{\frac{-S_0}{K_m} - 1}) + S_0 - S = k_{cat} * E * time \tag{3.2}$$

where the parameters are as in Eqn 3.2, but which have now been integrated with respect to time and are independent of concentration, instead relying on molecular quantities (in mols) [64]. To adapt this for our models, we solve for time and incorporate a relative emission efficiency product (REE) as a method of describing variation in light production that may be due to differences in intramolecular interactions between enzyme and substrate (e.g. photon yield or quantum efficiency). This produces the following equation:

$$time = \frac{K_m * log_{10}(\frac{\frac{-S}{K_m}-1}{\frac{-S_0}{K_m}-1}) + S_0 - S}{k_{cat} * E} * \frac{1}{REE} \tag{3.3}$$

Although this formulation is convenient to solve for the Michaelis-Menten equation in terms of time (which seems rarely done), the accuracy of this integral is an approximation to an infinite series. Instead, recent incorporations of the Lambert function (**W**) and certain reconfigurations permit Eqn S4 to be in terms of product formation in a finite reaction. We use the following interpretation to understand the difference in timing in

product formation:

$$P = REE * \left[S_0 - K_m * \mathbf{W} \left\{ \frac{S_0}{K_m} e^{\frac{S_0 - k_{cat} * E * time}{K_m}} \right\} \right] \tag{3.4}$$

Eqn. 3.4 now describes the amount of product (light) that has been produced after a given amount of time has passed under specific molecular conditions, and again with a term to capture the dynamics of variation in product production (REE) [108].

3.4.13 Ethics statement

All organisms were collected in accordance with the regulations of the Jamaican National Environment and Planning Agency (Permit Ref. # 18/27), the Belize Fisheries Department (Permit # 000003-16), the Honduran Department of Fish and Wildlife (Permit # DE-MO-082-2016), the Puerto Rican Department of Natural and Environmental Resources (DRNA; Permit # 2016-IC-113), and Panamanian Ministry of the Environment (MiAMBIENTE; Permit # SE/A-33-17).

3.4.14 Author Contributions

NMH designed experiments, performed research, analyzed data, and wrote the paper. EAE designed experiments, and collected and analyzed transcriptomes. NYL and DAT collected mammalian cell culture data, and NYL also generated cDNA libraries for cloning. JC generated yeast fusion constructs. AM designed emission spectra experiments and assisted with data collection and quality control. MT and DFG contributed resources for transcriptome generation and analysis. AWD provided resources for mammalian cell cultures. YM provided oversight and resources to yeast culture expression and insect cell expression. TJR, GAG, and ET provided resources, and collected biological specimens and morphological data. KM assisted with insect cell purification.

JAG developed tissue-specific transcriptomes and mapped RNA expression data. ESL provided bioinformatics support. JL provided advice on kinetics modeling. THO provided resources, analyzed and curated molecular data, and wrote the paper. All authors contributed to editing.

3.4.15 Acknowledgements

We thank C. Pham, T. Halvorsen, Y. Chiu, J. Russo, M. Pfau, T. Jessup, E. Youn and C. Martinez for assistance with cloning and expression. We acknowledge J. Lachat and Y. Nishimiya for assistance with the *Pichia* system and for providing the *C. noctiluca* construct used as a positive control, and M. Furubayashi and S. Kanie for their support during his visit to AIST. We are grateful to Z. Terner from the UCSB Statistical Consulting Laboratory for his advice on linear mixed effect modeling. We also extend our thanks to Y J. Li, S. Schulz, N. Reda, J. Morin, M D. Ramirez, C. Motta, and V. Gonzalez for assistance with animal collections.

3.4.16 Data, code, and materials

Transcriptomes have been deposited at BioProject: PRJNA589015. Most expression data and code for all analyses are available on GitHub: ostratodd/Cypridinidae_Emission: Raw data and analysis files for Bioluminescent Emission Spectra of Cypridinid ostracods. Code and data for ongoing analysis and modeling will be made available via another Github repository upon completion.

3.4.17 Funding

NMH was funded in part by an NSF EAPSI Fellowship (# 1713975), an NSF GROW Award as a part of the NSF Graduate Research Fellowship Program, and the UCSB

Research Mentorship Program run by Dr. Lina Kim. NSF DDIG (# 1702011) to EAE provided funding for transcriptomes. JC received funding from the UCSB URCA program. ET was funded by a CSUPERB Research Development Grant for transcriptomes, gene synthesis, and vector cloning. Authors THO, GAG, and ET were funded by NSF (# DEB-1457754, DEB-1457439, and DEB-1457462, respectively).

Chapter 4

Weak differences between female swimming behaviors in allopatry and sympatry among species of sea fireflies

4.1 Introduction

Reproductive isolation is the key step in speciation, whereby gene flow decreases between ancestrally mixed populations, allowing them to evolve independently from one another. Speciation is a temporally-dependent process, and investigating the variation in the rates and magnitudes of this process drives much of evolutionary research. As such, speciation biology has focused primarily on determining how extrinsic (i.e. geographic) and intrinsic (i.e. genetic, behavioral) characteristics contribute to reproductive isolation and influence speciation [36].

Theory and empirical work confirm that prezygotic reproductive isolation is important during speciation [37, 166]. In many species radiations, prezygotic isolation can rapidly evolve due to diverging mating behaviors. In allopatry, as most speciation occurs, there is little expectation for mate preferences to evolve early in speciation unless coupled with other processes like ecological selection (i.e. magic traits), assortative mating or divergent sexual selection (e.g. as in polymorphic populations), and drift (e.g. Kaneshiro processes, Mutation-order speciation) [169, 55]. In sympatry, divergence in mate preferences are expected to evolve early during speciation if they are causal in the process [77, 239], although many models still find it insufficient to cause speciation [5, 43]. Otherwise, much divergence in mating behaviors when in sympatry are most likely attributed to reinforcement processes on other reproductive isolating mechanisms (i.e. post-zygotic). Parsing out the relative contributions of differing processes to speciation, including how much reproductive isolation is due to divergence in mating behaviors [178], requires testing species at different levels of divergence, classically espoused by [37] and expanded in many other systems [132, 133, 142].

Regardless of whether divergence in mating behaviors drive speciation, they are prominent in intra- and interspecific interactions within ecological communities [68].

When conflict between shared resources arises during community assembly, evolution may push populations towards dissimilar optima of resource use to partition the shared niche [67]. This character displacement is famously recognized in reproductive characters from allopatric and sympatric species, both in the signals produced and the preferences for those signals [78, 198]. Increased community diversity may exacerbate reproductive character displacement and drive populations or species to evolve narrow ranges in their trait/preference values [210].

Because mating traits mediate the feedback between reproductive isolation, potential for reproductive interference, and speciation, measuring trait and preference values at varying ecological scales is critical. However, predicting which traits are important, especially in multivariate or multimodal mating systems, adds more complexity and which may have implications on the rate and magnitude of divergence in any of these processes [181]. For example, the shape of female preferences (open-ended versus closed) impacts the predicted change in trait distributions [210, 174, 227], which are at the crux of the interactions between these eco-evolutionary dynamics. We can begin to understand these complexities more robustly by taking a piecemeal, systematic approach to examining mating trait diversity.

Ostracods are small marine crustaceans (Cypridinidae) found world-wide that produce bioluminescence to deter predators. In Caribbean waters, males of about 100 species [29, 44] have co-opted this trait to generate species-specific mating displays, analogous to terrestrial fireflies and hence their moniker umihotaru ('sea firefly' in Japanese). Males produce these displays by secreting discrete packets of mucus in spatiotemporally varying trails (single displays are referred to as trains; [170]). Females use these trains as visual guides to anticipate and intercept the position of swimming males [171]. Other males can compete to attract the attention of females by adopting alternative mating tactics, such as entraining with their own display, inconspicuously sneaking on the display of another

male, or producing an independent train [172]. Within habitats, males from multiple species can display sympatrically, with up to nine species displaying at any one time ([59, 141], pers. obs.). This "cacophony" of lights is visually stunning for the casual human observer, but in theory poses a visual challenge to receptive females trying to locate conspecific mates among heterospecific distractors. The displays of sympatric males may have evolved under character displacement processes to partition the signaling niche ([59]; Gerrish et al., in prep.)

We hypothesized that the ability of a female ostracod to discriminately prefer her conspecific mating display would vary with the ecological context of the male's signaling environment. If community composition is a strong agent of selection, we predict that females from species whose males regularly display with other heterospecific males (Belize: *P. morini*, Panama: *P.* sp. "SFM") will have an increased discrimination ability against foreign displays. These females should bias their swimming trajectories and association time towards displays of conspecifics (artificial control) over heterospecifics (artificial experiments). Conversely, females whose mating arenas are not usually saturated with heterospecific signals (Belize: *P. annecohenae*, Panama: *P.* sp. "EGD") will be under weaker selection for discriminatory preferences, and therefore demonstrate swimming trajectories and association times equally between control and experimental displays.

4.2 Results

4.2.1 Four ostracod species vary in their displays

We recorded single females (N = 52) from four species with variable success. As with others [59, 141], the four ostracod species we studied have different displays (Fig.

4.1A). Based on our results from a multiple factor analysis with simulated data based on real field measures, the experimental programs we used to assay female discriminatory behavior varied in their multivariate "distance" from the control programs (Fig. 4.1B), the experimental programs we used to assay female discriminatory behavior varied in their multivariate distance from the control programs. The disparity between artificial control displays and artificial experimental displays differed for each species, as the Euclidean distances in multivariate space between artificial experimental display types are not equal. The first two factors describe approx. 21.54% of the variation between species, with significant but varying levels of overlap between them. Dimension 1 primarily captures variation in the display direction and pulse duration, while dimension 2 describes most of the variance in interpulse interval (Table 4.1).

Display character	Dimension 1	Dimension 2
Direction	0.59064	0.16984
Number of pulses	0.35355	0.00796
Pulse duration (PD)	0.64626	0.17497
Interpulse Interval (IPI)	0.14772	0.88836

Table 4.1: Dimension loadings for the first two dimensions from the multiple factor analysis describing display variation among four species of ostracod in the genus *Photeros*, as seen in Fig. 4.1A. Analysis based on focal characteristics, namely pulse duration (PD) and interpusle interval (IPI), which should not be interpreted as the primary axes of variation amongst all species' displays.

4.2.2 Females are more active during display periods

As a proxy for female activity, the number of trajectories detected before and after stimulus presentation differed ($N_{Before} = 311$, $N_{After} = 7{,}438$; binomial test, $p < 0.05$).

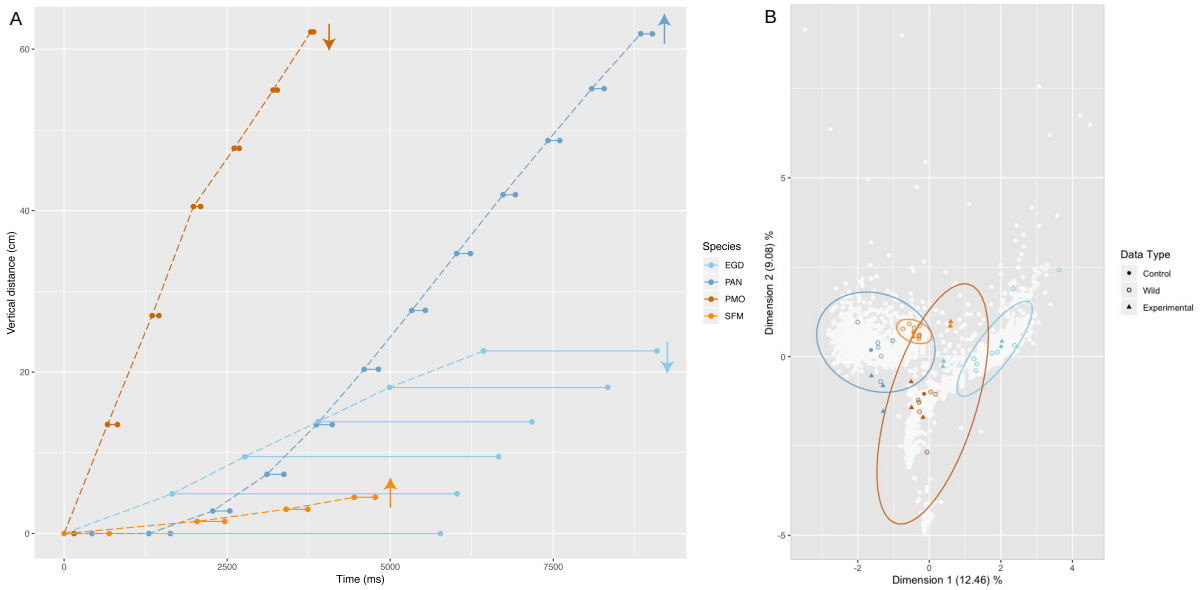

Figure 4.1: Species occupy distinct, partially overlapping regions of phenotypic space in their sexual displays. (A) Time-distance scatterplot (*sensu* Morin) of the display characteristics of the four species (uniquely colored) tested in this study. Arrows indicate the direction of pulse propagation (swimming direction, up or down) during a single display train. Each pair of data connected by a solid, horizontal line is a single pulse in the display, with the length of the line indicating the overall duration of the pulse (x-axis). Distances between pairs of data for a single pulse (y-axis) indicate the observed vertical distance between subsequent pulses in a display (dashed line). (B) Multiple factor analysis showing the potential variation in displays for each of the four species. Data are simulated (n = 1000 per species; white circles) based on the measured variation (N = 6 - 8 per species; empty circles) and reported ranges for 7 display variables. Projected into this multivariate space are both the artificial control (1 per species; as from Fig 4.1A; filled circles) and artificial experimental (3 per species; filled triangles) displays used for each species. Species in blue hues are allopatric with respect to other signaling species, while those in orange hues are spatiotemporally sympatric with other displaying ostracod species (not depicted).

4.2.3 Females swimming speeds are altered with artificial displays

Unlike [171], we find that females who are exposed to artificial displays have altered swimming speeds (Likelihood ratio test, p = 0.0024740; Fig. 4.2, Table C.2). However, this effect is mediated by ecological history (LRT, $p < 2.2 \times 10^{-16}$) and the interaction of these two variables (LRT, p = 0.0036389). Sympatric species have faster approach

trajectories. This pattern seems to be driven by the significantly bigger *P. morini* females, which are $\sim$ 16% larger in body size than their congener *P. annecohenae*. The other sympatric species, "SFM" from Panama, actually slows down (on average) after displays begin in the experimental trials.

The magnitude and direction of this change in speed is also affected by the type of display presented to females (LRT, $p < 0.0008869$; Table C.2), with interactions between display type and ecology (LRT, $p < 2.692 \times 10^{-07}$). Females from both sympatric and allopatric ecological histories consistently had increased speeds in the trajectories identified after displays began if they were presented with artificial displays that differed in pulse duration. For allopatric species, females exposed to stimuli with differences in the interpulse intervals have trajectories that are slowed compared to those identified before the onset of stimuli. Sympatric species generally increase their swimming speeds, but do so most pronouncedly in experiments presenting artificial experimental displays that have changes in pulse duration.

4.2.4 The directedness of female patterns is altered with artificial displays

The sinuosity of a female's trajectory is affected by the type of display (Likelihood ratio test, $p = 2.251 \times 10^{-05}$), ecological history (LRT, $p < 2.2 \times 10^{-16}$), and their interaction (LRT, $p = 5.871 \times 10^{-05}$). Although the sinuosity of female swimming trajectories is lower after stimuli have begun ($\mu_{\text{Before}} = 8.36$, $\mu_{\text{After}} = 7.98$), this is not statistically significant ($p = 0.2737$) nor were any of its interactions, and we removed timing from the subsequent analysis (Fig. 4.3; Table C.2).

Sympatric species havfe less direct approach trajectories, and the strength of this result is conditioned on the type of display in the experiment (Fig. 4.3A). In each treat-

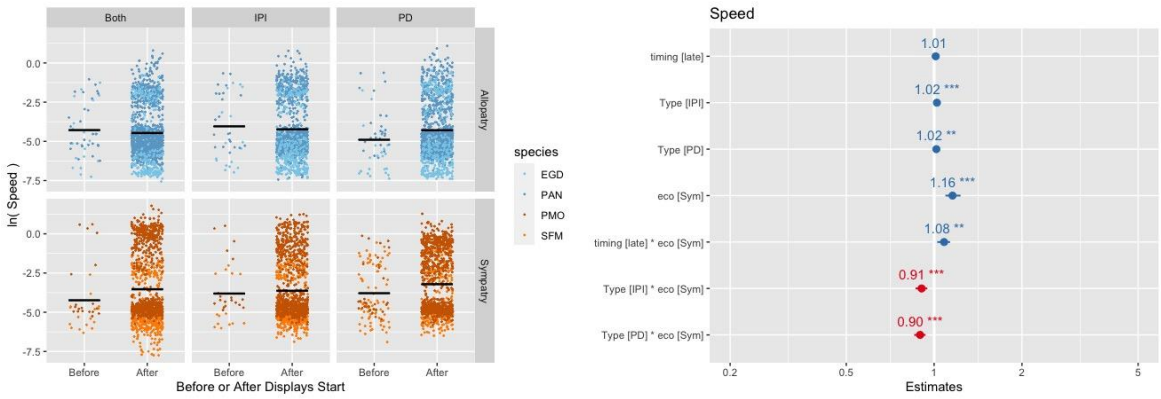

Figure 4.2: Changes in female swimming speed from trajectories identified before or after the onset of stimuli. (A; left) Females swimming speeds generally increase, but this depends on the type of stimuli presented. The magnitude of this change is also conditioned on the ecological history of the species (Blues = allopatric species, Oranges = sympatric species). Note that we present natural log-transformed speeds in Panel A simply for ease of interpretation. All models were run with untransformed speed measures as the response variable. (B; right) Effect size estimates with 95% confidence intervals for likelihood ratio tests on how subsequent addition and removal of each variable effects a generalized linear model describing how timing during an experimental trial (Early = Before stimulus onset, Late = After stimulus onset), ecological history (Allo = Allopatric, Sym = Sympatric), and display type (Both = Both IPI and PD altered, IPI = interpulse interval altered, PD = pulse duration altered) affects the speed of a female ostracod.

ment, sympatric animals exposed to artificial displays that differ in their pulse duration have less direct approaches than allopatric species. However, we caution the biological interpretation of this result. Sinuosity is dependent on other variables such as the step-size between consecutive measures of displacement. Given that these animals are moving at a faster speed than their allopatric congeners (Fig. 4.2A), this would also drive their step-sizes to increase and cause sinuosity to decrease. Indeed, we see a negative correlation between speed and sinuosity across trajectories (Pearson's product correlation = -0.4487; t = -44.197, df = 7747, p-value < 0.001). So although this metric incorporates information on the propensity to turn (cosine of angle of displacement), it may not accurately capture change in movement.

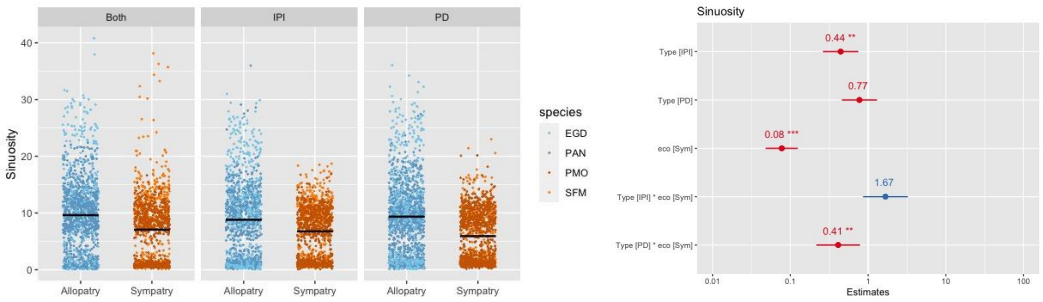

Figure 4.3: Changes in female swimming sinuosity. (A; left) Females swimming trajectories generally become less directed, but this depends on the ecological history of the species (Blues = allopatric species, Oranges = sympatric species). The magnitude of this change is also conditioned on the type of stimuli presented. (B; right) Effect size estimates with 95% confidence intervals for likelihood ratio tests on how subsequent addition and removal of each variable effects a generalized linear model describing how ecological history (Allo = Allopatric, Sym = Sympatric), and display type (Both = Both IPI and PD altered, IPI = interpulse interval altered, PD = pulse duration altered) affects the directedness of a female ostracod's path.

4.2.5 Females do not demonstrate strong patterns of choice

We examined the 55 confirmed trajectories to see if females would alter their swimming before and after the exact onset of a stimulus, producing 122 events. We find that the female swimming direction before or after a display (toward or away from it) is uncorrelated with the type of display observed or the ecology of the species (McNemar's tests, df = 1, $p > 0.05$ for each display type within each ecological condition). However, parsing our limited data into each category makes their sample sizes limited.

Increasing our power with a logistic regression, we find that females ostracods were more likely to change direction after seeing a display only if they were from an allopatric species (Wald Test; $p = 0.02048$), but not on which type of display they were headed towards (Wald Test; $p = 0.55872$) or the interaction of those test conditions (Wald Test; $p = 0.38835$). Females from allopatric communities switch their swimming direction about 33% of the time regardless of the signal observed, whereas females from sympatric species tend to remain on course 85% of the time regardless of display type (Fig. 4.4).

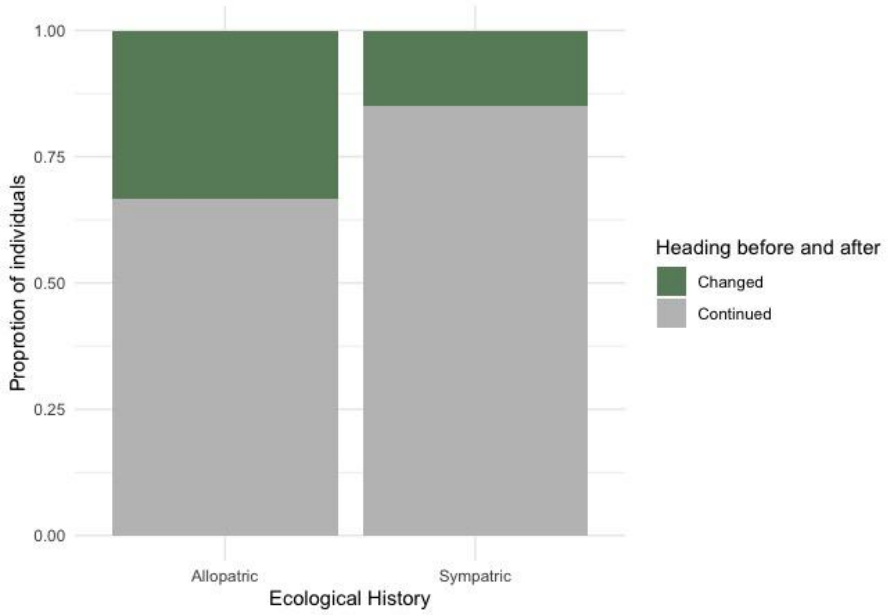

Figure 4.4: Proportion of individuals that changed (green) their heading or did not (grey) during a single trajectory after direct intervention of an artificial display. Allopatric species are slightly more likely to change their trajectory heading than sympatric species.

4.3 Discussion

Co-existence in complex communities should generate competition for shared resources. We tested the prediction that female receivers of different species that live in communities of varying heterospecific overlap should demonstrate different abilities to discriminate amongst proper conspecific mates. When the resource is access to mates, like in lekking species where command of space and time in common areas determine the opportunity to garner mating opportunities, selection to partition niches should facilitate coexistence. For successful communication in signal-receiver dynamics, partitioning of the signal niche may also be accompanied by receiver division of signal space through a number of mechanisms, from increased discimination via divergent sensory abilities to cognitive abilities. Using two species pairs of bioluminescent ostracods, each containing one species that lives allopatrically and one that lives sympatrically with other het-

erospecifics, we found that females from neither allopatric nor sympatric species demonstrate strong discriminatory behavior, although sympatric females are less likely to change heading after seeing a mate-like display. However, we do show that gross behavioral responses differ across experimental treatments. Namely, sympatric females increase their swimming speeds when exposed to artificial displays with differences in pulse duration. Below, we discuss the results of these analyses and the relevance of these behaviors in the context of speciation and ecological community dynamics.

Our results indicate that sympatric females are less likely to alter the heading of their trajectories when viewing a display, regardless of how divergent it may or may not be from a species-typical display (Fig. 4.4). This is counter to predictions under the reproductive character displacement hypothesis. We predicted that sympatric species should change heading more often and especially when viewing an artificial experimental display. Instead allopatric species alter their trajectory direction much more often. Although our sample sizes are low, this could be due to increased reproductive interference amongst sympatric species. If conspecific male density is reduced, the relative cost of mate searching may be higher in sympatric species. This may lead to sympatric females adopting different mate searching strategies [90], including being less choosy, than their allopatric compatriots. This system is primed for more in-depth classical behavioral ecology studies such as these.

Contrary to the results of our individual trajectory analysis, our bulk analysis of female behavior before or during the presentation of diverse displays follow the predictions of the reproductive character displacement hypothesis (Fig. 4.2). Different display traits may be more helpful to females during mate searching [19], and which may depend on their ecological history with heterospecifics. In our study, searching females from sympatric species always increased their swimming speed after displays began, and did so the most if presented with displays that differed in their pulse duration (or, pulse duration

and interpulse interval). Conversely, allopatric species only increased their swimming speeds when at least the pulse duration was different between displays. Responses to changes in interpulse interval were neither consistent nor as strong across treatments, suggesting that interpulse interval may have a reduced role in discrimination tasks for searching females. Variation in response to signal traits supports the hypothesis that display components may have evolved for a species recognition and/or mate recognition context.

Pulse duration may generally be important for female mate choice (Fig. 4.2B). Although different signal components may vary in their relevance to females between species, females of all species show an increase in speed during trials with stimuli that differ only in pulse duration. These differences may be adaptive. Pulse duration varies from milliseconds to tens of seconds across species [141], and for which we have a strong a priori understanding of its mechanistic basis. Recent molecular work connecting the enzymatic basis of light production with this signal phenotype has revealed candidate amino acid sites under diversifying selection (Chapter 3). Pairing molecular tools with more stringent behavioral assays may clarify what aspects of pulse duration - be it light intensity or actual duration - are important to receivers in this communication system.

The inconsistencies between our individual and bulk analyses may be explained by a few mechanisms. First, the display parameters we tested here may not be as important during individual choices during mate search. Ostracod bioluminescent displays are multivariate and many parameters differ within and between species [59]. The presence of signals generally may have increased female activity without necessarily requiring strong choice dynamics. Second, the differences in display parameters chosen during stimulus presentation may not have adequately covered differences in female perceptual ability, which is unknown. Although we cover an order of magnitude in pulse duration differences between species, how females view these differences remains to be tested. Third,

as our analysis is inherently noisy, identifying relevant trajectories with high confidence may obscure finer-scale patterns. Teasing apart which single traits are important, if any, requires more tests like ours.

Differences in community composition may shape the importance of different display components. Our results find inconsistent effects and magnitudes of pulse duration, and especially interpulse intervals, on producing changes in female behavior. Sympatric females demonstrate consistent increases in speed regardless of the display types presented, but show the strongest change with pulse duration experiments. Allopatric females show inconsistent changes in swimming speed, and only demonstrate an increase in speed with a change in pulse duration. The relative composition of heterospecifics in a community may shape how important differences in the overall display are to searching females, either in the magnitude of differences in single parameters or in the aggregate number of changes amongst different display traits. This may potentiate the number of heterospecifics that can coexist in any one lek if selection acts on different signal traits in different communities.

Multivariate signals may facilitate ecological and species diversity, as signal space can be partitioned by receivers along many different axes, including many not measured here. Previous research indicates that somes ostracod species partition the lek by altering which microhabitat (coral, sand, etc.) or when in the night (early, late, etc.) males, on average, display [59]. Although that work did not measure the contribution of the same display aspects we investigated here, regardless, it is possible that factors extrinsic to the display form itself may be more important during mate choice, and thus more labile during evolutionary divergence and/or community assembly. Of note is the divergence in display propagation direction with respect to the benthos (up, down, horizontally, angled, etc.), which differs widely within and between genera and seems to evolve quickly [167]. Our playback system will allow us to parse apart which characters are important and

evolving due to female choice, as opposed to randomly diverging or evolving primarily due to correlations between display characteristics.

The evolution of display disparity may not be as important during speciation, at least in the characters tested here. Species from the early diverging pair (Panamanian *Photeros*) show a much less pronounced difference in response to differences in trait characteristics than those from the distantly diverged pair (Belizean *Photeros*). If these traits are important during speciation, we expect that early-diverging lineages should demonstrate an equally strong magnitude of response. Instead, the variation in the magnitude of response is more consistent with divergence over time. This is corroborated by recent work within one of our focal species, *P. annecohenae*, which shows that behavioral divergence between populations is only very weakly correlated with genetic distance [29, 167]. So although these characteristics (pulse duration and interpulse interval) may play a role during female mate recognition and choice, it may not be a primary driver of speciation. This is in general agreement with models of speciation that argue for a more prominent effect of ecological speciation and secondary effects via sexual selection [169].

Conclusions In complex communities, mating opportunities between signalling males and searching females may be hindered by the presence of heterospecific signals - termed reproductive interference. Evolution may ameliorate the negative consequences of sympatry through reproductive character displacement, both in male signalling traits and female preferences for those traits. We find that in the bioluminescent mating displays of Caribbean ostracods, metrics of females response to male displays are inconsistent with predictions from reproductive character displacement. While female swimming speeds increase and respond to differences in male signals based on trait differences, individual trajectory headings do not. Both measures find ecological history an important determinant of female behavior, but with surprising results. These inconsistencies suggest that alternative metrics may be needed to accurately assess female choice, and that behavioral

divergence among this group may be a minor contributor to speciation dynamics.

4.4 Materials & Methods

4.4.1 Animal collection and care

Female *P. annecohenae* were collected from the grass beds off of Southwater Caye (16.812653, -88.082619) on either 29 March 2018 or 30 March 2018 using baited conical traps. A-I juvenile females (the last of five juvenile instars stages before the reproductive adult lifestage) were then sorted by eye the next day and kept in batch in 12-well cell culture dishes.. Each day we checked the health of individuals and changed their water; we fed them fish flakes (Seachem NutriDiet MarinePlus Enhanced Marine Flakes with Probiotics) everyday or every other day. Once animals molted into adult females, we separated them into their own individual wells until they were used in experiments. Experimental trials occurred nightly from 7 April 2018 to 11 April 2018 between 1900 hrs and 0200 hrs.

Female *P. morini* were collected from 11 April 2018 - 14 April 2018 using hand nets swept through the displays of male *P. morini* as described in Morin and Cohen (2010). We collected individuals from two locations: the patch reef off of South Water Caye (16.811801, -88.082628) or the patch reef of off Hangman Caye (16.823355, -88.150956). Because this species does not come to baited traps (Morin pers. communication), A-I females could not readily be collected; as such, we used any adult females collected from the water column. These females were caught in the mating spree and we assumed that this correlates with their receptivity to mating even though we cannot guarantee that they have not mated previously. Before our experiments, we noted the presence of developing eggs, brooding of deposited embryos into the marsupium, and/or parasites.

Experimental trials occurred from 13 April 2018 - 16 April 2018. After individual trials, individuals were preserved in 95% EtOH and later dissected to check for a spermatophore as another potential indicator of previous matings.

Off the coast of Bocas del Toro, Panama, we collected both female *Photeros* sp. "EGD" (21 September 2018 - 26 September 2018) and female *Photeros* sp. "SFM" (18 September 2018 - 27 September 2018) using traps. EGD were sampled from the grass bed of Punto Manglar (9.332464, -82.254105) and SFM were found in the mangrove roots adjacent to the site. Care for these animals was the same as described above. Experiments occurred nightly from 04 October 2018 to 13 October 2018 between 1900 hrs and 0400 hrs.

As with female *P. morini* described above, adult males of all four species were caught from active displays using hand nets and maintained in cell culture dishes until used in experiments. Because males frequently will not respond to other displays unless in high density (Rivers and Morin 2009), in experimental trials we used five males simultaneously in each trial. This prevents us from making conclusions about individual response curves to display differences because individuals are non-independent per trial. Instead, we present our results as averages generally, but with the understanding that our experimental conditions are more biologically relevant.

4.4.2 Experimental design and data collection

Tanks had two artificial displays, one running a control program that mimicked the native conspecific signal, and one running an experimental program with one of three experimental alterations (Fig. C.1). The experimental displays were as follows: (1) a program mimicking the conspecific display, like the control, except with the pulse durations of the heterospecific; (2) a program with only the interpulse interval changed to

that of the heterospecific; and (3) a program with both the pulse duration and interpulse interval of the heterospecific display. Before each trial, experimental animals were moved to a well-lit area to prevent them from experiencing nightfall. During an experimental trial, individuals were placed in the tank for 10 minutes while under bright illumination so they could adapt to the tank. I then turned off the light to simulate the onset of night. After 5 minutes in the dark, I began recording their behavior on camera without the presence of artificial displays, and gave them another 5 minutes in the dark. After these 10 minutes of dark adaptation, I began to expose them to artificial display trials. Every individual was exposed to all three experimental programs consecutively, with 5 minute intervals of darkness separating each condition. The presentation order of the experimental programs was randomized within trials via random number generator. During each trial, the artificial displays were each shown 10 times with 20 sec intervals between displays; because of differences in total display duration, this led to differences in overall trial duration across species. The tank was washed and dried during the day, with new sea water added nightly before experiments began.

All artificial displays (control and experimental programs) were written in Arduino and output to a NeoPixel LED strip. To best mimic the natural displays of each species, we used a custom fade function based on Gaussian curves. Using pulse width modulation, we could then calculate the change in light per time step based on the input pulse duration. Display characteristics like pulse duration, interpulse intervals, and interpulse distances were calculated from [170] for *P. annecohenae* and from [59] for *P. morini*. Display characteristics for *Photeros* sp. "EGD" and "SFM" came from video recordings obtained for Gerrish et al. (in prep), as well as in-field measurements. As a note, we could not fully measure the distances between pulses (IPD) for either SFM or EGD. For SFM, we used field measures of total display length and divided it by the number of pulses per display to calculate IPD; and for EGD, we calculated IPD from stereoscopic recordings

taken in the field (Oakley et. al, in prep). We adjusted the relative brightness between pulses in a single display train, as subsequent pulses after the first pulse in a display are dimmer [170]. These data were pulled from [170] for *P. annecohenae* or from natural pulses recorded in the lab for the other three species (*P. morini*, SFM, and EGD). To reduce the overall brightness of the LEDs in the artificial displays, we used a maximum brightness of 12/255 for the LED output and placed 5 layers of 0.3 One-stop Neutral Density filters (Cinegel) in front of the LED strips, outside the tank.

Videos were recorded on a Sony A7S with a Canon 24mm lens attached via a Metabones EF-F lens mount. The camera had been debayered to remove the infrared filter, allowing us to illuminate the tank with an infrared lighting array placed at the top. For videos filmed in Belize, we used two 150um paint strainers folded in half and suspended 5 cm beneath the array to disperse the IR light as evenly as possible through the water. We placed black felt behind the tank to increase contrast. The tank measured 60.96 cm x 15.24 cm x 60.96 cm (Length x Width x Height). After our initial set-up in Belize, we modified our design for Panama. This tank measured 38.10 cm x 7.62 cm x 60.96 cm (Length x Width x Height), and to increase contrast, we used adhesive, matte black vinyl to cover the back, bottom, and two sides of the tank. We also slightly offset the position of the displays from one another in the Width-axis by 6 cm. In this way, acrylic opposite the displays could then be covered in vinyl to prevent reflections from being produced when the artificial displays were on. Two 114-LED IR lights arrays (CM Vision) were suspended side-by-side, 18.5 cm above the water level to provide sufficient illumination for trials. See Fig. C.1 for a diagram/picture of the experimental set-up.

Because the depth of our experimental tank was 56 cm, and because the length of both total display train and interpulse distances differ between the species, we were limited on the number of pulses per display we could show between species. See Fig. 4.1 and Table 4.2 for a summary of the display differences between the four species.

Despite species differences in the number of pulses per display, displays from respective congeners in the same country always overlapped in the range of the number of pulses in one another's natural displays. As a note, due to minor programming error with the brightness, the artificial displays of EGD lacked the last pulse as it was too dim for the LED output, and instead had 5 pulses per display (within the range of natural displays; Table 4.2).

4.4.3 Characterizing Trait Space

In order to better understand how our artificial experimental displays placed within the potential phenotypic space of natural displays, we used the measured means and standard deviations for 6 display characteristics to randomly generate 1000 artificial displays per species. In each display, we sampled from log-normal distributions of the pulse durations and interpulse intervals separately for the initiation and trill phases of natural displays. We used this aggregate dataset, along with display direction, to perform a Multiple Factor Analysis in the package 'FactoMineR' [85] on these variables (Fig. 4.1B) from the simulated data set only. We then projected our measured, control, and experimental display data into this MFA space to see how our observed and experimental displays compared to the potential variation in the simulated data based on real measures.

4.4.4 Animal motion and artificial display tracking during video analysis

We used the DeepLabCut [150] pipeline to automatically track ostracods in our tanks. Although originally formulated to track individual postural changes, because our videos were filmed in environments with heterogeneous lighting environments (both within and between videos), other approaches were not tractable. Briefly, we annotated clips for the

Species (ID code)	**Country**	**N_{sp}**	**N_{ind}**	**N_{vid}**	**Direction**	**N_{pul}**	**Train length**	**Source**	**N_{frames}**
P. annecohenae (PAN)	Belize	0	16/21	41/54	Up	12 (9 - 19)	35 (na)	[141] [170]	805
P. morini (PMO)	Belize	4	16/19	36/57	Down	7 (10 - 20)	62 (na)	[141] [59] [216]	60
P. sp. "EGD" (EGD)	Panama	1 (rare)	10/26	22/78	Down	6 (4 - 8)	24 (18 - 30)	Appendix D	635
P. sp. "SFM" (SFM)	Panama	1 (common)	11/28	16/78	Up	4 (3 - 6)	15 (13 - 15)	Appendix D	80

Table 4.2: Summary table of observed variation in natural displays for each species. N_{sp} is the number of co-occurring species found at the same time during the display period. N_{ind} is the number of individuals tested and N_{vid} is the number of videos recorded. Each individual had multiple videos. Fractions are the number of successful records over the total number of attempts. Direction is display direction. N_{pul} is the average number of pulses per train with the range in parenthesis. Train length is the average distance of the train in cm. with the range in parenthesis. N_{frames} is the number of frames used to train the neural network model.

position of the ostracod body across a range of behaviors and video qualities, sampling clips from each species. See Table 1 for details on the number of frames used. We then trained a 101-layered neural network for 500,000 generations to reliably predict ostracod position in our videos over time (Pixel error, post-training: 1.45).

Although our data are filmed, we could not precisely record the exact timing of experimental stimulus projection. We therefore used custom Python scripts written with OpenCV to find where pixel values spike in brightness over the course of each video. We limited our analysis to 33% of the tank where the LED strips were localized (first third or last third, respectively) and did so separately for both sides of the tank because stimuli were not always presented in sync due to differences in interpulse intervals. Videos vary in quality due to field conditions, and identification of stimulus onset is noisy. We used the findpeaks function of the 'pracma' package [17] to locate semi-periodic spikes in pixel brightness and return the time points of the 10 brightest peaks, corresponding to the 10 times each stimulus was presented to an animal during the recording of a single video (i.e. a single experiment). See Fig. C.2 for examples of peak identification using this method.

4.4.5 Trajectory creation, filtering, and and behavioral analysis

Despite using 1,580 frames to train our model for 500,000 generations, false positive errors in body identification are possible due to small particulates in the water. Simultaneously, false negative calls may be prominent due to low levels of infrared illumination that reduce reflectivity and positive identification. As such, we used three stages of post-hoc filtering to reduce the level of misidentified points in each file.

Firstly, we assume that false positives (misidentification of similar sized particulates with slow moving speeds) accumulate randomly with respect to the true ostracod po-

sition in the tank. During tracking, because body position is correlated between time steps and changes with a given speed, both positions and changes in position should have a finite distribution. Of all identified points, we retain only those in the bottom 75th percentile of the interquartile range to control for misidentification that leads to erroneous and spontaneous "jumps" in position. Although this method can remove extreme outliers, particulates are evenly distributed across the tank and misidentification may not lead to large jumps in body position. Change in value with a temporal correlation can be modeled using autoregression with moving averages. We fit our once-filtered data with these arimax models (R package 'forecast' [87], command auto.arima) and removed position data that exceeded the 95% confidence interval from models estimated on either x-position or y-position over time. After twice-filtering, we used the R package 'trajR' [130] and its functions to convert ostracod positions (x, y, time data) into movement trajectories, which includes information on change in relative position re-centered on the animal and not to external frames of reference. This produced 223,885 individual tracks. We then filtered these by duration to require total durations greater than 30 frames (equivalent to 1 second), leaving 10,866 trajectories.

Average trajectory duration was 5.17 seconds and covers 0.516 cm (approximately 3 body lengths of an average ostracod). However, even with extensive filtering, the inclusion of erroneous body positions can result in wildly inaccurate trajectories. We calculated summary statistics like average positional speed across a trajectory, directional change, average turn angle magnitude, and the expected relative displacement (E_{max}) and used principal components to characterize all 10,866 trajectories in multivariate space. We then confirmed the accuracy of these metrics in predicting real trajectories by looking at a subset of 55 known trajectories; these trajectories loaded differently on principle components 1 and 3, whose eigenvalues we used to further reduce our dataset to a final count of 7,749 trajectories. We use these to describe general movement patterns (speed

and sinuosity) before and after the onset of stimuli during an experimental trial. From our 55 known trajectories, we further characterize specific timing of behavioral changes to the exact onset of individual stimuli. Using the identified peaks of pixel brightness from the left and right sides of the tank, we split each of these trajectories into two by the incident timing of the stimulus onset: 5 frames before and 5 frames after stimulus presentation. We then looked at whether animals were currently facing a display when the stimulus was presented, and if their heading had changed after the stimulus turned off.

4.4.6 Statistical analysis

To describe differences in movement patterns (speed, sinuosity) between species from different ecologies and/or during different times during different experimental trials, we used generalized linear models (with the family set to Gamma distribution). Speed is the linear speed of a detected animal. Sinuosity is a measure of the straightness of a trajectory based on the mean cosine of turning angles: the larger the value, the straighter the path [14]. We used McNemar tests to see if individual animals in the course of their trajectories changed direction towards or away from an artificial display (experimental or control) randomly or not. However, these tests have low samples sizes and may fail to detect true patterns. Redescritizing events from headed towards or away from a display to trajectories that changed or did not change heading after a stimulus, we used a generalized linear model (family set to binomial) to perform a logistic regression asking how ecological history and display type influence the probability a female ostracod will switch her course.

4.5 Relevant Supporting Information

4.5.1 Ethics statement

All animals were collected with permission from the Belizean and Panamanian governments, respectively the Belize Fisheries (Permit #006-18) and MiAmbiente (Permits #SE/A-54-18, #SEX/A-78-18).

4.5.2 Author Contributions

NMH conceived of the experiment with help from TJR and GAG. RS wrote the codes to make artificial displays, with input from TJR and NMH. NMH collected video and analyzed data. NMH, GAG, and THO provided field and financial support. NMH wrote the manuscript with comments from all other authors.

4.5.3 Acknowledgements

We thank Dr. Harilaos Lessios at the Smithsonian Tropical Research Institute (STRI) for his support, as well as members of the STRI Bocas del Toro Field Station, especially Marcos Alvarez, for their assistance in completion of this project. Thanks also to Ryan Langlo (UCSB EEMB Machine Shop) and Dr. Lauren Sumner-Rooney for advice in experimental setup; and to Jason Goodman, Alexander Hakansan, and Brooke Webster for help with initial analyses. We'd like to extend our warm regards and appreciation to Junior and Rosie David, and to Ben, Luke, and Alex Zagorski for their personal support during this work. We are also very grateful to Marie Sharp's and Cayo's for making extremely palatable hot sauce and honey, respectively.

4.5.4 Funding

NMH was supported by the NSF GRFP and a STRI Short-term Fellowship; he received a Sigma Xi Grants in Aid of Research (G20141015722209), a block grant from the Department of Ecology, Evolution, and Marine Biology at UCSB, and a Lerner-Grey Grant for Marine Research from the American Museum of Natural History to fund this work.

Appendix A

Supplement for Chapter 2

A.1 Introduction

Here we provide (A.2) sufficient background on Michaelis-Menten kinetics as a review and context for the interpretation of our results, (A.3) further details on methods used in the study, and (A.4) results and model exploration.

A.2 Review of Michaelis-Menten enzyme kinetics

To facilitate understanding of our hypotheses and predictions derived from enzymatic theory within the context of bioluminescence, we reproduce derivations of the Michaelis-Menten equation below. In enzymology, reactions are dependent on the introduction of enzyme (E) and substrate (S), which react to form an enzyme-substrate complex (ES) and then dissociate with the generation of products (P) and the return to the enzyme's original state:

$$E + S \underset{\leftarrow k_r}{\overset{\rightarrow k_f}{}} ES \overset{k_{cat}}{\rightarrow} E + P$$

We assume that the reverse reaction of $E + P$ forming ES is negligible, or extremely unlikely. Different steps in the reaction can take place at different rates (denoted by k): production of the ES complex occurs at a forward reaction rate (k_f), the reverse reaction can theoretically occur at a rate k_r, and degeneration of the ES complex occurs at rate k_{cat}. In terms of cypridinid bioluminescence, this means that:

$$c - luciferase \ + \ vargulin \ + \ O_2$$

$$\underset{\leftarrow k_r}{\overset{\rightarrow k_f}{\rightleftharpoons}}$$

$$c - luciferase : vargulin$$

$$\xrightarrow{k_{cat}}$$

$$c - luciferase \ + \ light \ + \ oxyvargulin \ + \ CO_2$$

In sea firefly bioluminescence, molecular oxygen is assumed to be freely available in sea water; this assumption is validated because enzyme kinetic analysis show that the reaction is first-order (dependent on the concentration of one substrate - vargulin - as opposed to two substrates). The products oxyvargulin and carbon dioxide are inert with respect to our measured variable of light. We can further describe the rate of change in these variables in a system of equations that relate the concentration of each (denoted by square brackets [ ]) to rates k and their contribution to both formation and degradation:

$$\begin{aligned}
\tfrac{dS}{dt} &= -k_f[E][S] \ + \ k_r[ES] \\
\tfrac{dE}{dt} &= -k_f[E][S] + k_r[ES] + k_{cat}[ES] \\
\tfrac{dES}{dt} &= k_f[E][S] - k_r[ES] - k_{cat}[ES] \\
\tfrac{dP}{dt} &= k_{cat}[ES]
\end{aligned}$$

Michaelis-Menten dynamics assume a steady-state reaction such that the rate of change in ES complex formation is equal to zero during substrate saturation. Further, we know that the total amount of enzyme is constant in the reaction, making both E and ES add to some E_{tot}. So in order to calculate the change in product over time

($\frac{dP}{dt}$), we must solve for the concentration of the ES complex. Given these substitutions:

$$k_f[E][S] = k_r[ES] \ + \ k_cat[ES] = (k_r \ + \ k_{cat})[ES]$$

$$k_f([E]_{tot} \ - \ [ES])[S] = (k_r \ + \ k_{cat})[ES]$$

$$k_f[E]_{tot}[S] \ - \ k_f[ES][S] = (k_r \ + \ k_{cat})[ES]$$

$$(k_r \ + \ k_{cat})[ES] \ + \ k_f[ES][S] = k_f[E]_{tot}[S]$$

$$[ES] = \frac{k_f[E]_{tot}[S]}{(k_r \ + \ k_{cat}) \ + \ k_f[S]} = \frac{[E]_{tot}[S]}{(\frac{k_r + k_{cat}}{k_f}) \ + \ [S]}$$

$$\frac{dP}{dt} = \frac{k_{cat}[E]_{tot}[S]}{(\frac{k_r + k_{cat}}{k_f}) \ + \ [S]}$$

This final equation gives us the relationship between the change in product (light) over time in terms of a few measurable variables and some composite metrics of the reaction. Namely the composite metrics are the biochemical parameters V_{max} and K_m, defined as:

$$V_{max} = k_{cat}[E]_{tot} \tag{A.1}$$

$$K_m = \frac{k_r \ + \ k_{cat}}{k_f} \tag{A.2}$$

Which when substituted into $\frac{dP}{dt}$ gives the Michaelis-Menten equation in terms of product formation. As shown here, V_{max} relates directly to the amount of enzyme available to the reaction, whereas K_m relates the different k rates in the reaction to one another, independent of any concentration. Both these biochemical parameters rely on k_{cat}. To increase the rate of product formation for any given amount of substrate and enzyme, you can either raise the maximum reaction rate (V_{max}) or decrease the enzyme affinity for the substrate (K_m).

A.3 Materials & Methods

A.3.1 Notes on induced bioluminescent phenotyping

We attempted to record from 630 individuals, but not all animals produced bioluminescence of quality for downstream analysis. Of the 376 individuals successfully recorded from, we identified 837 defensive pulses with our program. See summaries for Tables A.4 - A.6 for sampling details.

Animals were subjected to two different stimulation regimes depending on their length of time within the vial; electrical impulse programs were written via custom Arduino scripts. We initially stimulated all animals with three 12.5 V bursts for 10 ms, with 5 ms intervals separating each electrical pulse (low-stim condition). If no bioluminescence was detected, they were given approximately 10 s to recover before applying another stimulus; if the animal generated bioluminescence, that pulse was allowed to fade and the animal was given 10 s before application of another stimulus. If an animal failed to bioluminesce within the first six stimulations, they were subjected to a single 12.5 V stimulus burst for 50 ms (high-stim condition). We used experience developed during preliminary trials to judge when to switch between high and low-stim programs. If an animal reacted to the stimulus, they were subjected to more stimulation until, at most, 3 clean light pulses were recorded. We deemed light pulses as adequate and "clean" if they were produced without multiple peaks and if light output eventually faded back down to undetectable levels from background. If an animal failed to react within 5 minutes of testing, they were removed.

To note, using intensity is an inaccurate estimation of product formation as it is unknown what the quantum yield (i.e. photon release) per substrate oxidized is, or if this differs by species. Quantum yield can vary due to pH, salinity, or even temperature [193]. To address this, we attempted to standardize conditions by using location-available

seawater at ambient temperatures (24 - 26). Variation could also be compounded by the PMT, which has a biased sensitivity and propagates more voltage to certain wavelengths (maximum sensitivity: 380 nm; Burle Electronic Tubes). Cypridinid bioluminescence is primarily blue (around 470 nm; [86]), but there is seemingly some variation in this trait [74]. At worst, our PMT has a 10% drop in sensitivity for light propagating from 450 to 500 nm, which is most likely a greater difference in peak emission than the differences we observe. Thus, any error because of a mismatch with peak wavelength emission or due to quantum yield fluctuations should be minor.

Although decays could vary because of differences in encounter rate between enzyme and substrate, the stimulated pulses were in a finite volume of seawater and much smaller than defensive pulses produced during predation. We cannot fully discount this possibility, but our methodological controls and replicates help separate inter-individual noise from true differences between species.

A.3.2 Notes on induced bioluminescent phenotyping data analysis and results

Each file, exported from .DAQ to .CSV using the WinDAQ program, was parsed to remove background values and small fluctuations in measurement due to electrical noise (Fig. 2.1A #2). Backgrounds were calculated as the average amount of light from the first ten time points per file plus the absolute value of the lowest of those ten points. We required waveforms to have a minimum peak height of 1 V after background normalization, and each had to be separated by at least 0.03 s to be considered a separate pulse (Fig. 2.1A inset). We cropped each waveform from its highest point until it decayed back to the minimum level recorded (background; Fig. 2.1A blue shaded region); the background value was calculated from the average of first 10 time points of the file (Fig.

2.1A #1) and used to initiate starting conditions in our models (I_0 and S_0). Waveforms were normalized after background removal by calculating the difference between 1 - background and rescaling the y-axis (Fig. 2.1A #2). In order to find the exponential decay of the waveform, we then calculated the slope between consecutive time point pairs and restricted the data to be from the point at which the steepest slope occurred down to the background (Fig. 2.1A #3), whose slope value is used to initiate V_{max} estimates. These decays were required to have a minimum of 20 data points for proper modeling downstream. After waveform identification, the time was rescaled to be from 0 msec until the time at which light levels returned to background levels. To initiate values of K_m for model fitting, we identified the voltage at which the reaction is at half its maximum slope or the time point at which the reaction has reached half its maximum length, although these two values are not necessarily the same point (Fig. 2.1A #4). Decay length was calculated as the last datum retained above the background (Fig. 2.1A #5). For species from Panama, we had to back-calculate time intervals post-sampling due to experimental error. We used the known sampling rate (120 Hz) and total number of data points to generate time points every 0.017 s, which approximates the true time points to the 0.0001 s.

When fitting models during data exploration, we actually fit all waveform data to 3 different models. The second model (below) was an exponential decay based on first-order reaction kinetics that collapses Euler's number and the λ parameter into a single estimated constant that can then be then further partitioned into enzyme kinetic parameters as in [232]:

$$I = I_0(1 - \alpha)^t \tag{A.3}$$

We provide the results of this model here in the supporting information (Fig. A.3). All methods used when calculating *lambda* from Eqn 2.1 in the main text were also used with

this model. Decay estimates for the log-transformed α constant were different between species (Fig. A.3, Fig. A.4, Linear mixed effect model, Species $p < 0.001$, Max Intensity $p = 0.2411$).

Both Eqn 2.1 and Eqn A.3 cannot infer the biochemical parameters relevant in steady-state Michaelis-Menten kinetics (V_{max} and K_m [5], Eqn A.4), which describe the change in substrate (S) over time by relating substrate concentration with: V_{max}, the maximum reaction rate; and K_m, the substrate concentration at half the maximum rate (a metric of enzyme affinity for a given substrate). To estimate these parameters from decay (not steady-state), we applied a third model that uses a real-time, integrated solution of Michaelis-Menten kinetics from [65]:

$$S = K_m \times \mathbf{W}\left\{ \frac{S_0}{K_m} e^{\frac{S_0 - V_{max} * t}{K_m}} \right\} \tag{A.4}$$

In Eqn A.4, S and S_0 are the concentration of substrate at time t and the initial concentration of substrate at $t = 0$, respectively. Because the relationship between substrate and product is the same as substrate oxidation and light production in our case, we substituted in the amount of light produced (I and I_0 as in Eqn 2.1) for S and S_0 values. In Eqn A.4, $\mathbf{W}$ is the Lambert function, and S_0 (now I_0), V_{max} and K_m are estimated parameters. For quality control, we visually inspected all decays and model fits post-processing.

In order to obtain reasonable starting values to initiate each model, we started I_0 at the background level of voltage (described above), similar to [7]. In Eqn 2.1, we initially set λ as the natural log of 2 divided by the time point at which the decay had proceeded to half its total length (Fig. 2.1A #4). In Eqn A.3, α was set at 1 minus the natural log of 2 divided by the time point at which the decay had proceeded to half its total length. In Eqn A.4, we initiated V_{max} at the greatest difference between consecutive time points

(i.e. the greatest slope along the length of the curve), and K_m at the voltage level at half the maximum slope. We constrained all parameters between (0, +Inf) during likelihood searching. During visual model inspection, model fits were drawn graphically onto the observed decays: λ models of Eqn 2.1 are in red, dashed lines, α models of Eqn A.3 are in blue, and real-time Michaelis-Menten models of Eqn A.4 are in green. After adjusting for model fit and potential editing errors, each model retained a variable number of defensive pulses: 322 pulses remained from 180 individuals of 34 species when estimating when estimating λ (Table A.4); 312 defensive pulses remained from 175 individuals of 34 species α (Table A.5); and 287 defensive pulses remained from 161 individuals of 38 species when estimating V_{max} and K_m (Table A.6). In most cases, Eqn 2.1 and Eqn A.3 were equivalent in fitting the observed data. When possible to compare between models, Eqn A.4 was always a better fit than Eqn 2.1 or Eqn A.3.

Methodological sources of variation may be inherent to the model fitting procedure, as seen when comparing the level of decay variation between λ and $\alpha$for each species (Fig. 1 and Fig. A.3). Estimates of α for each species have much higher levels of variation than those for λ, despite the models' relatively equitable fit to the data (AICc comparisons between these two models are nearly always identical; see Tables A.4 and A.5). However, this should contribute minor levels of variation equally across our sampling, and most likely does not explain larger patterns of variation across species.

From the literature, we pulled decay data for *Vargula hilgendorfii* (previously *Cypridina hilgendorfii*) from Figures 3C and 4A of [73], and Figure 1B of [204], and for *Cypridina serrata* from Figure 2 of [220] using WebPlotDigitizer. As a note, *V. hilgendorfii* decays are from mixtures of organismal extracts, not living animals. Because these species were interpolated from previously published graphs, we did not enforce a minimum number of data points. We could not ensure that each waveform was from a single individual, and therefore independent, so we averaged these data to give a single datum for each species.

Our data further formalize the pattern of variation more broadly across the group, greatly expanding the taxonomic sampling as well as the amount of variation across species. Some species appear more variable than others in their decay constants. We recapitulate the previous findings for *V. hilgendorfii*, *C. serrata* and *P. annecohenae*, but to varying degrees. For *P. annecohenae*, our results match well within the range of decays measured for defensive displays from [173]. For *V. hilgendorfii* and *C. serrata*, we do not recover the same decay constants as [220] but their exponential model is unspecified, and data fitting procedure predates our computational methods. Generally, these results are in agreement with previous studies.

A caveat to our estimation of enzyme parameters is that we cannot directly measure substrate concentrations, and instead used maximum light intensity as a proxy for the amount of product (i.e. light) generated in the reaction. In this way, we cannot make comparisons to the known values of V_{max} or K_m for the two species *V. hilgendorfii* and *C. noctiluca*. Also, the correlation between V_{max} and K_m only represents an upper limit to how much k_{cat} influences both biochemical parameters. This is because k_{cat} may or may not be correlated with other rates in the reaction (k_f and/or k_r), which contribute to the magnitude of K_m as well. However, we can conclude that k_{cat} is non-zero because of the strong correlation between V_{max} and K_m after controlling for maximum intensity of stimulated defensive pulses.

Maximum intensity does significantly explain patterns of decay variation, but so does species level identification. From a mechanistic perspective, the decay of our initial model (Eqn 2.1) is simply a different way to measure the variables from the other equations (Eqn A.3 and A.4). Thus λ from Eqn 2.1 is due to compound action from the variables in Eqn A.4, namely K_m, V_{max}, and S. Variation in any one of these parameters may explain variation in our estimates of lambda. Our continued analysis in this supplement provides evidence that variation in enzyme function (k_{cat}) is real (see below). We include

maximum intensity as a co-variate in our models to control for noise due to these factors. Other mechanisms may describe intraspecific variation in decay including interindividual variation in c-luciferase sequence, or differences in the regulation of other secretion components with the c-luciferase/vargulin complex. The latter is most likely the difference between context-dependent decay rates in defensive versus courtship display pulses in *P. annecohenae* [173].

A.3.3 Notes on courtship pulse duration data

In WebPlotDigitizer, each species' courtship pulse duration data was analyzed separately using their respective colours to differentiate them. We extracted each data point corresponding to the beginning and ending of the first three courtship pulses and exported the file into Microsoft Excel. To calculate duration for the first pulse, we subtracted the end time point (x-axis value) for pulse 1 from the beginning time point for pulse 1; this was repeated for pulses 2 and 3. We averaged the first three courtship pulse durations per species.

A.3.4 Notes on transcriptome processing and phylogeny

UUsing Magic-BLAST v1.1.0 [151], we queried forward and reverse reads against a blast database of the *V. hilgendorfii* mitochondrial genome. The resulting hits were extracted using SeqTK v1.2 [190] to create new forward and reverse reads containing potential blast hits of each species' mitochondrial genes. We used Geneious [99] to annotate the *V. hilgendorfii* reference mitochondrial genome into individual genes. We then used the Smith-Waterman algorithm in BWA v0.5.9 [112] to annotate assembled contigs. As transcriptomes were prepared from up to 10 individuals, we created consensus sequences and denoted polymorphic sites with an N. We performed a second search using

all mitochondrial hits as bait in MagicBlast to recover more mitochondrial sequences, using the steps described above. We aligned individual gene datasets using MAFFT v7.305 [96], and used trimAl v1.2 [26] as a site-trimmer with the automated1 function. We concatenated the genes using Phylocatenator v2.0 implemented in Osiris [156].

In constructing a phylogeny with our taxa for PGNLS, we recovered monophyly of previously proposed genera: *Photeros* (P), *Kornickeria* (K), and an unnamed "H"- group (H) [141, 59, 140]. As a note on species identity, in previous publications, Bz SVU is also called MWU and Bz SVD is also called ZZD. Recent work as named the "H"-group as the genus *Maristella* and named Bz MSH as *Maristella chicoi* [168].

For use in phylogenetic comparative regressions, it is advised to use an ultrametric tree [56]. To make our tree ultrametric, we used the "chronopl" function in 'ape', setting the maximum age of the tree to 1.0 and using cross validation option as CV=TRUE. We did this across a range of lambda smoothing values, ultimately choosing a smoothing value that minimized the cross validation. The tree was then transformed using a lambda value of 10,000 to make it ultrametric and ready for PGNLS analysis.

A.3.5 Notes on model comparisons, outliers, and model selection

In our comparisons with other linear and non-linear models, we discovered the species "Ro GPH" is sometimes but not always a statistical outlier, hinting at its strong influence in our analyses generally. We also performed our model comparisons without this species, which did change the residual squared error of the models (Table A.1, Fig. A.6).

For the species "Ja PJA" we could only obtain a single value for its decay. This prevented us from calculating a standard error, and in turn, from using it in our weighting scheme. To address this, we performed two types of analyses: (1) as described in [89],

we used the standard error of lambda from the whole dataset and assumed it to suffice for the individual standard error of lambda for "Ja PJA", or (2) we excluded "Ja PJA" from the analysis. From Table A.2, any results with a weighting scheme not explicitly excluding "Ja PJA" uses the former strategy in order to include that species.

A.4 Results

A.4.1 No other estimated model parameter describes courtship pulse duration

Other metrics of c-luciferase identity (natural log of α, V_{max}, and K_m) did not describe differences in courtship pulse duration between species (Fig. A.7A natural log-α, Linear regression $p = 0.3719$, Bonferroni corrected $p = 1.000$; Fig. A.7B natural log-V_{max}, Linear regression $p = 0.1231$, Bonferroni corrected $p = 0.4923$; Fig. A.7C natural log-K_m, Linear regression $p = 0.0806$, Bonferroni corrected $p = 0.3224$). The lack of significance between other parameters could be due to a few reasons. First, small sample size may limit our power to detect a pattern. Second, insufficient contributions by either enzymatic parameter (V_{max}, K_m) separately to the phenotype may not describe overall enzyme kinetic dynamics sufficiently as they may act synergistically. Third, decay rates from defensive pulses and courtship pulses have been found to differ [173] and although we find that the defensive pulse decay constant correlates with courtship pulse duration generally, noise around these other estimates of defensive pulse decay may decrease our power to detect a pattern.

A.4.2 Methodological controls for differences in c-luciferase function reveal variation in k_{cat} between species

Variability in our decay measures may be due to differences in the total concentration of enzyme available, as well as differences in the enzyme ability (k_{cat} in Eqns A.1 and A.2), neither of which were directly measurable but both contribute to the maximum amount of light per pulse. We can infer differences between species in enzyme function by analyzing the relationship between two different enzyme parameters V_{max} and K_m; these parameters share an underlying mechanism, the enzyme ability k_{cat}, but only V_{max} is affected by enzyme amount. We could not measure enzyme amount or k_{cat} directly, but by using variation in the maximum intensity per defensive pulse and then comparing the relationship between V_{max} and K_m, we can infer differences in k_{cat}. To see if species ID contributed to V_{max}, K_m, and the strength of their correlation (k_{cat}) after controlling for the brightness of each pulse, we performed a series of reduced dimension analyses ("rda" function in the 'vegan' package) using natural log-transformed V_{max} and K_m as the independent variables, and maximum intensity and species ID as explanatory variables in a full RDA model *sensu* [18]. We alternated each dependent variable (max intensity or species ID) as a conditional variable to partition the contribution of each to the observed levels of variation in the estimates of natural log-transformed V_{max} and K_m. To see how strongly enzyme amount affected enzyme function estimates, we used 'atan2' to compare the strength of correlation between log-transformed V_{max} and K_m in the full and conditioned models.

There were statistically different enzyme kinetic parameters between species (natural log V_{max}, Kruskal-Wallis test p = 0.0005; natural log K_m, Kruskal-Wallis test p = 0.0139). We find that species identity does significantly explain variation in ln V_{max} and ln K_m (Fig. A.5, $F_{39,246} = 3.233$, p = 0.001). A full RDA model explained 61.6% of the

variation in ln V_{max} and ln K_m; when partitioning variance between different explanatory variables (using conditioned RDA models), maximum intensity explained 14.55% of the variation, and species status explained 33.20%. Of these, both species status and brightness shared 4.24% of the explained variance. We detected a correlation between V_{max} and K_m as indicated by angle of their eigenvectors in RDA space (Fig. A.5, 32.14°or 84.67% correlation). Thus, species have different abilities to produce light, reflected in k_{cat} as a factor of enzyme identity.

A.5 Supplementary Tables for Chapter 2

For Tables A.3 - A.6, please see Dryad Digital Repository. We provide the captions below for ease.

Model	Relationship	RSE (all species)	RSE (without Ro GPH)	Color in Fig. A6
$P = \lambda$	Linear	2.1514	1.9915	Red
$P = ln(\lambda)$	Linear	2.1048	1.7302	Blue
$P = e^{-\lambda}$	Non-linear	2.9294	1.9151	Green
$P = \lambda + \frac{1}{\lambda}$	Non-linear	4.2887	4.4372	Purple
$P = \lambda$	Non-linear	4.1799	4.3126	Orange
$P = \lambda$	Non-linear	**2.4937**	**1.6274**	Black
$P = \lambda$	Non-linear	2.8619	1.6472	Grey

Table A.1: Models results and residual standard error (RSE) for different linear and nonlinear models used to explore the relationship between courtship pulse duration (P) and enzyme identity (λ). After initial data plotting determined the relationship was nonlinear, the best model was chosen using minimized RSE for further PGLS analysis, highlighted in bold. As indicated in the columns, RSE values correspond to Fig. A.6.

Dataset	Phylogeny	Weights	Model	Intercept	P-value	RSE	AICc	ΔAIC	Prefer phylo?
All	No	No	Inverse	7.739006	1.16×10^{-5}	2.493704	78.5371	2.08622	no
All	No	Yes	Inverse	9.058946	1.37×10^{-6}	1.570038	76.45088	0	no
All	Yes	No	Inverse	3.594654	0.1028	6.459745	89.00902	12.55814	-
All	Yes	Yes	Inverse	4.012306	0.2017	4.158752	87.63622	11.18534	-
noPJA	No	No	Inverse	7.01501	4.28×10^{-5}	2.333949	71.96011	0.54664	same
noPJA	No	Yes	Inverse	8.845426	4.27×10^{-6}	1.589833	71.41347	0	no
noPJA	Yes	No	Inverse	1.745401	0.2388	4.242951	71.89939	0.48592	-
noPJA	Yes	Yes	Inverse	2.908101	0.3186	3.812809	79.66394	8.25047	-
noGPH	No	No	Inverse	9.770998	3.45×10^{-8}	1.627425	61.14323	0	no
noGPH	No	Yes	Inverse	9.953529	1.78×10^{-7}	1.327073	65.99205	4.84882	no
noGPH	Yes	No	Inverse	11.20271	4.12×10^{-4}	4.610553	74.80346	13.66023	-
noGPH	Yes	Yes	Inverse	8.896747	3.61×10^{-2}	3.875672	80.56412	19.42089	-
minus2	No	No	Inverse	Intercept	1.82×10^{-7}	1.519753	55.50301	0	no
minus2	No	Yes	Inverse	Intercept	6.82×10^{-7}	1.348477	61.40441	5.9014	no
minus2	Yes	No	Inverse	Intercept	4.93×10^{-2}	3.957051	66.6856	11.18259	-
minus2	Yes	Yes	Inverse	Intercept	0.1464	3.773347	74.60399	19.10098	-

Table A.2: Inverse model comparisons from Table A.1 with and without weights, phylogeny, and/or certain species. Dataset indicates whether all 16 species were used in the analysis ('All'); whether data from a species was excluded: 'noGPH' indicates Ro GPH was excluded because it was highly influential in the model exploration phase, while 'noPJA' excludes Ja PJA because we only had one measure of its decay values; 'minus2' indicates that both species mentioned were removed for a total of 14 species. The intercept column indicates if the estimated coefficient of the inverse model; P is the p-value of the model; RSE is the residual standard deviation of the error. RSE and AICc are from ML estimates. With phylo indicates, for any pair of models that only differ in their inclusion of the phylogeny, which is best supported by AICc

Table A.3: Species identified and average length, heights, eye, keel, and length:height measurements used for identification along with sample size (N) and standard errors for each (SE). Initials of researcher who performed collection or measurements as in the acknowledgements of the main text. All measures are in millimeters (mm). Citations for species descriptions are found on the 2nd tab of the file.

Table A.4: Individual model results for all identified pulses for lambda (λ) models of Equation 2.1. Brightness is the maximum intensity (in volts) recorded per identified peak (peakID) for an individual (ind). Time is the length of decay until return to background. RSS is the residual squared error, AIC is the model fit, and quality is a binary assessment ("n" for n) of whether the model fit is acceptable. Only models deemed acceptable were used for downstream analysis. Estimated parameters are Lambda (λ) and the asymptote of the decay (asymp_L), which corresponds to the initial intensity (I_0).

Table A.5: Individual model results for all identified pulses for alpha (α) models of Equation A.3. Brightness is the maximum intensity (in volts) recorded per identified peak (peakID) for an individual (ind). Time is the length of decay until return to background. RSS is the residual squared error, AIC is the model fit, and quality is a binary assessment ("n" for n) of whether the model fit is acceptable. Only models deemed acceptable were used for downstream analysis. Estimate parameters are Alpha (α) and the asymptote of the decay (asymp_A), which corresponds to the initial intensity (I_0).

Table A.6: Individual model results for all identified pulses for Michaelis-Menten models of Equation A.4. Brightness is the maximum intensity (in volts) recorded per identified peak (peakID) for an individual (ind). Time is the length of decay until return to background. AIC is the model fit, and quality is a binary assessment ("n" for n) of whether the model fit is acceptable. Only models deemed acceptable were used for downstream analysis. Estimated parameters are K_m, V_{max}, and S (substrate concentration at time t, but measured in intensity). See methods for details.

A.6 Supplementary Figures for Chapter 2

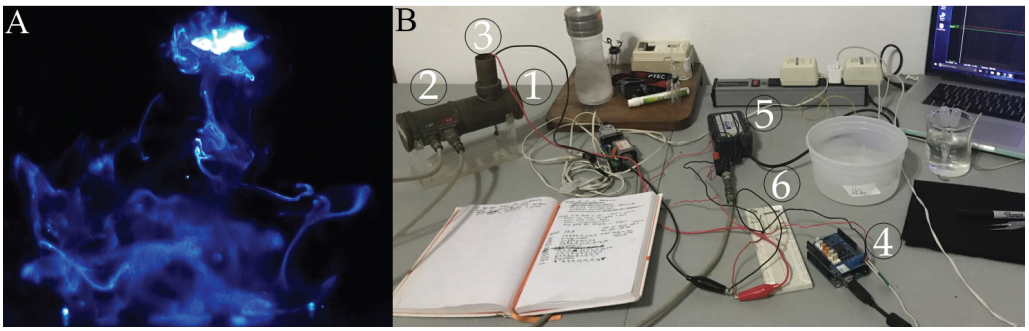

Figure A.1: (A) An ostracod secreting bioluminescence in response to attack. The fish is illuminated with bioluminescence in its gut; its eye is visible as the dark circle. (B) Experimental setup to record stimulated defensive pulses. Labels are: (1) photomultiplier tube (PMT) and housing to collect light output over time, (2) PMT power supply and data output, (3) scintillation vial for live individuals, (4) Arduino Uno for stimulation, (5) DATAQ data collector, (6) breadboard to integrate data input and stimulation output.

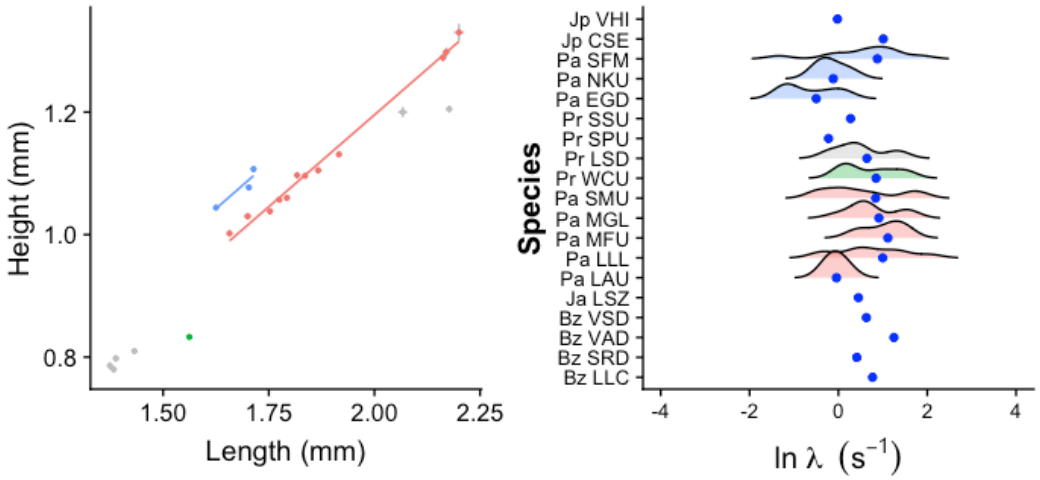

Figure A.2: Different decay constants (λ) between species indicate differences in enzyme activity. Panels are the same as in Fig. 2.2, but without phylogeny. (A) Length and height measures for the remaining 20 species of bioluminescent ostracod; genera position is inferred from measures in Table A.3. (B) Density plots with means (blue dots) are the interpolated distribution of each species' decay constant. For species with less than 3 estimates, no density plot could be generated. Note the x-axis is scaled to match that of Fig 2.2B in the main text to ease comparisons. The first two letters of each ID are country of origin (Bz = Belize, Ja = Jamaica, Pa = Panama, Jp = Japan, Pr = Puerto Rico, Ro = Roatan), followed by a species-specific identifier. Most are undescribed, but described species are as follows: VHI = *Vargula hilgendorfii*, CSE = *Cypridina serrata*.

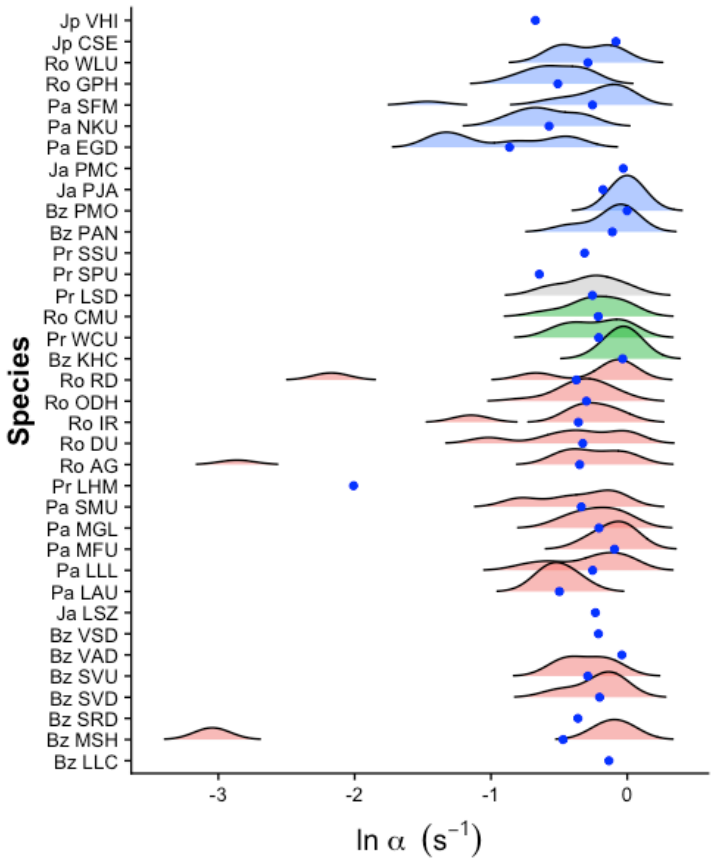

Figure A.3: Different species have different decay constants. The α constant from Eqn A.3. Density plots with means (blue dots) are the distribution of each species' decay constant. For species with less than 3 estimates, no density plot could be generated. Ordered and colored by genus: *Photeros* = blue, equivocal between *Kornickeria* or *Maristella* = grey, *Kornickeria* = green, and *Maristella* = red). First two letters of each ID are country of origin (Bz = Belize, Ja = Jamaica, Pa = Panama, Jp = Japan, Pr = Puerto Rico, Ro = Roatan), followed by a species-specific identifier. Most are undescribed, but described species are as follows: VHI = *Vargula hilgendorfii*, CSE = *Cypridina serrata*.

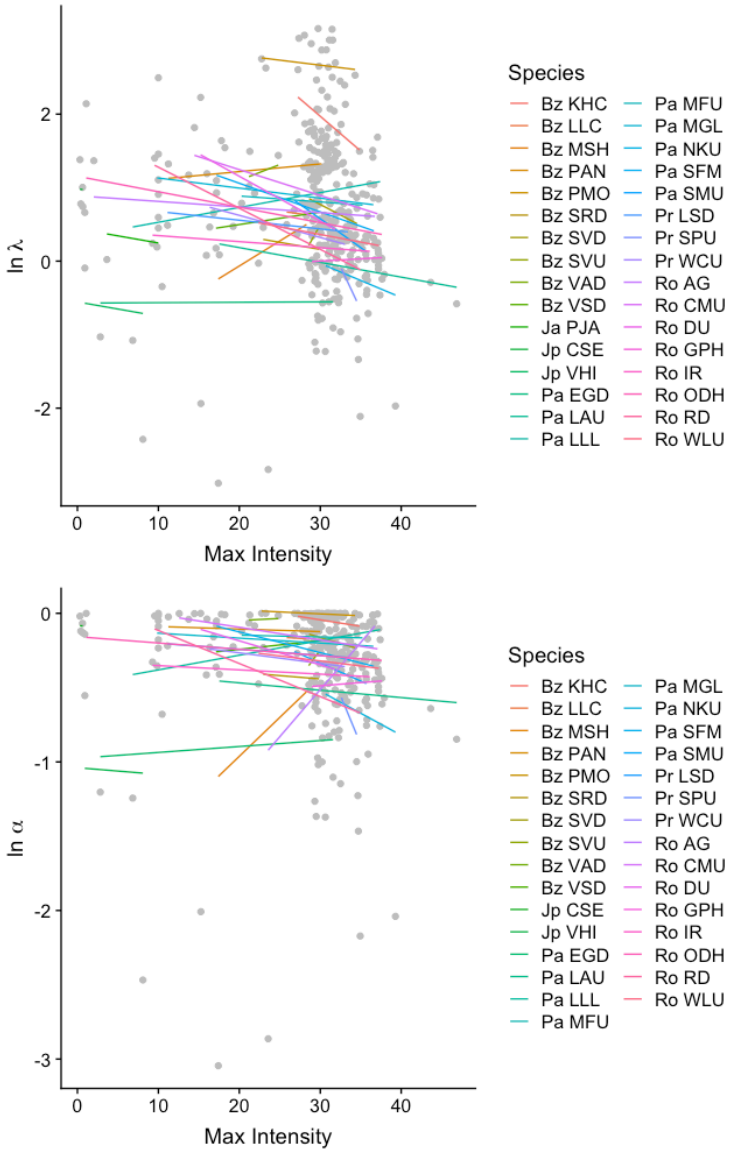

Figure A.4: Linear mixed effect model results describing differences between species in transformed decay constants (A) λ and (B) α. Note that species have drastically different slopes and intercepts generally. Grey data are individual decay parameter estimates from Tables A.4 and A.5, respectively.

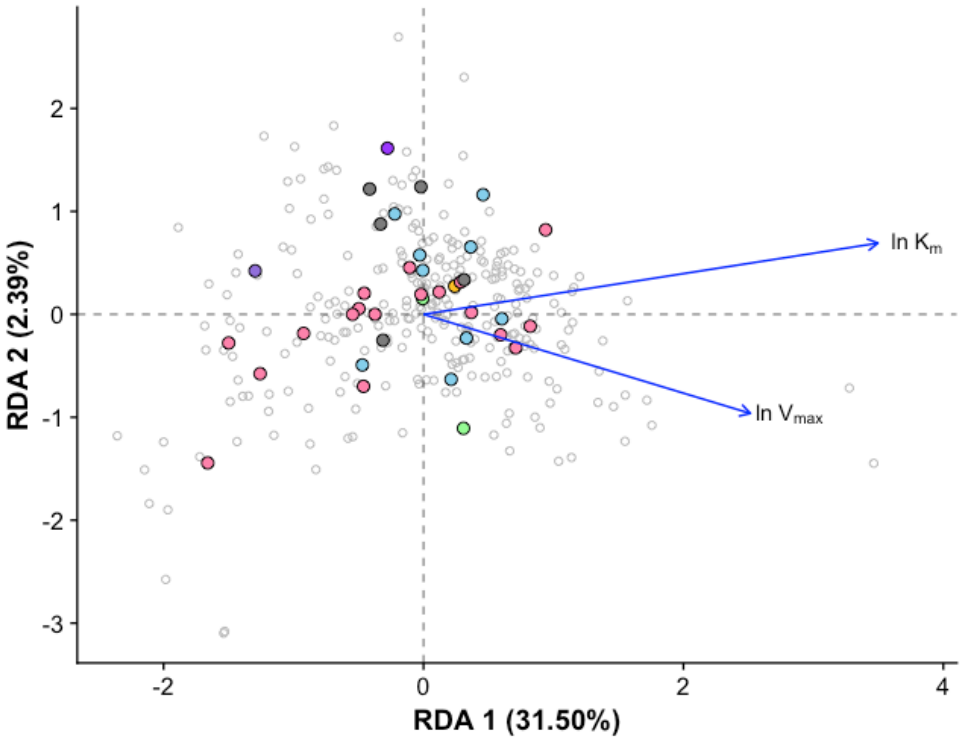

Figure A.5: Different biochemical parameters (natural log-V_{max} and natural log-K_m) between species reveal strength of inherent enzyme ability (k_{cat}) as a component of identity. Results from reduced dimensions analysis with individual data as open circles. Blue arrows are projections of natural log-V_{max} and natural log-K_m after controlling for the maximum intensity per defensive pulse. Centroid values for each species are coloured by genus: *Photeros* = blue, equivocal between *Kornickeria* or *Maristella* = grey, *Kornickeria* = green, *Maristella* = red, "C"-group = purple, non-signaling out groups from the literature = gold). Biplot scaled to response variable depicting correlational structure of the model. As both enzyme ability and enzyme amount contribute to variation in estimates of V_{max}, controlling for maximum intensity accounts for changes in available enzyme. The power of enzyme ability, k_{cat}, can then be inferred from the strong correlation between V_{max} and K_m. If there were no differences in enzyme ability between species, V_{max} and K_m would not be correlated (90° from one another).

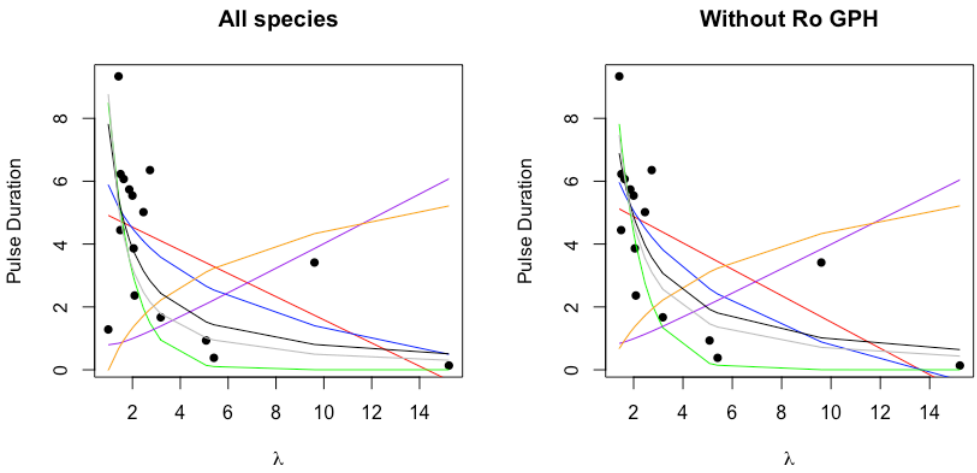

Figure A.6: Model fit between courtship pulse duration and c-luciferase identity (λ). Models fits from Table A.1. Raw data are black dots. Each model is drawn in the corresponding color from Table A.1. Note that in red is a linear model and all other models are nonlinear.

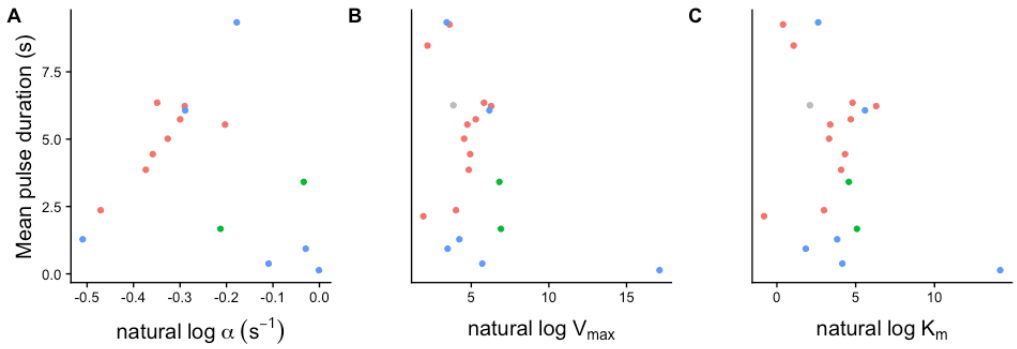

Figure A.7: Courtship pulse duration does not relate to other estimates of c-luciferase identity. (A) α from Eqn A.2, and (B) ln V_{max}, and (C) ln K_m from Eqn A.4.

Appendix B

Supplement for Chapter 3

B.1 Supplementary Tables for Chapter 3

Please see the Github Repository linked in Chapter 3 for all these data. Statistical results and summary tables are repeated herein for ease of reference.

Culture	Comp.	Test	Value	Std. Error	DF	T	P	Corr.
Mammal	HEK & P_mor	T	na	na	8.39	-4.76	0.0000	0.0000
Mammal	HEK & M_SVU	T	na	na	11.92	-14.91	0.0000	0.0000
Mammal	HEK & V_tsu	T	na	na	11.25	-15.92	0.0000	0.0000
Yeast	Before & After (C_noc)	T	na	na	8.75	5.79	0.0000	0.0000
Yeast	Before & After (K_has)	T	na	na	4.68	3.18	0.0300	0.1100
Yeast	Before & After (M_SVU)	T	na	na	11.50	2.62	0.0200	0.0900
Yeast	Before & After (V_tsu)	T	na	na	4.60	4.88	0.0100	0.0200
	Model effects							
Yeast	*Pichia* after	LMEM	2.13	0.85	53.00	2.50	0.0200	
Yeast	C_noc	LMEM	3.17	0.98	19.00	3.23	0.0000	
Yeast	K_has	LMEM	0.88	1.04	19.00	0.85	0.4100	
Yeast	M_SVU	LMEM	0.57	0.95	19.00	0.60	0.5500	
Yeast	V_tsu	LMEM	0.49	1.04	19.00	0.47	0.6500	
Yeast	Before	LMEM	-0.09	0.28	40.00	-0.31	0.7500	
Yeast	C_noc * Before	LMEM	-2.83	0.36	40.00	-7.87	0.0000	
Yeast	K_has * Before	LMEM	-2	0.39	40.00	-5.09	0.0000	
Yeast	M_SVU * Before	LMEM	-0.7	0.32	40.00	-2.19	0.0300	
Yeast	V_tsu * Before	LMEM	-1.26	0.39	40.00	-3.21	0.0000	

Table B.1: Statistical results for luciferase expression *in vitro* from key comparisons. Test is either: T-test (T) or Linear Mixed Effect Model (LMEM). Culture is the cell culture type compared. Comp. are the groups being compared within each culture type. Before and/or After refer to the timing of substrate addition to the culture media in each test. T is the T-value from the respective test. P is the p-value from the respective test. Corr. is the corrected p-value for multiple comparisons, if needed.

Species	# Genes BLAST-p	Proteins Expressed
Vargula hilgendorfii	145	81
Maristella sp. "SVU"	116	61
Photeros annecohenae	99	32
Kornickeria hastingsi carriebowae	183	56

Table B.2: Summarized BLAST search and Tag-seq mapping results.

Model	AIC or AICc	AIC / AICc	Dataset
OLS	AICc	261.1865	Old mutagenesis, new color, & tx-ome combined
BM	AICc	355.176	Old mutagenesis, new color, & tx-ome combined
OLS	AIC	-3.98076	New color & tx-ome only
BM	AIC	3.636894	New color & tx-ome only
OLS	AICc	-285.7653	Previously published decay & new tx-ome only
BM	AICc	-244.4218	Previously published decay & new tx-ome only

Table B.3: Comparison between phylogenetically uncorrected (OLS) or corrected (BM) models. Models were compared only within datasets by lowest AIC or AICc score.

Primer name	**Target species**	**Sequence**	**Purpose**
KHC Forward	*Kornickeria hastingsi carriebowae*	GGACTCGAGAAGAGAGA GGCTAAAGATTGTTTTG AATCATCTTTCC	Amplify from cDNA
KHC Reverse	*Kornickeria hastingsi carriebowae*	AGCGGCCGCTTTGGTGC ATTGAGGTGG	Amplify from cDNA
PMO Forward	*Photeros morini*	TAACTCGAGAAGAGAGA GGCTCAAGAATGCGCTC AGACA	Amplify from cDNA
PMO Reverse	*Photeros morini*	AGCGGCCGCCTGGCATA TGGCTGGTAC	Amplify from cDNA
SVU Forward	SVU (undescribed)	GGGCTCGAGAAGAGAGA GGCTCAAGATTGTTATG AATTCACA	Amplify from cDNA
SVU Reverse	SVU (undescribed)	AGCGGCCGCTTTACACTG AGGGGGATA	Amplify from cDNA
SVD Forward	SVD (undescribed)	GTGCTCGAGAAGAGAGA GGCTGAAGATTGTTATG AATTCACATG	Amplify from cDNA
SVD Reverse	SVD (undescribed)	AGCGGCCGCTTTACACTG AGGTGGATAC	Amplify from cDNA
MSH Forward	*Maristella chicoi*	CGGCTCGAGAAGAGAG AGGCTGAAGATTGTTAT GAATTCACAT	Amplify from cDNA
MSH Reverse	*Maristella chicoi*	AGCGGCCGCTTTACACT GAGGGGGATAC	Amplify from cDNA
VTS Forward	*Vargula tsujii*	CCGCTCGAGAAGAGAG AGGCTCAAGATTGTTAT GAATCAACATG	Amplify from cDNA
VTS Reverse	*Vargula tsujii*	AGCGGCCGCTTTACACT GAGGAGGATACT	Amplify from cDNA
454-Forward-Vt	*Vargula tsujii*	CTCGAGATCAGTCGAG AAACGAAACGTGATA	Amplify from cDNA
454-Reverse-Vt	*Vargula tsujii*	GAATTCCTTTACACTGA GGGGGATACTG	Amplify from cDNA
AOX Forward	n/a	GACTGGTTCCAATTGACAAGC	Sequence from clones
AOX Reverse	n/a	GCAAATGGCATTCTGACATCC	Sequence from clones

Table B.4: Primers used to amplify c-luciferases for cloning or confirm insert sequences

B.2 Supplementary Figures for Chapter 3

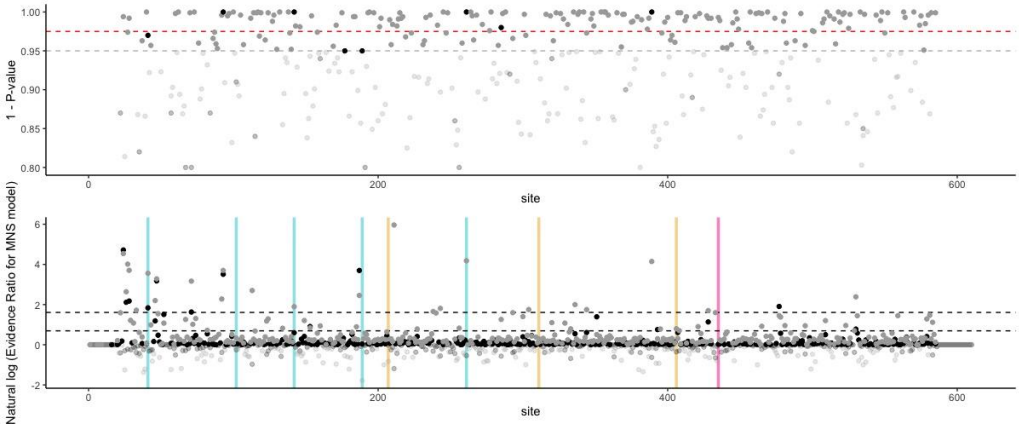

Figure B.1: Plots of significance tests (top panel) and evidence ratios (bottom panel) for each codon site. Top panel: 1 - p-values from HyPhy MEME tests (black) or FEL (gray). Dashed lines are significance level at p 0.05 (grey) or q 0.025 (corrected for multiple tests). Sites above the dotted lines have signatures of diversifying or purifying selection. Bottom panel: Natural log of the evidence ratio from HyPhy Multihit tests comparing the support for a model with a dinucleotide mutation over a single mutation (gray), or the support for a model with a trinucleotide mutation over a single hit (black). Opaque data have an evidence ratio greater than 1. Dashed horizontal lines are evidence ratio levels supporting a model with a multinucleotide substitution over a model with a single nucleotide substitution by 2x (lower line) or 5x (upper line) greater chance of support. Note that evidence ratio support is continuous between alternative models with no distinct cut-off; lines are added for aid in interpretation. Horizontal colored bars correspond to sites with functional correlates from Table 1. Bar colors represent dn:ds values consistent with diversifying selection (blue), purifying selection (red), or neutral (yellow).

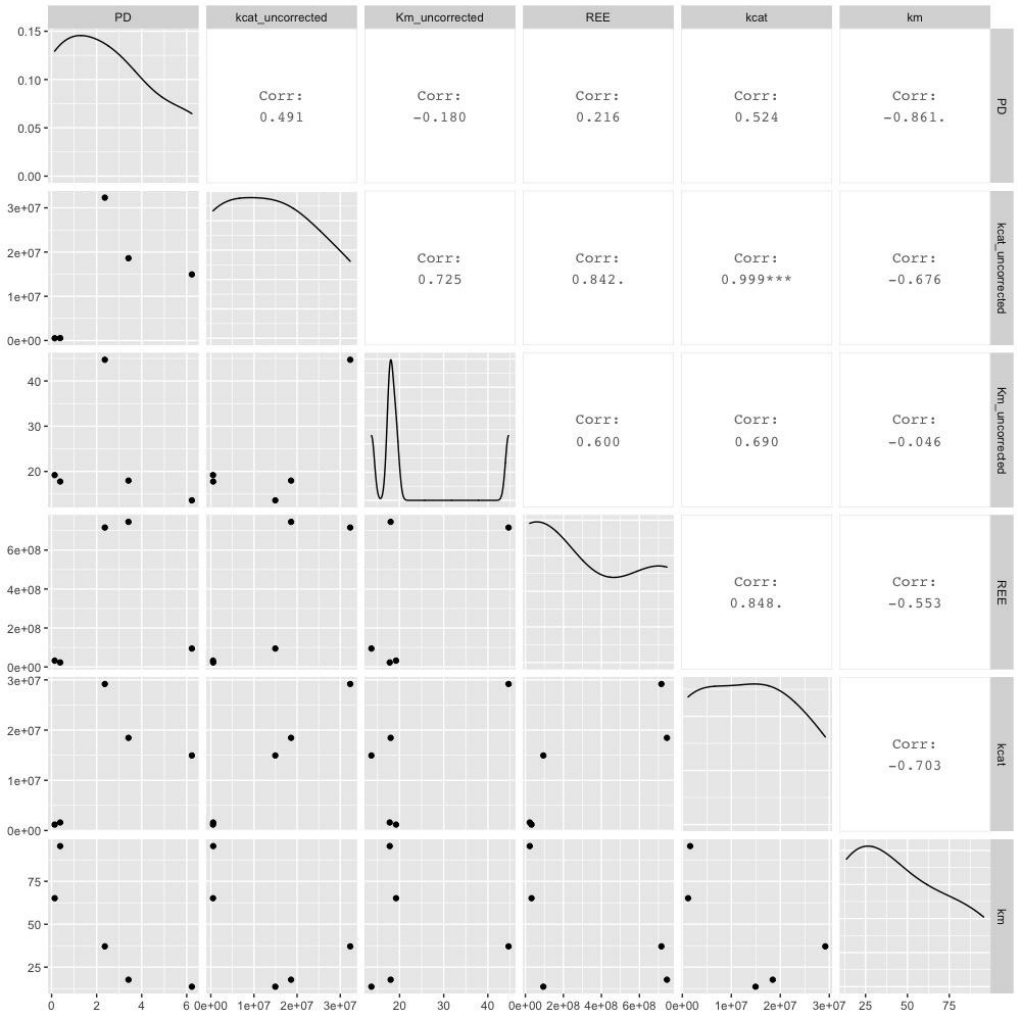

Figure B.2: Correlations between pulse duration data from [76] and kinetic parameters measured in this study. Statistically significant observations ($p < 0.05$) are marked with an asterisk in the correlation value.

Appendix C

Supplement for Chapter 4

C.1 Supplementary Tables for Chapter 4

Species	Individual	Eggs	Brooding	Parasite	Dissection Date	Genital morphology
PMO	1	eggs	brooding	none	24October2019	none
PMO	2	eggs	none	none	28October2019	spermatophore
PMO	3	none	none	none	31October2019	none
PMO	4	eggs	none	none	04November2019	spermatophore
PMO	5	none	none	none	07November2019	spermatophore
PMO	6	eggs	none	none	14November2019	spermatophore
PMO	7	eggs	none	none	18November2019	none
PMO	8	none	none	none	21November2019	none
PMO	9	eggs	none	none	25November2019	none
PMO	10	eggs	none	none	05December2019	ambiguous
PMO	11	none	none	none	13January2020	none
PMO	12	none	none	parasite	15January2020	spermatophore
PMO	13	eggs	none	none	22January2020	none
PMO	14	none	brooding	parasite	27January2020	spermatophore
PMO	15	eggs	none	parasite	29January2020	spermatophore
PMO	16	eggs	none	none	03February2020	ambiguous
PMO	17	none	none	none	12Feb2020	none
PMO	18	none	brooding	none	19February2020	spermatophore
PMO	19	none	brooding	none	24February2020	spermatophore

Table C.1: Reproductive history as assessed from the absence/ presence of eggs, spermatophores, or broods in female *P. morini* used in the experiments of Chapter 4.

Model Response	Predictor	Estimate	SE	t value	P-value
Speed (Fig. 4.2)	Intercept (Timing "Early", Both, & Allopatry)	0.0492	0.0120	4.0890	0.0000
	After displays started ("Late")	0.0128	0.0121	1.0600	0.2893
	IPI	0.0222	0.0066	3.3710	0.0008
	PD	0.0177	0.0060	2.9210	0.0035
	Sympatric	0.1451	0.0300	4.8420	0.0000
	Late & Sympatric	0.0788	0.0248	3.1760	0.0015
	IPI & Sympatric	-0.0988	0.0236	-4.1940	0.0000
	PD & Sympatric	-0.1107	0.0228	-4.8580	0.0000
Sinuosity (Fig. 4.3)	Intercept (Both & Allopatry)	9.6180	0.1910	50.3460	0.0000
	IPI	-0.8139	0.2669	-3.0490	0.0023
	PD	-0.2571	0.2650	-0.9700	0.3319
	Sympatric	-2.5571	0.2434	-10.5060	0.0000
	IPI & Sympatric	0.5133	0.3381	1.5180	0.1290
	PD & Sympatric	-0.8870	0.3293	-2.6940	0.0071

Table C.2: Results of generalized linear model outputs for models describing changes in sinuosity and swimming speed of female ostracods.

C.2 Supplementary Figures for Chapter 4

Figure C.1: Experimental set-up for dichotomous choice assays of female behaviors. (A; left) tank filled with seawater. On the top of the tank is a large infrared LED light source, suspended above the water line. In between the water line and the light are two folded paint strainers to diffuse the directionality of the light. (B; right). Close-up on the LED light strips used to provide stimuli to single females in the tank. On both left and right sides were single tracks of LEDs controlled by Arduino and loaded with custom-written programs to stimulate displays. Black cloth is used to enhance contrast behind the transparent tank. Set-up as in Belize, but differs slightly in practice from set-up in Panama for logistical reasons.

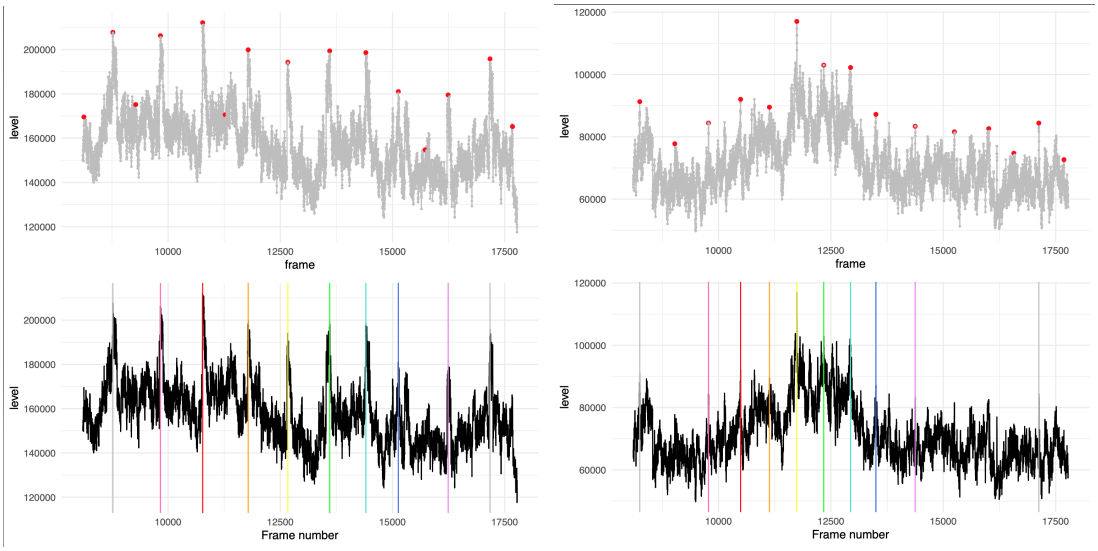

Figure C.2: Exemplar peaks for (A; left two panels) obvious and (B; right two panels) noisy identification of stimulus presentation. Data in top and bottom panels are the same: pixel brightness value over time. Identified semi-regular peaks are highlighted with red dots on the top panels. Bottom panels have top 10 highest values peaks annotated with a colored line. These data are from the same experiment, each representing one stimulus on one side of the tank. Note the difference in pixel values even between a single tank, both pattern of change and absolute level.

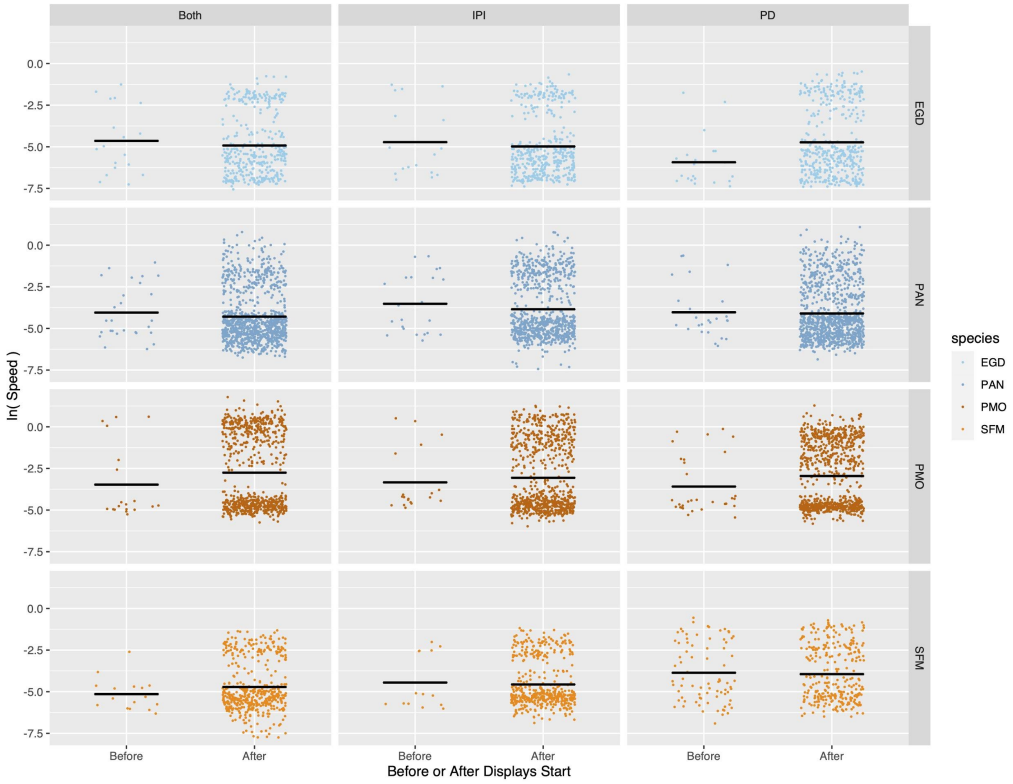

Figure C.3: Change in female swimming speed as by species and experiment type. Warmer colors are sympatric species, and cooler colors are allopatric species.

Appendix D

Hybrid offspring and differences in life-history between two new species (genus *Photeros*) from Bocas del Toro, Panama

D.1 Introduction

Reducing gene flow between diverging populations is essential to complete the speciation process [36]. Barriers to gene flow are myriad and best represented in the many different theoretical models of speciation, including where species diversity is driven by increasing geographic obstacles, ecological adaptation to different niches, or even sexual radiations based on mate choice and/or competition [61, 123]. Given sufficient gene flow between populations, speciation can slow or even stop as shared genetic material homogenizes groups (e.g. de-speciation, [103]). In reality, many of these mechanisms interact to produce population divergence. Classically, local adaption between allopatric populations can prevent populations from exchanging genetic material if or when they come back into contact because locally adapted alleles will reduce hybrid offspring (e.g. Dobzhansky-Muller incompatibility, [52]). And magic traits, phenotypes that are under disruptive selection due to both ecological and sexual selection, are theoretically poised to generate rapid bouts of speciation [186]. Assessing the individual contribution of these joint processes on reducing gene flow can give us better insight into their necessary prevalence and strength in generating biodiversity.

Documenting successful hybridization between species not only provides evidence that post-copulatory mechanisms may be weakly contributing to speciation within a clade (if at all; [34]), but the hybrids themselves represent valuable biological specimens to better understand complex trait development. Gene flow between diverging groups is generally considered to produce malapated hybrids [37], although hybrid vigor is possible (e.g. [53]). Especially when the opportunity for gene flow is high such as during secondary contact or sympatric speciation, selection against hybrids can be strong and multiple mechanisms can evolve to prevent interspecific mating. Most notably, pre-copulatory mechanisms like mating displays [117] or "lock-and-key" copulatory organs [124] can

prevent hybrids from ever forming. In animals, detection of hybrids in nature is fairly rare, perchance due to strong negative selection or ephemeral opportunity, and most studies on hybrids come from lab crosses. Hybrids represent a unique genomic event to probe the development of complex phenotypes because recombination shuffles parental alleles amongst progeny, allowing us to tease apart causal loci given sufficient numbers and rigorous methodologies [118].

Hybridization can also be an important driver in phenotypic and species diversity, like during adaptive introgression [75]. In this study we document the first evidence that hybridization is possible between two closely related species of bioluminescent ostracod, both new to science. As millimeter-sized crustaceans, ostracods are mostly benthic meiofauna found in waters around the world. In marine habitats of the Caribbean, 75 different species (mostly undescribed) are bioluminescent, whereby males produce species-specific luminous patterns to attract mates [141]. Females use these displays to track the male's position [171]. Given their species specificity and implication in mate choice, these displays are thought to be a strong reproductive barrier between species and important in the widespread diversification of this monophyletic group [217, 45]. Along with wide behavioral and ecological disparity [29], these species have a number of morphological features that separate them, including notable reproductive characteristics [140]. In some freshwater ostracod species (Family Cyprididae), phylogenetically distinct from bioluminescent cypridinids, hybridization has been linked with increased genetic and phenotypic diversity. Many of these species consist of unisexual clones, but with large variation in their ploidy levels and/or clonal diversity. [221] found that increases in clonal genetic diversity between populations within a species were associated with females mating with males from other closely related species.

To our knowledge, no one has ever explicitly tested the role that post-copulatory mechanisms may play in reproductive isolation amongst species of bioluminescent os-

tracods. Thus it remains to be seen how strongly factors like behavior, morphology, or even genetic incompatibilities contribute to speciation in sea fireflies. Herein, we describe two new species of Caribbean ostracod that successfully produced offspring when housed in lab conditions. Our classical morphological and phylogenetic assessments place these nominal species in the genus Photeros, and we also provide data on noted life-history phenomenon. We conclude with a discussion on the relative contribution of pre- versus post-copulatory mechanisms in generating such a speciose group of charismatic crustaceans.

D.2 Results

D.2.1 Species have different displays and are found in different habitats

Males of *Photeros* sp. "EGD" produce a downward display, consisting of 3-8 pulses per display. Displays begin 25 cm above the substrate, with each pulse lasting 4-6 seconds. The entire display train length is approximately 0.18 m long, usually ending 5-7 cm above the sea grass. Pulses are about 1-1.5 seconds apart, spaced evenly about 4-5 cm from one another. A single co-occurring species has been documented signaling in the same habitat as *Photeros* sp. "EGD" , but very rarely and no sample has been collected for identification. Displays are abundant in sea grass, as males heavily entrain off of one another to produce synchronous interindividual displays.

Males of *Photeros* sp. "SFM" produce upward displays, consisting of 1-4 pulses per display. Displays begin 5-7 cm above the substrate, each pulse lasting $\sim$0.5 seconds. The entire display train length is approximately 0.2 m long, usually ending 0.25 m above the substrate; for this species, this is most often at the water surface. Pulses are about 1.5-2 seconds apart, spaced evenly about 10-15 cm from one another. A single co-occurring

species is often found (field designation "MFU" in the nominal genus *Maristella*) signaling alongside *Photeros* sp. "SFM" , but whose displays are visibly distinct in pulse duration and number. Displays are abundant beneath mangrove prop roots and many are within visible range, usually less than 0.25 m apart and often within centimeters of one another.

For a summary of species differences, see Fig. D.1 and Tables D.1 and 4.2

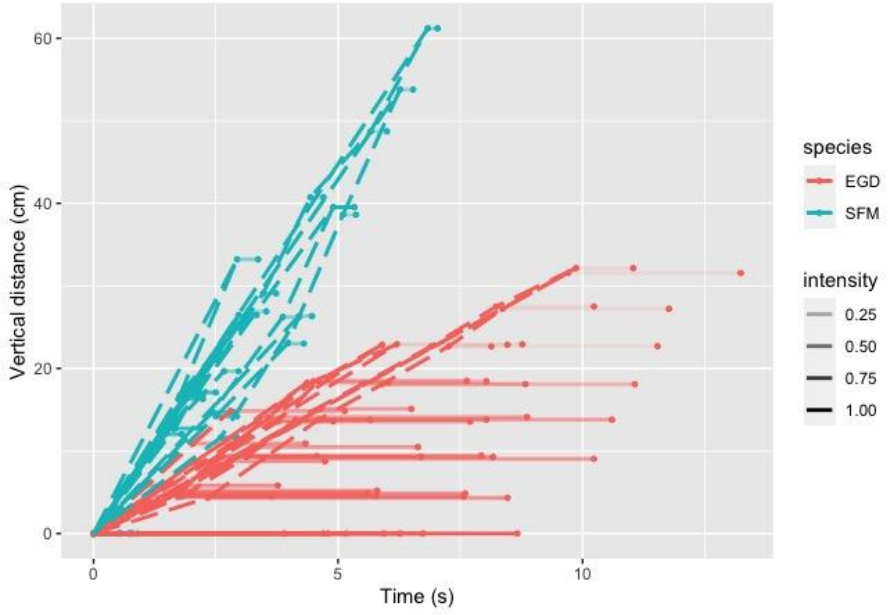

Figure D.1: Measured display characteristics from nominal *Photeros* species "EGD" (N = 8, orange), and "SFM" (N = 8, blue). Each pair of data connected by a solid, horizontal line is a single pulse in the display, with the length of the line indicating the overall duration of the pulse (x-axis, seconds). Distances between pairs of data for a single pulse (y-axis, cm) indicate the observed vertical distance between subsequent pulses in a display (dashed line). Note, "EGD" pulses propagate downwards while "SFM" pulses propagate upwards over time. For the vertical distance between pulses (dashed lines), we did not have exact measures that paired with the same individuals as measured for the pulse durations. Instead, interpulse distances are randomly sampled from a distribution measured from the original 8 individuals. Intensity of the transparency of horizontal bars are the relative intensity of a pulse compared to the first pulse in the display. These are measures from up to 3 individuals for each species, taken with a PMT at a fixed distance while individuals were kept in captivity.

D.2.2 Morphological measures place nominal species within the *Photeros* genus

Measurements taken via ImageJ with known scale to calculate the length:height ratio (a reliable genus level measure) place species EGD and SFM into the *Photeros* clade (Fig. D.2).

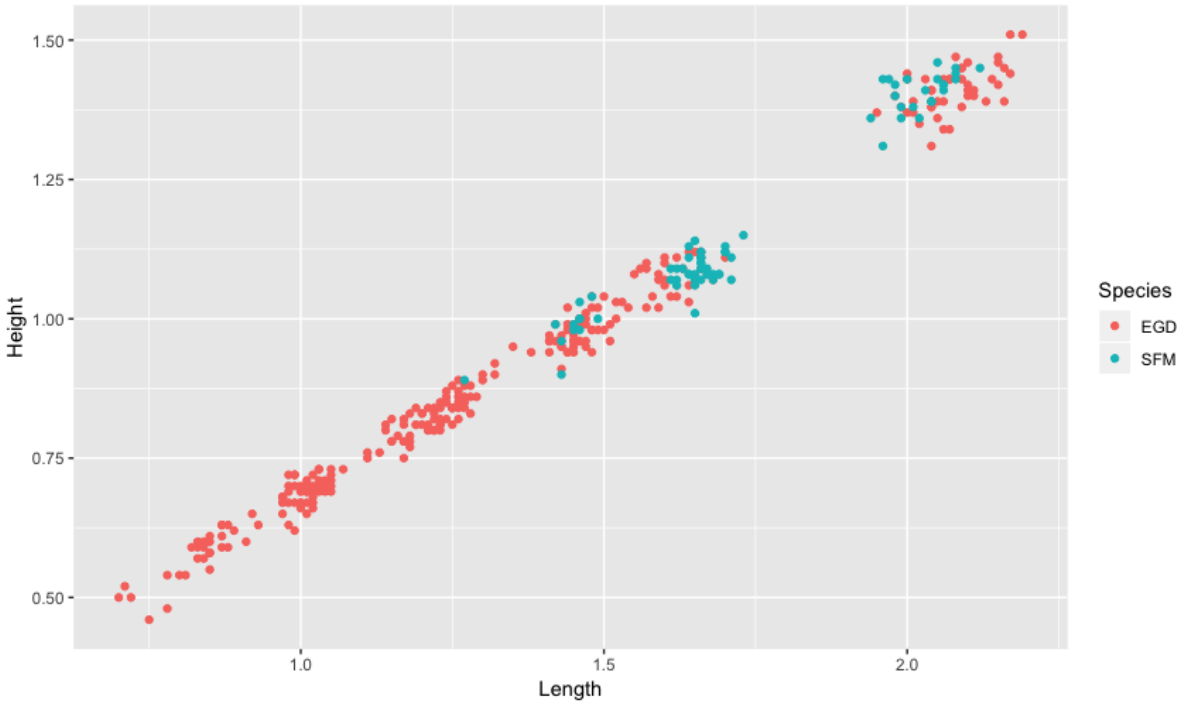

Figure D.2: Length and height measurements across life stages for the two species described herein. Animals were caught via baited trap. When compared to congener *P. annecohenae*, we find similar clusters based on size classes but do not infer developmental stage from these wild-caught individuals besides adult females (uppermost group). We did not catch smaller sizes of species "SFM".

D.2.3 Mitochondrial phylogeny confirms genera assignment

A mitochondrial phylogeny with 8 genes confirms the placement of these two new species within the genus *Photeros* (Fig. D.3). When compared with other species from

different genera (*Vargula hilgendorfii, Vargula tsujii, Cypridina denata, Kornickeria hastingsi carriebowae*) and congeners (*Photeros annecohenae, P. morini, P. mcelroyi, P. jamescasei*, and other undescribed *Photeros* 'WLU', 'NOL', and 'GPH'), both 'EGD' and 'SFM' fall more closely with *Photeros* and to one another. Although bootstrap values across the tree are variable, the *Photeros* clade has 100% bootstrap support across 1,000 trees.

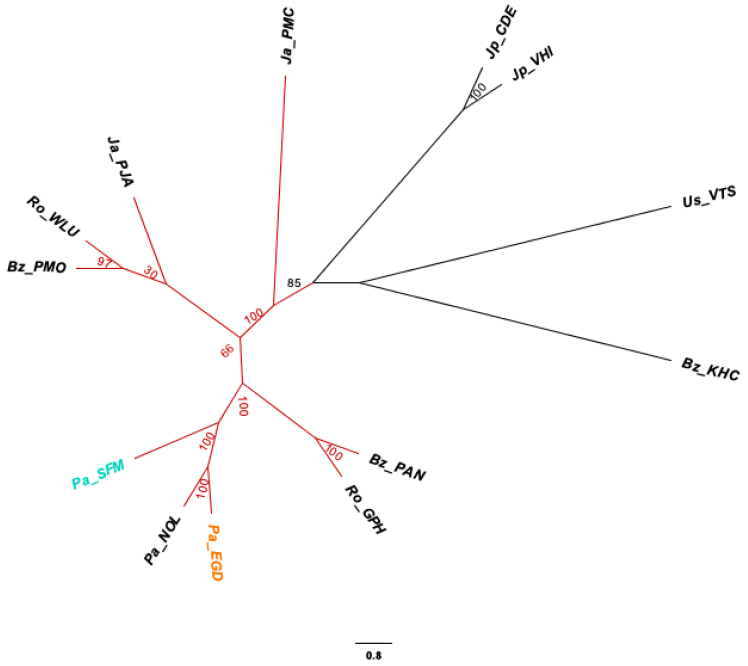

Figure D.3: Unrooted, maximum-likelihood mitochondrial DNA phylogeny (# of informative sites = 16,859; # of bootstraps = 1000) confirm the placement of these two nominal species within the genus *Photeros* (red branches). Focal taxa highlighted (EGD: orange; Blue: SFM).

D.2.4 Two species differ in life-history timing

EGD spends less time as an A-1 instar, having a shorter developmental time molting from immature (A-1) to adult (A) (Fig. D.4, ANOVA $p < 0.05$). As with congener *P. annecohenae*, there is no evidence of sexually dimorphic patterns in developmental

timing [58], at least during this life stage (Fig. D.4, ANOVA $p > 0.05$).

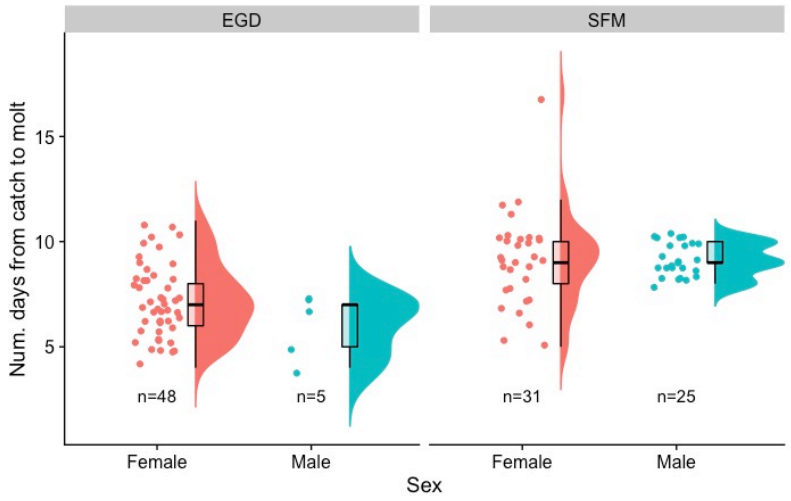

Figure D.4: EGD spends less time as a juvenile (A-I) than SFM. Cloud plot depicting time to molt from the last immature instar to mature adult by species and by sex. EGD spends an average of 7 days (post captivity) as an A-I, whereas SFM spends an average of 9 days as a juvenile before molting.

D.2.5 Variable success of interspecific crosses and embryonic development

Breeding attempts had variable, generally low success rates (Table D.3). Females varied in the amount of time to ovigery, as well as to subsequent egg deposition and juvenile hatching. In approx. 30% of cases, no offspring were produced from the crosses, either conspecific or heterospecific. We note that female ostracods, once observed in a developmental state (either ovigerous or brooding young in the marsupium), did revert back to an empty state on subsequent days (Fig. D.5, Table D.3). Whether this was loss and ejection of developing progeny, or resorption of the tissue, is unknown.

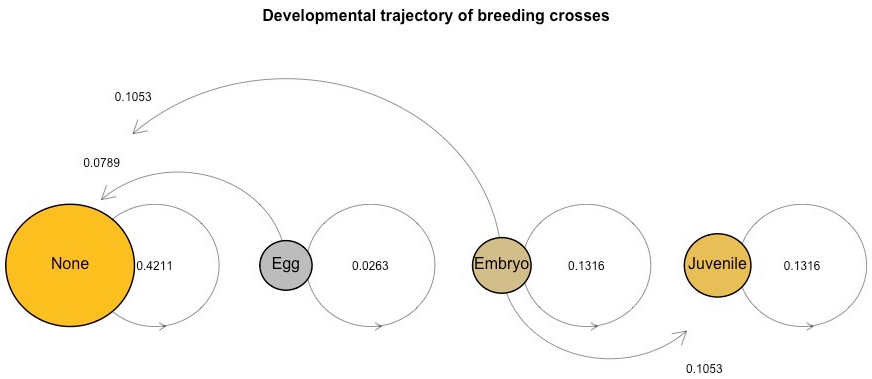

Figure D.5: Transition probabilities between developmental states across the developmental trajectory for females ostracods during all breeding attempts (control and experimental). Development progresses from no apparent signs of reproductive output ("None", left) to the presence of live offspring outside the mother ("Juvenile", right). States are scaled and color coded by the percent of observations (larger, brighter = more observations).

D.2.6 Intraspecific and interspecific juveniles

Reciprocal crosses in both directions resulted in living juveniles (Fig. D.6). Note that of intraspecific mating attempts, only EGD produced juveniles.

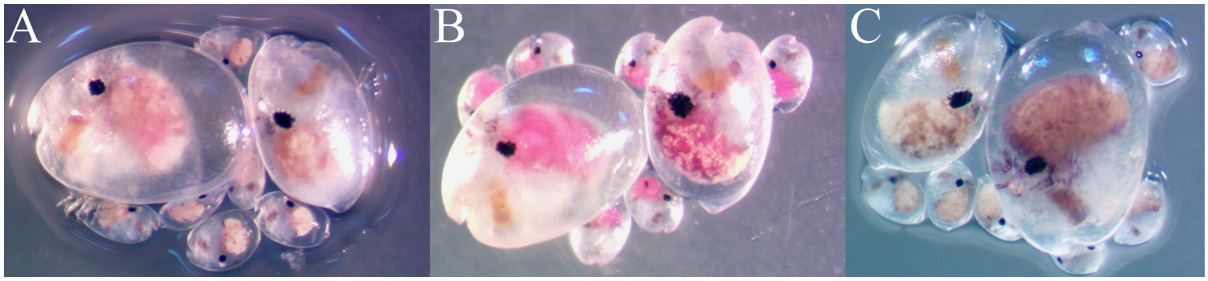

Figure D.6: Images of successful crosses between an intraspecific pair, and reciprocal crosses between males and females of different species. (A; left) A control mating of male (right; smaller) and female (left; larger) from the same species, "EGD". Note both have white bellies, as do their offspring (surrounding; tiny). (B; middle) A mating between a female "EGD" and a male "SFM". Note the freckled, darker stomach of the "SFM" male (right). (C; right) A mating between a female "SFM" (larger with dark stomach; right) and a male "EGD".

Species	**Country**	**Location**	**Habitat**	**Capture method**
Photeros sp. 'EGD'	Bocas del Toro, Panama	Lat: 9.332464 Long: -82.254105	Grassbeds of mixed *Thalassia testudinalis* and *Syringodium filiforme* (0.5 - 4 m deep)	Baited conical traps; males from displays
Photeros sp. 'SFM'	Bocas del Toro, Panama	Lat: 9.332464 Long: -82.254105	Amongst and next to the prop roots of mangroves above very fine sand or other litter (Depth < 0.5 m)	Baited conical traps; males from displays

Table D.1: Summary of locality, collection, and habitat information for two species.

Species	**RNA Yield (μg)**	**# Raw Reads**	**N50**	**BUSCO Score**
Photeros sp. 'EGD'	0.093	19,072,925	697	62.2 %
Photeros sp. 'SFM'	0.238	18,330,042	742	69.9 %

Table D.2: RNA yield and summary statistics for transcriptome assemblies for each species.

Observation	**Control Crosses**	**Experimental Crosses**
Successful juveniles	28.6 % (2/7)	33.3 % (4/12)
Eggs/Embryo gone	28.6 % (2/7)	41.7 % (5/12)
Nothing observed	42.9 % (3/7)	25.0 % (3/12)

Table D.3: Summary of breeding attempts between conspecific and heterospecific individuals, and different states of female/juvenile development during the attempts. Results of the reciprocal crosses are pooled. Percent observed with number of observations over attempts in parentheses.

D.3 Discussion

We document the first morphological, behavioral, and DNA evidence of two new, closely related species and place them in the genus *Photeros* [141, 30]. We also show that these species have diverged in life-history traits, and that broods in gestating females can show complex developmental trajectories. Despite these differences between species, they are able to produce living offspring through parturition to their first instat (A-V). Although we lack explicit pedigree analysis to confirm parental assignment, our experiments are the first to test the role of post-zygotic barriers in this species radiation associated with sexual selection.

Pre-zygotic reproductive barriers may be more important in ostracod speciation than post-zygotic barriers. The successful, although admittedly low, hybridization between these two closely related species suggests that reproductive barriers between them have not yet evolved. During speciation, different types of reproductive isolation may be more important at different times in the process; testing which mechanisms influence initial lineage furcation is important to understand how microevolutionary processes can lead to patterns of species diversity at longer timescales. Our data suggest that post-zygotic mechanisms (e.g. like as mediated by selection against maladaptive hybrids) may not contribute much isolation to the initial speciation process amongst cypridinid ostracods.

Regardless of post-zygotic mechanisms, many pre-zyogtic mechanisms can contribute to speciation. Besides wide disparity in sexual signals between species, Caribbean cypridinids also demonstrate extreme differences in reproductive morphology [29]. Thorough morphological investigations have revealed that ostracods may possess "lock-and-key"-like reproductive morphologies between females and males. Males are also known to leave spermatophores on female reproductive organs, seemingly to function as copulatory plugs [28]. And in at least one species, females only sire offspring from one male

(although low-levels of multiple paternity were not reliably detectable in this study, [32]). These lines of evidence support the role of strong sexual selection acting on both pre- and post- copulatory mechanisms, potentially which also generate reproductive isolation during speciation. Thus, multiple types of pre-zygotic reproductive isolation, including behavioral and morphological divergence, may contribute to speciation in this system.

Allopatric speciation by vicariance may be a large contributor to ostracod speciation, as assumed for much of metazoan biodiversity [36]. In Caribbean ostracods, isolation by barrier effects has recently been detected in divergent populations of another *Photeros* species [167], despite the surprisingly strong ability for such small-bodied individuals to disperse (upwards of 400 m; [60]). As benthic meiofauna, is it unsurprising that these organisms would suffer from strong geographic isolating mechanisms. Across large and intermediate spatial scales (1000 to 10s of kilometers), different species are quite endemic (pers. obser.). However, many different species can co-occur in sympatry, dividing up habitats into characteristic arenas within which they perform species-specific bioluminescent mating displays [59]. Understanding which geographical barriers, including habitat preferences, are important to ostracod divergence will take a much more thorough sampling across closely related species.

All together, it seems that pre-zygotic barriers like geography and sexually selected pre-copulatory mechanisms are setting the stage for sea firefly speciation. The role of hybridization in this process is unknown. Recent phylogenetics of the group revealed historical patterns of both introgression and incomplete lineage sorting may be present in this family, and even in the past divergence within the *Photeros* genus [44]. To our knowledge, we are first to document that hybridization can occur in cypridinids. Exploring if this process has a role in the diversification or adaptation of these charismatic crustaceans remains to be seen and will require future tests on F1 hybrid fecundity. In many species, hybridization has been associated with adaptive increases in genetic

variation, including in other ostracod families.

Conclusions Through simple reciprocal crosses, we show that recently diverged ostracod species can interbreed and produce living offspring. These two new species are relatively closely related and show wide disparity in behavior, life history, and habitat, but are similar in gross morphology. This suggests that pre-zygotic barriers to reproduction may drive speciation amongst sea fireflies, including vicariance and sexual selection. By recording these two species, we hope to develop them as a model for asking questions on the evolution and architecture of complex behavioral traits like bioluminescent mating displays.

D.4 Materials & Methods

D.4.1 Animal collection, husbandry, and breeding design

We collected both *Photeros* sp. "EGD" (21 September 2018 - 26 September 2018) and *Photeros* sp. "SFM" (18 September 2018 - 27 September 2018) using baited conical traps [31]. EGD were sampled from the grass bed of Punto Manglar (9.332464, -82.254105) and SFM were found in the mangrove roots adjacent to the site. Besides from traps, males of each species were caught via handnets [31] to guarantee that males came from the appropriate species' displays.

In the lab, individuals were visually inspected and sorted using a dissecting microscope. Animals were photographed in batches with a reference for later measurement. Individual animals were then housed in a single well of a 12-well culture dish kept at ambient temperature (25°C). We checked animals daily for molting and a subsequent water change; individuals were fed every other day on fish flakes (Seachem NutriDiet MarinePlus Enhanced Marine Flakes with Probiotics) before any water change.

To create hybrid crosses, adult males of one species and newly molted, adult females ("virgin") were housed together in a single well for a minimum of three days, and until one of them died or until termination of the experiment.

D.4.2 Display characterization

As described in [76]. Briefly, displays were filmed using a Sony A7S with an Atomos Shogun, all inside a custom underwater housing. Measurements on display timing (pulse duration, interpulse interval) were then estimated from videos. Because SFM occurs in shallow, obstructed habitat, we could not film with a reference in frame. Instead, after filming, we placed a reference of known length (field slate) alongside displays and estimated by eye the total length of the display (sensu [141]). We then interpolate interpulse distances as the number of pulses per display divided by the maximum display length for the species. For EGD, we used stereoscopic recordings from custom underwater housing (Oakley et al., in prep.) to estimate interpulse distance and display length. For each species, multiple individuals were filmed.

D.4.3 Morphological description

For the majority of individuals, classical measures (body length and height, eye, and keel length) were recorded from photographs with a known reference file (FIJI). Most individuals were photographed in batches, allowing for many measures per image.

D.4.4 Transcriptome processing & phylogeny

Two males of each species caught via handnet were stored in RNALater after fresh collection in Panama. RNA was isolated with a Qiagen RNeasy mini kit for total RNA isolation from both individuals together. Although these yielded very low RNA quan-

tities, samples were sent for subsequent sequencing (Novogene). We assembled de novo transcriptomes using Trinity (v.2.8.5) [71] and assessed assembly quality with BUSCO (v.3) [233] and N50 score. We then extracted mitochondrial genes using MitoFinder (v.1.0.1) [3] with published sequences from other bioluminescent myodocopids (Vargula tsujii, Vargula hilgendorfii) as the bait sequences.

We aligned mitochondrial sequences for each gene family separately with MAFFT (v7.429) [97], and settings as –globalpair –maxiterate 1000. Sequences were concatenated with catfasta2phyml (optional flags as: -c -s -f), generating a partition file and keeping all genes for all species despite varying levels of maxtrix occupancy. After specifying protein coding genes as "CODON5" and ribosomal RNA as "DNA" in the partition, we used IQTree (v.1.6.6) [135] to implement ModelFinder [94]. Finding that 5 partitions were best via BIC, we used IQTree (v.1.6.6) with this partitioning scheme to perform 1000 bootstraps (-bb 1000 -bnni), creating both maximum likelihood and consensus trees with congruent topologies.

D.5 Relevant Supporting Information

D.5.1 Ethics Statement

All animals were collected with permission from the Panamanian government (Mi-Ambiente Permits #SE/A-54-18 and #SEX/A-78-18).

D.5.2 Author Contributions

NMH conceived the study, designed the experiments, collected and analyzed data, secured funding, and wrote the manuscript with input from all other authors. KP collected data (morphological measurements), and assisted with analysis and writing. NML

assisted in data collection (animal husbandry); GAG and TJR assisted in data collection (display characterization). THO assisted with data collection (morphological description) and secured funding.

D.5.3 Acknowledgements

We would like to thank H. Lessios for his sponsorship of NMH at the Smithsonian Tropical Research Institute, as well as all facilities personnel at the Bocas del Toro station. We also would like to thank E. Ellis and J. Goodheart for advice with phylogenetics.

D.5.4 Funding

NMH was supported by the NSF GRFP and a STRI Short-term Fellowship. He also received a block grant from the Department of Ecology, Evolution, and Marine Biology at UCSB, supplemental funds from the American Microscopical Society Student Research Fellowship, and a Worster Award with KP to fund this work.

Bibliography

[1] W J Albery and J R Knowles. "Efficiency and evolution of enzyme catalysis". en. In: *Angew. Chem. Int. Ed Engl.* 16.5 (May 1977), pp. 285–293.

[2] H Allen Orr. "The genetics of species differences". en. In: *Trends Ecol. Evol.* 16.7 (July 2001), pp. 343–350.

[3] Rémi Allio et al. "MitoFinder: Efficient automated large-scale extraction of mitogenomic data in target enrichment phylogenomics". In: *Mol. Ecol. Resour.* 20.4 (July 2020), pp. 892–905.

[4] Martin N Andersson, Christer Löfstedt, and Richard D Newcomb. "Insect olfaction and the evolution of receptor tuning". In: *Functional Characterization of Insect Chemoreceptors: Receptivity Range, Expression and Evolution* (2017), p. 49.

[5] Matthew E Arnegard and Alexey S Kondrashov. "Sympatric speciation by sexual selection alone is unlikely". en. In: *Evolution* 58.2 (Feb. 2004), pp. 222–237.

[6] Matthew E Arnegard et al. "Sexual signal evolution outpaces ecological divergence during electric fish species radiation". en. In: *Am. Nat.* 176.3 (Sept. 2010), pp. 335–356.

[7] Stevan J Arnold and Lynne D Houck. "Can the Fisher-Lande Process Account for Birds of Paradise and Other Sexual Radiations?" In: *Am. Nat.* 187.6 (2016), pp. 717–735.

[8] *Babraham Bioinformatics - Trim Galore!* `http://www.bioinformatics.babraham.ac.uk/projects/trim_galore/`. Accessed: 2017-10-20.

[9] Simon W Baxter et al. "Genomic hotspots for adaptation: the population genetics of Müllerian mimicry in the Heliconius melpomene clade". en. In: *PLoS Genet.* 6.2 (Feb. 2010), e1000794.

[10] Patricia Beldade, Kees Koops, and Paul M Brakefield. "Modularity, individuality, and evo-devo in butterfly wings". en. In: *Proc. Natl. Acad. Sci. U. S. A.* 99.22 (Oct. 2002), pp. 14262–14267.

[11] Patrıcia Beldade and Paul M Brakefield. "The genetics and evo–devo of butterfly wing patterns". In: *Nat. Rev. Genet.* 3.6 (June 2002), pp. 442–452.

[12] Andres Bendesky and Cornelia I Bargmann. "Genetic contributions to behavioural diversity at the gene–environment interface". en. In: *Nat. Rev. Genet.* 12.12 (Nov. 2011), pp. 809–820.

[13] Jannick Dyrløv Bendtsen et al. "Improved prediction of signal peptides: SignalP 3.0". en. In: *J. Mol. Biol.* 340.4 (July 2004), pp. 783–795.

[14] Simon Benhamou. "How to reliably estimate the tortuosity of an animal's path: straightness, sinuosity, or fractal dimension?" en. In: *J. Theor. Biol.* 229.2 (July 2004), pp. 209–220.

[15] Todd A Blackledge and Rosemary G Gillespie. "Convergent evolution of behavior in an adaptive radiation of Hawaiian web-building spiders". en. In: *Proc. Natl. Acad. Sci. U. S. A.* 101.46 (Nov. 2004), pp. 16228–16233.

[16] Thomas Blankers et al. "The Genomic Architecture of a Rapid Island Radiation: Recombination Rate Variation, Chromosome Structure, and Genome Assembly of the Hawaiian Cricket Laupala". en. In: *Genetics* 209.4 (Aug. 2018), pp. 1329–1344.

[17] Hans Werner Borchers. "Pracma: practical numerical math functions". In: *R package version* 1.3 (2015).

[18] Zeineb Bouhlel et al. "Interspecies comparison of the mechanical properties and biochemical composition of byssal threads". en. In: *J. Exp. Biol.* 220.Pt 6 (Mar. 2017), pp. 984–994.

[19] Jack W Bradbury and Sandra L Vehrencamp. *Principles of Animal Communication*. en. Sinauer, Aug. 2011.

[20] Bruce R Branchini et al. "A Photinus pyralis and Luciola italica chimeric firefly luciferase produces enhanced bioluminescence". en. In: *Biochemistry* 53.40 (Oct. 2014), pp. 6287–6289.

[21] Philipp Brand et al. "The evolution of sexual signaling is linked to odorant receptor tuning in perfume-collecting orchid bees". en. In: *Nat. Commun.* 11.1 (Jan. 2020), p. 244.

[22] Brett Calcott and Arnon Levy. *Modeling and Simulation in Evo-Devo*. 2020.

[23] Christiam Camacho et al. "BLAST+: architecture and applications". en. In: *BMC Bioinformatics* 10 (Dec. 2009), p. 421.

[24] Jessica Cande, Benjamin Prud'homme, and Nicolas Gompel. "Smells like evolution: the role of chemoreceptor evolution in behavioral change". en. In: *Curr. Opin. Neurobiol.* 23.1 (Feb. 2013), pp. 152–158.

[25] Jessica Cande et al. "Looking under the lamp post: neither fruitless nor doublesex has evolved to generate divergent male courtship in Drosophila". en. In: *Cell Rep.* 8.2 (July 2014), pp. 363–370.

[26] Salvador Capella-Gutiérrez, José M Silla-Martınez, and Toni Gabaldón. "trimAl: a tool for automated alignment trimming in large-scale phylogenetic analyses". en. In: *Bioinformatics* 25.15 (Aug. 2009), pp. 1972–1973.

[27] William W Chen, Mario Niepel, and Peter K Sorger. "Classic and contemporary approaches to modeling biochemical reactions". en. In: *Genes Dev.* 24.17 (Sept. 2010), pp. 1861–1875.

[28] Anne C Cohen and James G Morin. "External Anatomy of the Female Genital (Eighth) Limbs and the Setose Openings in Myodocopid Ostracodes (Cypridinidae)". In: *Acta Zool.* 78.2 (Apr. 1997), pp. 85–96.

[29] Anne C Cohen and James G Morin. "Sexual morphology, reproduction and the evolution of bioluminescence in Ostracoda". In: *Paleontological Society Papers* 9 (2003), p. 37.

[30] Anne C Cohen and James G Morin. "Two New Bioluminescent Ostracode Genera, Enewton And Photeros (Myodocopida: Cypridinidae), with Three New Species from Jamaica". In: *J. Crustacean Biol.* 30.1 (Jan. 2010), pp. 1–55.

[31] Anne C Cohen and Todd H Oakley. "Collecting and processing marine ostracods". In: *J. Crustacean Biol.* 37.3 (May 2017), pp. 347–352.

[32] Nathaniel Conley and Gretchen A Gerrish. "Testing for multiple paternity in broods of the bioluminescent ostracod Photeros annecohenae (Torres & Morin, 2007) (Myodocopida: Cypridinidae)". In: *J. Crustacean Biol.* 39.3 (May 2019), pp. 213–217.

[33] Kimberly L Cooper. "Self-organization in the limb: a Turing mechanism for digit development". en. In: *Curr. Opin. Genet. Dev.* 32 (June 2015), pp. 92–97.

[34] Jenn M Coughlan and Daniel R Matute. "The importance of intrinsic postzygotic barriers throughout the speciation process". en. In: *Philos. Trans. R. Soc. Lond. B Biol. Sci.* 375.1806 (Aug. 2020), p. 20190533.

[35] Virginie Courtier-Orgogozo et al. "Gephebase, a database of genotype–phenotype relationships for natural and domesticated variation in Eukaryotes". In: *Nucleic Acids Res.* 48.D1 (Jan. 2020), pp. D696–D703.

[36] Jerry A Coyne and H Allen Orr. *Speciation*. en. Sinauer, June 2004.

[37] Jerry A Coyne and H Allen Orr. "PATTERNS OF SPECIATION IN DROSOPHILA". en. In: *Evolution* 43.2 (Mar. 1989), pp. 362–381.

[38] Charles Darwin. *The Descent of Man, and Selection in Relation to Sex*. en. D. Appleton, 1871.

[39] Brigitte Dauwalder. "The Roles of Fruitless and Doublesex in the Control of Male Courtship". In: *Recent advances in the use of Drosophila in neurobiology and neurodegeneration*. Vol. 99. International Review of Neurobiology. Elsevier, 2011, pp. 87–105.

[40] Antony M Dean and Joseph W Thornton. "Mechanistic approaches to the study of evolution: the functional synthesis". en. In: *Nat. Rev. Genet.* 8.9 (Sept. 2007), pp. 675–688.

[41] Yun Ding et al. "Natural courtship song variation caused by an intronic retroelement in an ion channel gene". en. In: *Nature* 536.7616 (Aug. 2016), pp. 329–332.

[42] Rui Diogo. "Where is, in 2017, the evo in evo-devo (evolutionary developmental biology)?" en. In: *J. Exp. Zool. B Mol. Dev. Evol.* 330.1 (Jan. 2018), pp. 15–22.

[43] G Sander van Doorn, Ulf Dieckmann, and Franz J Weissing. "Sympatric speciation by sexual selection: a critical reevaluation". en. In: *Am. Nat.* 163.5 (May 2004), pp. 709–725.

[44] Emily A Ellis. "Macroevolutionary consequences of rapid species accumulation due to sexual selection". PhD thesis. University of California, Santa Barbara, 2019.

[45] Emily A Ellis and Todd H Oakley. "High Rates of Species Accumulation in Animals with Bioluminescent Courtship Displays". en. In: *Curr. Biol.* 26.14 (July 2016), pp. 1916–1921.

[46] Timur V Elzhov et al. "R interface to the Levenberg-Marquardt nonlinear least-squares algorithm found in MINPACK". In: *Plus support for bounds* (2010), pp. 1–2.

[47] John A Endler. "Signals, Signal Conditions, and the Direction of Evolution". In: *Am. Nat.* 139 (1992), S125–S153.

[48] Adam Eyre-Walker and Peter D Keightley. "The distribution of fitness effects of new mutations". en. In: *Nat. Rev. Genet.* 8.8 (Aug. 2007), pp. 610–618.

[49] Timothy R Fallon et al. "Firefly genomes illuminate parallel origins of bioluminescence in beetles". en. In: *Elife* 7 (Oct. 2018).

[50] Pu Fan et al. "Genetic and neural mechanisms that inhibit Drosophila from mating with other species". en. In: *Cell* 154.1 (July 2013), pp. 89–102.

[51] R A Fisher. *The genetical theory of natural selection*. en.

[52] Llla Fishman and John H Willis. "Evidence for Dobzhansky-Muller incompatibilites contributing to the sterility of hybrids between Mimulus guttatus and M. nasutus". In: *Evolution* 55.10 (2001), pp. 1932–1942.

[53] Benjamin M Fitzpatrick and H Bradley Shaffer. "Hybrid vigor between native and introduced salamanders raises new challenges for conservation". en. In: *Proc. Natl. Acad. Sci. U. S. A.* 104.40 (Oct. 2007), pp. 15793–15798.

[54] Tamara A Franz-Odendaal and Dorit Hockman. "Non-model organisms and unique approaches are needed for the future of evo-devo". In: *Dev. Dyn.* 248.8 (Aug. 2019), pp. 618–619.

[55] Daniel J Funk, Patrik Nosil, and William J Etges. "Ecological divergence exhibits consistently positive associations with reproductive isolation across disparate taxa". en. In: *Proc. Natl. Acad. Sci. U. S. A.* 103.9 (Feb. 2006), pp. 3209–3213.

[56] László Zsolt Garamszegi, ed. *Modern Phylogenetic Comparative Methods and Their Application in Evolutionary Biology: Concepts and Practice*. 2014.

[57] Małgorzata A Gazda et al. "A genetic mechanism for sexual dichromatism in birds". en. In: *Science* 368.6496 (June 2020), pp. 1270–1274.

[58] Gretchen A Gerrish and James G Morin. "Life Cycle of a Bioluminescent Marine Ostracode, Vargula Annecohenae (Myodocopida: Cypridinidae)". In: *J. Crustacean Biol.* 28.4 (Jan. 2008), pp. 669–674.

[59] Gretchen A Gerrish and James G Morin. "Living in sympatry via differentiation in time, space and display characters of courtship behaviors of bioluminescent marine ostracods". en. In: *Mar. Biol.* 163.9 (Aug. 2016), p. 190.

[60] Gretchen Anne Gerrish. "Spatial and temporal habitat use by bioluminescent marine ostracods". In: (2008).

[61] Rosemary G Gillespie et al. "Comparing Adaptive Radiations Across Space, Time, and Taxa". en. In: *J. Hered.* 111.1 (Feb. 2020), pp. 1–20.

[62] J M Gleason et al. "Identification of quantitative trait loci function through analysis of multiple cuticular hydrocarbons differing between Drosophila simulans and Drosophila sechellia females". en. In: *Heredity* 103.5 (Nov. 2009), pp. 416–424.

[63] Jennifer M Gleason. "Mutations and natural genetic variation in the courtship song of Drosophila". en. In: *Behav. Genet.* 35.3 (May 2005), pp. 265–277.

[64] Marko Goličnik. "Explicit reformulations of time-dependent solution for a Michaelis–Menten enzyme reaction model". In: *Anal. Biochem.* 406.1 (Nov. 2010), pp. 94–96.

[65] Chetan T Goudar et al. "Progress curve analysis for enzyme and microbial kinetic reactions using explicit solutions based on the Lambert W function". en. In: *J. Microbiol. Methods* 59.3 (Dec. 2004), pp. 317–326.

[66] Manfred G Grabherr et al. "Full-length transcriptome assembly from RNA-Seq data without a reference genome". In: *Nat. Biotechnol.* 29.7 (July 2011), pp. 644–652.

[67] Peter R Grant and B Rosemary Grant. "Evolution of character displacement in Darwin's finches". en. In: *Science* 313.5784 (July 2006), pp. 224–226.

[68] Julia Gröning and Axel Hochkirch. *Reproductive Interference Between Animal Species*. 2008.

[69] Astrid T Groot, Teun Dekker, and David G Heckel. "The Genetic Basis of Pheromone Evolution in Moths". en. In: *Annu. Rev. Entomol.* 61 (2016), pp. 99–117.

[70] Jonathan D Gruber et al. “Contrasting properties of gene-specific regulatory, coding, and copy number mutations in Saccharomyces cerevisiae: frequency, effects, and dominance”. en. In: *PLoS Genet.* 8.2 (Feb. 2012), e1002497.

[71] Brian J Haas et al. “De novo transcript sequence reconstruction from RNA-seq using the Trinity platform for reference generation and analysis”. In: *Nat. Protoc.* 8.8 (Aug. 2013), pp. 1494–1512.

[72] Peter W Harrison et al. “Sexual selection drives evolution and rapid turnover of male gene expression”. en. In: *Proc. Natl. Acad. Sci. U. S. A.* 112.14 (Apr. 2015), pp. 4393–4398.

[73] E N Harvey and P A Snell. “THE ANALYSIS OF BIOLUMINESCENCES OF SHORT DURATION, RECORDED WITH PHOTOELECTRIC CELL AND STRING GALVANOMETER”. en. In: *J. Gen. Physiol.* 14.4 (Mar. 1931), pp. 529–545.

[74] E Newton Harvey. “STUDIES ON BIOLUMINESCENCE”. In: *American Journal of Physiology–Legacy Content* 70.3 (1924), pp. 619–623.

[75] Philip W Hedrick. “Adaptive introgression in animals: examples and comparison to new mutation and standing variation as sources of adaptive variation”. en. In: *Mol. Ecol.* 22.18 (Sept. 2013), pp. 4606–4618.

[76] Nicholai M Hensley et al. “Phenotypic evolution shaped by current enzyme function in the bioluminescent courtship signals of sea fireflies”. en. In: *Proc. Biol. Sci.* 286.1894 (Jan. 2019), p. 20182621.

[77] M Higashi, G Takimoto, and N Yamamura. “Sympatric speciation by sexual selection”. en. In: *Nature* 402.6761 (Dec. 1999), pp. 523–526.

[78] M Higgie, S Chenoweth, and M W Blows. “Natural selection and the reinforcement of mate recognition”. en. In: *Science* 290.5491 (Oct. 2000), pp. 519–521.

[79] Hopi E Hoekstra and Jerry A Coyne. “The locus of evolution: evo devo and the genetics of adaptation”. en. In: *Evolution* 61.5 (May 2007), pp. 995–1016.

[80] Kim L Hoke et al. “Co-opting evo-devo concepts for new insights into mechanisms of behavioural diversity”. en. In: *J. Exp. Biol.* 222.Pt 8 (Apr. 2019).

[81] Ralph W Howard and Gary J Blomquist. “Ecological, behavioral, and biochemical aspects of insect hydrocarbons”. en. In: *Annu. Rev. Entomol.* 50 (2005), pp. 371–393.

[82] X Huang and A Madan. “CAP3: A DNA sequence assembly program”. In: *Genome Res.* 9.9 (Sept. 1999), pp. 868–877.

[83] A L Hughes and M Nei. “Pattern of nucleotide substitution at major histocompatibility complex class I loci reveals overdominant selection”. en. In: *Nature* 335.6186 (Sept. 1988), pp. 167–170.

[84] Eric A Hunt et al. “Expression of a soluble truncated Vargula luciferase in Escherichia coli”. en. In: *Protein Expr. Purif.* 132 (Apr. 2017), pp. 68–74.

[85] Francois Husson et al. “FactoMineR: multivariate exploratory data analysis and data mining with R”. In: *R package version* 1.1.29 (2013).

[86] Andrea L Huvard. “Analysis of visual pigment absorbance and luminescence emission spectra in marine ostracodes (Crustacea: Ostracoda)”. In: *Comp. Biochem. Physiol. A Physiol.* 104.2 (Feb. 1993), pp. 333–338.

[87] Rob J Hyndman, Yeasmin Khandakar, et al. *Automatic time series for forecasting: the forecast package for R*. Monash University, Department of Econometrics and Business Statistics . . ., 2007.

[88] Satoshi Inouye and Yuiko Sahara. “Soluble protein expression in E. coli cells using IgG-binding domain of protein A as a solubilizing partner in the cold induced system”. en. In: *Biochem. Biophys. Res. Commun.* 376.3 (Nov. 2008), pp. 448–453.

[89] Anthony R Ives, Peter E Midford, and Theodore Garland Jr. “Within-species variation and measurement error in phylogenetic comparative methods”. en. In: *Syst. Biol.* 56.2 (Apr. 2007), pp. 252–270.

[90] Anthony C Janetos. “Strategies of female mate choice: A theoretical analysis”. In: *Behav. Ecol. Sociobiol.* 7.2 (July 1980), pp. 107–112.

[91] Chris D Jiggins, Richard W R Wallbank, and Joseph J Hanly. “Waiting in the wings: what can we learn about gene co-option from the diversification of butterfly wing patterns?” en. In: *Philos. Trans. R. Soc. Lond. B Biol. Sci.* 372.1713 (Feb. 2017).

[92] Kenneth A Johnson and Roger S Goody. “The Original Michaelis Constant: Translation of the 1913 Michaelis–Menten Paper”. In: *Biochemistry* 50.39 (Oct. 2011), pp. 8264–8269.

[93] M Joron et al. “Heliconius wing patterns: an evo-devo model for understanding phenotypic diversity”. en. In: *Heredity* 97.3 (Sept. 2006), pp. 157–167.

[94] Subha Kalyaanamoorthy et al. “ModelFinder: fast model selection for accurate phylogenetic estimates”. en. In: *Nat. Methods* 14.6 (June 2017), pp. 587–589.

[95] David Karig et al. “Stochastic Turing patterns in a synthetic bacterial population”. en. In: *Proc. Natl. Acad. Sci. U. S. A.* 115.26 (June 2018), pp. 6572–6577.

[96] Kazutaka Katoh, George Asimenos, and Hiroyuki Toh. “Multiple alignment of DNA sequences with MAFFT”. en. In: *Methods Mol. Biol.* 537 (2009), pp. 39–64.

[97] Kazutaka Katoh and Daron M Standley. “MAFFT multiple sequence alignment software version 7: improvements in performance and usability”. In: *Mol. Biol. Evol.* 30.4 (Apr. 2013), pp. 772–780.

[98] Kosei Kawasaki et al. “Mutant luciferase”. 8147842. Apr. 2012.

[99] Matthew Kearse et al. “Geneious Basic: an integrated and extendable desktop software platform for the organization and analysis of sequence data”. en. In: *Bioinformatics* 28.12 (June 2012), pp. 1647–1649.

[100] Mohammed A Khallaf et al. “Mate discrimination among subspecies through a conserved olfactory pathway”. In: *bioRxiv* (2020).

[101] Anna Kicheva, Michael Cohen, and James Briscoe. “Developmental pattern formation: insights from physics and biology”. en. In: *Science* 338.6104 (Oct. 2012), pp. 210–212.

[102] M Kimura. “Preponderance of synonymous changes as evidence for the neutral theory of molecular evolution”. en. In: *Nature* 267.5608 (May 1977), pp. 275–276.

[103] Sonia Kleindorfer et al. “Species collapse via hybridization in Darwin’s tree finches”. en. In: *Am. Nat.* 183.3 (Mar. 2014), pp. 325–341.

[104] Koji Kobayashi et al. “PURIFICATION AND PROPERTIES OF THE LUCIFERASE FROM THE MARINE OSTRACOD Vargula hilgendorfii”. In: *Bioluminescence And Chemiluminescence*. books.google.com, 2001, pp. 87–90.

[105] Hanna Kokko, Michael D Jennions, and Robert Brooks. “Unifying and Testing Models of Sexual Selection”. In: *Annu. Rev. Ecol. Evol. Syst.* 37.1 (Nov. 2006), pp. 43–66.

[106] Sergei L Kosakovsky Pond and Simon D W Frost. “Not so different after all: a comparison of methods for detecting amino acid sites under selection”. en. In: *Mol. Biol. Evol.* 22.5 (May 2005), pp. 1208–1222.

[107] Clemens Küpper et al. “A supergene determines highly divergent male reproductive morphs in the ruff”. en. In: *Nat. Genet.* 48.1 (Jan. 2016), pp. 79–83.

[108] Petr Kuzmic. *Integrated Michaelis-Menten equation in DynaFit. 2. Application to 5α-ketosteroid reductase*. Tech. rep. BioKin Ltd Technical Note TN-2016-02, http://www. biokin. com/TN/2016/02 ..., 2016.

[109] R Lande. “Models of speciation by sexual selection on polygenic traits”. en. In: *Proc. Natl. Acad. Sci. U. S. A.* 78.6 (June 1981), pp. 3721–3725.

[110] R Lande. “The minimum number of genes contributing to quantitative variation between and within populations”. en. In: *Genetics* 99.3-4 (Nov. 1981), pp. 541–553.

[111] Meghan Laturney and Amanda J Moehring. “The Genetic Basis of Female Mate Preference and Species Isolation in Drosophila”. en. In: *Int. J. Evol. Biol.* 2012 (Aug. 2012).

[112] Heng Li and Richard Durbin. “Fast and accurate long-read alignment with Burrows-Wheeler transform”. en. In: *Bioinformatics* 26.5 (Mar. 2010), pp. 589–595.

[113] Denis Limousin et al. “Genetic architecture of sexual selection: QTL mapping of male song and female receiver traits in an acoustic moth”. en. In: *PLoS One* 7.9 (Sept. 2012), e44554.

[114] Olle Lind et al. “Coevolution of coloration and colour vision?” en. In: *Philos. Trans. R. Soc. Lond. B Biol. Sci.* 372.1724 (July 2017).

[115] Charles E Linn Jr et al. “Behavioral evidence for fruit odor discrimination and sympatric host races of Rhagoletis pomonella flies in the Western United States”. en. In: *Evolution* 66.11 (Nov. 2012), pp. 3632–3641.

[116] Alexander G Lucaci et al. “Extra base hits: widespread empirical support for instantaneous multiple-nucleotide changes”. en. May 2020.

[117] Martine E Maan and Ole Seehausen. “Ecology, sexual selection and speciation”. en. In: *Ecol. Lett.* 14.6 (June 2011), pp. 591–602.

[118] T F Mackay. “The genetic architecture of quantitative traits”. en. In: *Annu. Rev. Genet.* 35 (2001), pp. 303–339.

[119] Philip K Maini et al. “Turing’s model for biological pattern formation and the robustness problem”. en. In: *Interface Focus* 2.4 (Aug. 2012), pp. 487–496.

[120] Judith E Mank. “The transcriptional architecture of phenotypic dimorphism”. In: *Nature Ecology & Evolution* 1 (2017), p. 0006.

[121] Svetlana V Markova et al. “The smallest natural high-active luciferase: cloning and characterization of novel 16.5-kDa luciferase from copepod Metridia longa”. en. In: *Biochem. Biophys. Res. Commun.* 457.1 (Jan. 2015), pp. 77–82.

[122] Arnaud Martin and Virginie Orgogozo. “The Loci of repeated evolution: a catalog of genetic hotspots of phenotypic variation”. en. In: *Evolution* 67.5 (May 2013), pp. 1235–1250.

[123] Christopher H Martin and Emilie J Richards. “The Paradox Behind the Pattern of Rapid Adaptive Radiation: How Can the Speciation Process Sustain Itself Through an Early Burst?” In: *Annu. Rev. Ecol. Evol. Syst.* 50.1 (Nov. 2019), pp. 569–593.

[124] John P Masly. “170 Years of “Lock-and-Key”: Genital Morphology and Reproductive Isolation”. en. In: *Int. J. Evol. Biol.* 2012 (Dec. 2011).

[125] A Mazo-Vargas and R D Reed. “Single master regulatory gene coordinates the evolution and development of butterfly color and iridescence”. In: *Proceedings of the* (2017).

[126] Carolyn S McBride. “Rapid evolution of smell and taste receptor genes during host specialization in Drosophila sechellia”. en. In: *Proc. Natl. Acad. Sci. U. S. A.* 104.12 (Mar. 2007), pp. 4996–5001.

[127] Carolyn S McBride et al. “Evolution of mosquito preference for humans linked to an odorant receptor”. en. In: *Nature* 515.7526 (Nov. 2014), pp. 222–227.

[128] W D McELROY and A M Chase. “Purification of Cypridina luciferase”. en. In: *J. Cell. Comp. Physiol.* 38.3 (Dec. 1951), pp. 401–408.

[129] Alistair P McGregor et al. “Morphological evolution through multiple cis-regulatory mutations at a single gene”. en. In: *Nature* 448.7153 (Aug. 2007), pp. 587–590.

[130] Donald James McLean and Marta A Skowron Volponi. “trajr : An R package for characterisation of animal trajectories”. In: *Ethology* 124.6 (June 2018). Ed. by T Tregenza, pp. 440–448.

[131] Louise S Mead and Stevan J Arnold. “Quantitative genetic models of sexual selection”. en. In: *Trends Ecol. Evol.* 19.5 (May 2004), pp. 264–271.

[132] Tamra C Mendelson. “Sexual isolation evolves faster than hybrid inviability in a diverse and sexually dimorphic genus of fish (Percidae: Etheostoma)”. en. In: *Evolution* 57.2 (Feb. 2003), pp. 317–327.

[133] C Mérot et al. “What shapes the continuum of reproductive isolation? Lessons from Heliconius butterflies”. en. In: *Proc. Biol. Sci.* 284.1856 (June 2017).

[134] Meredith C Miles et al. “Macroevolutionary patterning of woodpecker drums reveals how sexual selection elaborates signals under constraint”. en. In: *Proc. Biol. Sci.* 285.1873 (Feb. 2018).

[135] Bui Quang Minh et al. “IQ-TREE 2: New Models and Efficient Methods for Phylogenetic Inference in the Genomic Era”. en. In: *Mol. Biol. Evol.* 37.5 (May 2020), pp. 1530–1534.

[136] Yasuo Mitani et al. “Efficient production of glycosylated Cypridina luciferase using plant cells”. en. In: *Protein Expr. Purif.* 133 (May 2017), pp. 102–109.

[137] *Modern Phylogenetic Comparative Methods and Their Application in Evolutionary Biology — SpringerLink*. `https://link.springer.com/content/pdf/10.1007/978-3-662-43550-2.pdf`. Accessed: 2018-8-27.

[138] James G Morin. “Based on a review of the data, use of the term ‘cypridinid’solves the Cypridina/Vargula dilemma for naming the constituents of the luminescent system of ostracods in the family Cypridinidae”. In: *Luminescence* 26.1 (2011), pp. 1–4.

[139] James G Morin. “Firefleas of the Sea: Luminescent Signaling in Marine Ostracode Crustaceans”. In: *Fla. Entomol.* 69.1 (1986), pp. 105–121.

[140] James G Morin and Anne C Cohen. “A guide to the morphology of bioluminescent signaling Cypridinid Ostracods from the Caribbean Sea, and a tabular key to the genera”. In: *Zootaxa* 4303.3 (2017), pp. 301–349.

[141] James G Morin and Anne C Cohen. “It’s All About Sex: Bioluminescent Courtship Displays, Morphological Variation and Sexual Selection in Two New Genera of Caribbean Ostracodes”. In: *J. Crustacean Biol.* 30.1 (Jan. 2010), pp. 56–67.

[142] Leonie C Moyle, Matthew S Olson, and Peter Tiffin. "Patterns of reproductive isolation in three angiosperm genera". en. In: *Evolution* 58.6 (June 2004), pp. 1195–1208.

[143] Barton K MuMIn. *Multi-Model inference. R package version 1.15. 6. 2016*. 2018.

[144] Ben Murrell et al. *Detecting Individual Sites Subject to Episodic Diversifying Selection*. 2012.

[145] Takao Nakagawa et al. "Insect sex-pheromone signals mediated by specific combinations of olfactory receptors". en. In: *Science* 307.5715 (Mar. 2005), pp. 1638–1642.

[146] Yoshihiro Nakajima et al. "cDNA cloning and characterization of a secreted luciferase from the luminous Japanese ostracod, Cypridina noctiluca". In: *Biosci. Biotechnol. Biochem.* 68.3 (Mar. 2004), pp. 565–570.

[147] Chandrasekhar Natarajan et al. *Convergent Evolution of Hemoglobin Function in High-Altitude Andean Waterfowl Involves Limited Parallelism at the Molecular Sequence Level*. 2015.

[148] Chandrasekhar Natarajan et al. "Epistasis among adaptive mutations in deer mouse hemoglobin". en. In: *Science* 340.6138 (June 2013), pp. 1324–1327.

[149] Chandrasekhar Natarajan et al. "Predictable convergence in hemoglobin function has unpredictable molecular underpinnings". In: *Science* 354.6310 (2016), pp. 336–339.

[150] Tanmay Nath et al. "Using DeepLabCut for 3D markerless pose estimation across species and behaviors". en. In: *Nat. Protoc.* 14.7 (July 2019), pp. 2152–2176.

[151] *NCBI Magic-BLAST : NCBI Magic-BLAST Documentation*. `https://ncbi.github.io/magicblast/`. Accessed: 2017-11-13.

[152] E Newton Harvey and Peter A Snell. *The Analysis of Bioluminescences of Short Duration, recorded with photoelectric cell and string galvinometer*.

[153] Lam-Tung Nguyen et al. "IQ-TREE: a fast and effective stochastic algorithm for estimating maximum-likelihood phylogenies". en. In: *Mol. Biol. Evol.* 32.1 (Jan. 2015), pp. 268–274.

[154] Kazuki Niwa, Yoshiro Ichino, and Yoshihiro Ohmiya. "Quantum yield measurements of firefly bioluminescence reactions using a commercial luminometer". In: *Chem. Lett.* 39.3 (2010), pp. 291–293.

[155] T H Oakley. "Myodocopa (Crustacea: Ostracoda) as models for evolutionary studies of light and vision: multiple origins of bioluminescence and extreme sexual dimorphism". In: *Hydrobiologia*. 179th ser. 538 (2005), pp. 179–192.

[156] Todd H Oakley et al. "Osiris: accessible and reproducible phylogenetic and phylogenomic analyses within the Galaxy workflow management system". In: *BMC Bioinformatics* 15 (July 2014), p. 230.

[157] K P Oh et al. “Interspecific genetics of speciation phenotypes: song and preference coevolution in Hawaiian crickets”. en. In: *J. Evol. Biol.* 25.8 (Aug. 2012), pp. 1500–1512.

[158] Y Ohmiya, T Hirano, and M Ohashi. “The structural origin of the color differences in the bioluminescence of firefly luciferase”. en. In: *FEBS Lett.* 384.1 (Apr. 1996), pp. 83–86.

[159] Koh Onimaru et al. “The fin-to-limb transition as the re-organization of a Turing pattern”. In: *Nat. Commun.* 7.1 (2016), pp. 1–9.

[160] Eric A Ortlund et al. “Crystal structure of an ancient protein: evolution by conformational epistasis”. In: *Science* 317.5844 (2007), pp. 1544–1548.

[161] David C Plachetzki, Bernard M Degnan, and Todd H Oakley. “The origins of novel protein interactions during animal opsin evolution”. In: *PLoS One* 2.10 (Jan. 2007), e1054.

[162] Jeffrey Podos. “A PERFORMANCE CONSTRAINT ON THE EVOLUTION OF TRILLED VOCALIZATIONS IN A SONGBIRD FAMILY (PASSERIFORMES: EMBERIZIDAE)”. en. In: *Evolution* 51.2 (Apr. 1997), pp. 537–551.

[163] Sergei L Kosakovsky Pond et al. *HyPhy 2.5—A Customizable Platform for Evolutionary Hypothesis Testing Using Phylogenies*. 2019.

[164] J Jordan Price and Scott M Lanyon. “Reconstructing the evolution of complex bird song in the oropendolas”. en. In: *Evolution* 56.7 (July 2002), pp. 1514–1529.

[165] A Y Prokuda and D A Roff. “The quantitative genetics of sexually selected traits, preferred traits and preference: a review and analysis of the data”. en. In: *J. Evol. Biol.* 27.11 (Nov. 2014), pp. 2283–2296.

[166] Daniel L Rabosky and Daniel R Matute. “Macroevolutionary speciation rates are decoupled from the evolution of intrinsic reproductive isolation in Drosophila and birds”. en. In: *Proc. Natl. Acad. Sci. U. S. A.* 110.38 (Sept. 2013), pp. 15354–15359.

[167] Nicholas J Reda. “Capturing speciation in action: Rapid population divergence in the Caribbean bioluminescent ostracod Photeros annecohenae (Myodocopida: Cypridinidae)”. PhD thesis. 2019.

[168] Nicholas J Reda et al. “Maristella, a new bioluminescent ostracod genus in the Myodocopida (Cypridinidae)”. In: *Zool. J. Linn. Soc.* (Oct. 2019).

[169] Michael G Ritchie. “Sexual Selection and Speciation”. In: *Annu. Rev. Ecol. Evol. Syst.* 38.1 (Dec. 2007), pp. 79–102.

[170] Trevor J Rivers and James G Morin. “Complex sexual courtship displays by luminescent male marine ostracods”. en. In: *J. Exp. Biol.* 211.Pt 14 (July 2008), pp. 2252–2262.

[171] Trevor J Rivers and James G Morin. "Female ostracods respond to and intercept artificial conspecific male luminescent courtship displays". In: *Behav. Ecol.* 24.4 (July 2013), pp. 877–887.

[172] Trevor J Rivers and James G Morin. "Plasticity of male mating behaviour in a marine bioluminescent ostracod in both time and space". In: *Anim. Behav.* 78.3 (2009), pp. 723–734.

[173] Trevor J Rivers and James G Morin. "The relative cost of using luminescence for sex and defense: light budgets in cypridinid ostracods". en. In: *J. Exp. Biol.* 215.Pt 16 (Aug. 2012), pp. 2860–2868.

[174] Donelle M Robinson, M Scarlett Tudor, and Molly R Morris. *Female preference and the evolution of an exaggerated male ornament: the shape of the preference function matters*. 2011.

[175] A Rohatgi. "WebPlotDigitizer". In: *URL http://arohatgi. info/WebPlotDigitizer/app* (2011).

[176] Erica Bree Rosenblum et al. "Molecular and functional basis of phenotypic convergence in white lizards at White Sands". en. In: *Proc. Natl. Acad. Sci. U. S. A.* 107.5 (Feb. 2010), pp. 2113–2117.

[177] Gonzalo Sabarıs et al. "Actors with Multiple Roles: Pleiotropic Enhancers and the Paradigm of Enhancer Modularity". en. In: *Trends Genet.* 35.6 (June 2019), pp. 423–433.

[178] Rebecca J Safran et al. "Contributions of natural and sexual selection to the evolution of premating reproductive isolation: a research agenda". en. In: *Trends Ecol. Evol.* 28.11 (Nov. 2013), pp. 643–650.

[179] Aaron A Sandel et al. "Assessing sources of error in comparative analyses of primate behavior: Intraspecific variation in group size and the social brain hypothesis". en. In: *J. Hum. Evol.* 94 (May 2016), pp. 126–133.

[180] Thomas J Sanger and Rajendhran Rajakumar. "How a growing organismal perspective is adding new depth to integrative studies of morphological evolution". en. In: *Biol. Rev. Camb. Philos. Soc.* (July 2018).

[181] H Martin Schaefer and Graeme D Ruxton. "Signal Diversity, Sexual Selection, and Speciation". In: *Annu. Rev. Ecol. Evol. Syst.* 46.1 (Dec. 2015), pp. 573–592.

[182] Christine E Schnitzler et al. "Genomic organization, evolution, and expression of photoprotein and opsin genes in Mnemiopsis leidyi: a new view of ctenophore photocytes". en. In: *BMC Biol.* 10 (Dec. 2012), p. 107.

[183] Bas van Schooten et al. "Divergence of chemosensing during the early stages of speciation". en. In: *Proc. Natl. Acad. Sci. U. S. A.* 117.28 (July 2020), pp. 16438–16447.

[184] Ole Seehausen et al. “Speciation through sensory drive in cichlid fish”. en. In: *Nature* 455.7213 (Oct. 2008), pp. 620–626.

[185] Ryohei Seki et al. “Functional roles of Aves class-specific cis-regulatory elements on macroevolution of bird-specific features”. en. In: *Nat. Commun.* 8 (Feb. 2017), p. 14229.

[186] Maria R Servedio et al. “Magic traits in speciation:‘magic’but not rare?” In: *Trends Ecol. Evol.* 26.8 (2011), pp. 389–397.

[187] Kerry L Shaw. *Sequential Radiations and Patterns of Speciation in the Hawaiian Cricket Genus Laupala Inferred from DNA Sequences*. 1996.

[188] Kerry L Shaw and Sky C Lesnick. “Genomic linkage of male song and female acoustic preference QTL underlying a rapid species radiation”. en. In: *Proc. Natl. Acad. Sci. U. S. A.* 106.24 (June 2009), pp. 9737–9742.

[189] Michael J Sheehan, Judy Jinn, and Elizabeth A Tibbetts. *Coevolution of visual signals and eye morphology in Polistes paper wasps*. 2014.

[190] Wei Shen et al. “SeqKit: A Cross-Platform and Ultrafast Toolkit for FASTA/Q File Manipulation”. en. In: *PLoS One* 11.10 (Oct. 2016), e0163962.

[191] R Sheth et al. *Hox Genes Regulate Digit Patterning by Controlling the Wavelength of a Turing-Type Mechanism*. 2012.

[192] O Shimomura and F H Johnson. “Mechanism of the luminescent oxidation of cypridina luciferin”. en. In: *Biochem. Biophys. Res. Commun.* 44.2 (July 1971), pp. 340–346.

[193] O Shimomura and F H Johnson. “Mechanisms in the quantum yield of Cypridina bioluminescence”. en. In: *Photochem. Photobiol.* 12.4 (Oct. 1970), pp. 291–295.

[194] B Sinervo et al. “The role of pleiotropy vs signaller-receiver gene epistasis in life history trade-offs: dissecting the genomic architecture of organismal design in social systems”. en. In: *Heredity* 101.3 (Sept. 2008), pp. 197–211.

[195] Saurabh Sinha et al. “Behavior-related gene regulatory networks: A new level of organization in the brain”. en. In: *Proc. Natl. Acad. Sci. U. S. A.* (July 2020).

[196] Martin D Smith et al. “Less is more: an adaptive branch-site random effects model for efficient detection of episodic diversifying selection”. en. In: *Mol. Biol. Evol.* 32.5 (May 2015), pp. 1342–1353.

[197] Masayo Soma and László Z Garamszegi. “Evolution of courtship display in Estrildid finches: dance in relation to female song and plumage ornamentation”. en. In: *Front. Ecol. Evol.* 3 (2015).

[198] Kathrin F Stanger-Hall and James E Lloyd. “Flash signal evolution in Photinus fireflies: character displacement and signal exploitation in a visual communication system”. en. In: *Evolution* 69.3 (Mar. 2015), pp. 666–682.

[199] Tyler N Starr et al. “Pervasive contingency and entrenchment in a billion years of Hsp90 evolution”. en. In: *Proc. Natl. Acad. Sci. U. S. A.* 115.17 (Apr. 2018), pp. 4453–4458.

[200] Galina A Stepanyuk et al. “Expression, purification and characterization of the secreted luciferase of the copepod Metridia longa from Sf9 insect cells”. en. In: *Protein Expr. Purif.* 61.2 (Oct. 2008), pp. 142–148.

[201] David L Stern. “The genetic causes of convergent evolution”. en. In: *Nat. Rev. Genet.* 14.11 (Nov. 2013), pp. 751–764.

[202] David L Stern and Virginie Orgogozo. “Is genetic evolution predictable?” en. In: *Science* 323.5915 (Feb. 2009), pp. 746–751.

[203] David L Stern and Virginie Orgogozo. “The loci of evolution: how predictable is genetic evolution?” en. In: *Evolution* 62.9 (Sept. 2008), pp. 2155–2177.

[204] K P Stevens. “STUDIES ON THE AMOUNT OF LIGHT EMITTED BY MIXTURES OF CYPRIDINA LUCIFERIN AND LUCIFERASE”. en. In: *J. Gen. Physiol.* 10.6 (July 1927), pp. 859–873.

[205] Mary Caswell Stoddard and Mark E Hauber. “Colour, vision and coevolution in avian brood parasitism”. en. In: *Philos. Trans. R. Soc. Lond. B Biol. Sci.* 372.1724 (July 2017).

[206] Jay F Storz. “Hemoglobin-oxygen affinity in high-altitude vertebrates: is there evidence for an adaptive trend?” en. In: *J. Exp. Biol.* 219.Pt 20 (Oct. 2016), pp. 3190–3203.

[207] Elio Sucena et al. “Regulatory evolution of shavenbaby/ovo underlies multiple cases of morphological parallelism”. In: *Nature* 424.6951 (Aug. 2003), pp. 935–938.

[208] Mikita Suyama, David Torrents, and Peer Bork. “PAL2NAL: robust conversion of protein sequence alignments into the corresponding codon alignments”. en. In: *Nucleic Acids Res.* 34.Web Server issue (July 2006), W609–12.

[209] Immani Swapna et al. “Electrostatic Tuning of a Potassium Channel in Electric Fish”. en. In: *Curr. Biol.* 28.13 (July 2018), 2094–2102.e5.

[210] Laurel B Symes. “Community composition affects the shape of mate response functions”. en. In: *Evolution* 68.7 (July 2014), pp. 2005–2013.

[211] Yasuhiro Takenaka et al. “Evolution of bioluminescence in marine planktonic copepods”. en. In: *Mol. Biol. Evol.* 29.6 (June 2012), pp. 1669–1681.

[212] Yasuhiro Takenaka et al. “Two forms of secreted and thermostable luciferases from the marine copepod crustacean, Metridia pacifica”. en. In: *Gene* 425.1-2 (Dec. 2008), pp. 28–35.

[213] E M Thompson, S Nagata, and F I Tsuji. "Cloning and expression of cDNA for the luciferase from the marine ostracod Vargula hilgendorfii". In: *Proc. Natl. Acad. Sci. U. S. A.* 86.17 (Sept. 1989), pp. 6567–6571.

[214] Yuki Tochigi et al. "Sensitive and convenient yeast reporter assay for high-throughput analysis by using a secretory luciferase from Cypridina noctiluca". en. In: *Anal. Chem.* 82.13 (July 2010), pp. 5768–5776.

[215] Nobuhiko Tokuriki et al. "How protein stability and new functions trade off". en. In: *PLoS Comput. Biol.* 4.2 (Feb. 2008), e1000002.

[216] Elizabeth Torres and Anne C Cohen. "Vargula morini, a new species of bioluminescent ostracode (Myodocopida: Cypridinidae) from Belize and an associated copepod (Copepoda: Siphonostomatoida: Nicothoidae)". In: *J. Crustacean Biol.* 25.1 (2005), pp. 11–24.

[217] Elizabeth Torres and Vanessa L Gonzalez. "MOLECULAR PHYLOGENY OF CYPRIDINID OSTRACODES AND THE EVOLUTION OF BIOLUMINESCENCE". In: *Bioluminescence and Chemiluminescence*. San Diego, USA: WORLD SCIENTIFIC, July 2007, pp. 269–272.

[218] F I Tsuji, R V Lynch 3rd, and C L Stevens. "Some properties of luciferase from the bioluminescent crustacean, Cypridina hilgendorfii". en. In: *Biochemistry* 13.25 (Dec. 1974), pp. 5204–5209.

[219] F I Tsuji and R Sowinski. "Purification and molecular weight of Cypridina luciferase". en. In: *J. Cell. Comp. Physiol.* 58 (Oct. 1961), pp. 125–129.

[220] Frederick I Tsuji, Richard V Lynch, and Yata Haneda. "Studies on the Bioluminescence of the Marine Ostracod Crustacean Cypridina serrata". In: *Biol. Bull.* 139.2 (1970), pp. 386–401.

[221] Julie Turgeon and Paul D N Hebert. "Evolutionary interactions between sexual and all-female taxa of Cyprinotus (Ostracoda: Cyprididae)". In: *Evolution* 48.6 (1994), pp. 1855–1865.

[222] A M Turing. "The chemical theory of morphogenesis". In: *Phil. Trans. Roy. Soc* 13.1 (1952).

[223] Leslie M Turner et al. "Monogamy evolves through multiple mechanisms: evidence from V1aR in deer mice". en. In: *Mol. Biol. Evol.* 27.6 (June 2010), pp. 1269–1278.

[224] Elaina M Tuttle et al. "Divergence and Functional Degradation of a Sex Chromosome-like Supergene". en. In: *Curr. Biol.* 26.3 (Feb. 2016), pp. 344–350.

[225] Valen Van and L Van Valen. "A new evolutionary law". In: (1973).

[226] Aarti Venkat, Matthew W Hahn, and Joseph W Thornton. *Multinucleotide mutations cause false inferences of lineage-specific positive selection*. 2018.

[227] Machteld N Verzijden, Robert F Lachlan, and Maria R Servedio. "Female mate-choice behavior and sympatric speciation". In: *Evolution* 59.10 (2005), pp. 2097–2108.

[228] Vadim R Viviani and Y Ohmiya. "Bovine serum albumin displays luciferase-like activity in presence of luciferyl adenylate: insights on the origin of protoluciferase activity and bioluminescence colours". In: *Luminescence* 21.4 (2006), pp. 262–267.

[229] Vadim R Viviani et al. "A new blue-shifted luciferase from the Brazilian Amydetes fanestratus (Coleoptera: Lampyridae) firefly: molecular evolution and structural/functional properties". en. In: *Photochem. Photobiol. Sci.* 10.12 (Dec. 2011), pp. 1879–1886.

[230] Peter C Wainwright et al. "Many-to-One Mapping of Form to Function: A General Principle in Organismal Design?" en. In: *Integr. Comp. Biol.* 45.2 (Apr. 2005), pp. 256–262.

[231] Richard W R Wallbank et al. "Evolutionary Novelty in a Butterfly Wing Pattern through Enhancer Shuffling". en. In: *PLoS Biol.* 14.1 (Jan. 2016), e1002353.

[232] Ryan Walsh, Earl Martin, and Sultan Darvesh. "A method to describe enzyme-catalyzed reactions by combining steady state and time course enzyme kinetic parameters". en. In: *Biochim. Biophys. Acta* 1800.1 (Jan. 2010), pp. 1–5.

[233] Robert M Waterhouse et al. "BUSCO applications from quality assessments to gene prediction and phylogenomics". en. In: *Mol. Biol. Evol.* (Dec. 2017).

[234] Chris Wiley and Kerry L Shaw. "Multiple genetic linkages between female preference and male signal in rapidly speciating Hawaiian crickets". en. In: *Evolution* 64.8 (Aug. 2010), pp. 2238–2245.

[235] Steffen Wischmann, Dario Floreano, and Laurent Keller. "Historical contingency affects signaling strategies and competitive abilities in evolving populations of simulated robots". en. In: *Proc. Natl. Acad. Sci. U. S. A.* 109.3 (Jan. 2012), pp. 864–868.

[236] Sadie R Wisotsky et al. "Synonymous site-to-site substitution rate variation dramatically inflates false positive rates of selection analyses: ignore at your own peril". en. In: *Mol. Biol. Evol.* (Feb. 2020).

[237] Gregory A Wray. "The evolutionary significance of cis-regulatory mutations". en. In: *Nat. Rev. Genet.* 8.3 (Mar. 2007), pp. 206–216.

[238] Kathleen T Xie et al. "DNA fragility in the parallel evolution of pelvic reduction in stickleback fish". en. In: *Science* 363.6422 (Jan. 2019), pp. 81–84.

[239] Yusan Yang, Maria R Servedio, and Corinne L Richards-Zawacki. "Imprinting sets the stage for speciation". en. In: *Nature* 574.7776 (Oct. 2019), pp. 99–102.

[240] Rie Yasuno, Yasuo Mitani, and Yoshihiro Ohmiya. "Effects of N-Glycosylation Deletions on Cypridina Luciferase Activity". In: *Photochem. Photobiol.* 94.2 (2018), pp. 338–342.

[241] Shozo Yokoyama, Hui Yang, and William T Starmer. "Molecular basis of spectral tuning in the red- and green-sensitive (M/LWS) pigments in vertebrates". en. In: *Genetics* 179.4 (Aug. 2008), pp. 2037–2043.

[242] Shozo Yokoyama et al. "Elucidation of phenotypic adaptations: Molecular analyses of dim-light vision proteins in vertebrates". en. In: *Proc. Natl. Acad. Sci. U. S. A.* 105.36 (Sept. 2008), pp. 13480–13485.

[243] Shozo Yokoyama et al. "Epistatic adaptive evolution of human color vision". en. In: *PLoS Genet.* 10.12 (Dec. 2014), e1004884.

[244] Ryan York. *The genetic landscape of animal behavior.*

[245] Ryan A York and Russell D Fernald. "The Repeated Evolution of Behavior". In: *Frontiers in Ecology and Evolution* 4 (2017), p. 143.

[246] Ryan A York et al. "Evolution of bower building in Lake Malawi cichlid fish: phylogeny, morphology, and behavior". In: *Frontiers in Ecology and Evolution* 3 (2015), p. 18.

[247] Nathan M Young et al. "Craniofacial diversification in the domestic pigeon and the evolution of the avian skull". In: *Nature Ecology & Evolution* 1.4 (2017), s41559–017.